

ROTATION-INVARIANT WEB BASES FROM HOURGLASS PLABIC GRAPHS

CHRISTIAN GAETZ, OLIVER PECHENIK, STEPHAN PFANNERER, JESSICA STRIKER,
AND JOSHUA P. SWANSON

ABSTRACT. Webs give a diagrammatic calculus for spaces of tensor invariants. We introduce *hourglass plabic graphs* as a new avatar of webs, and use these to give the first rotation-invariant $U_q(\mathfrak{sl}_4)$ -web basis, a long-sought object. The characterization of our basis webs relies on the combinatorics of these new plabic graphs and associated configurations of a symmetrized six-vertex model. We give growth rules, based on a novel crystal-theoretic technique, for generating our basis webs from tableaux and we use skein relations to give an algorithm for expressing arbitrary webs in the basis. We also discuss how previously known rotation-invariant web bases can be unified in our framework of hourglass plabic graphs.

CONTENTS

1. Introduction	1
2. Preliminaries	7
3. Hourglass plabic graphs and symmetrized six-vertex configurations	13
4. Fluctuating tableaux and separation labelings	25
5. Growth rules from crystals	32
6. The hourglass web basis	51
7. Uncrossing and reduction relations	54
8. Combinatorial applications of the web basis	56
9. Hourglass plabic graphs recover known web bases	59
Acknowledgements	63
References	63

1. INTRODUCTION

Over the last four decades, the classical theory of spaces of $SL_r(\mathbb{C})$ -invariants has been extended with the aid of diagrams called *webs*, whose calculus has powerful topological applications. For SL_2 , the *Temperley–Lieb basis* consists of tensor invariants of non-crossing matchings of points around a disk and can be used to compute the *Jones polynomial*. For SL_3 , Kuperberg [Kup96b] introduced the remarkable *non-elliptic web basis* with many beautiful properties. However, a rotation-invariant extension of Kuperberg’s basis to higher ranks has proven elusive ever since its introduction in 1996. Our main result provides the first such basis for SL_4 , and indeed for its quantum deformation $U_q(\mathfrak{sl}_4)$.

Theorem A (See Theorem 6.8). *The collection \mathcal{B}_q^c of tensor invariants of top fully reduced hourglass plabic graphs of type \underline{c} is a rotation-invariant web basis for the invariant space $\text{Inv}_{U_q(\mathfrak{sl}_4)}(\bigwedge_q^{\underline{c}} V_q)$.*

Date: June 19, 2024.

Gaetz was supported by NSF fellowship DMS-2103121. Pechenik was partially supported by a Discovery Grant (RGPIN-2021-02391) and Launch Supplement (DGEER-2021-00010) from the Natural Sciences and Engineering Research Council of Canada. Pfannerer was partially supported by the Austrian Science Fund (FWF) P29275 and is a recipient of a DOC Fellowship of the Austrian Academy of Sciences. Striker was partially supported by Simons Foundation gifts MP-TSM-00002802 and 527204 and NSF grant DMS-2247089. Swanson was partially supported by NSF grant DMS-2348843.

Such a rotation-invariant basis has long been desired by those developing the theory of webs; see, e.g., [Wes12, Fon12, FLL19, Fra20, Fra23] for such remarks. The lack heretofore of suitable generalizations of the SL_3 -web basis to higher rank has also been specifically lamented in applications of webs to cluster algebras [FP16], enumerative combinatorics [PPR09], representation theory [RT22], quantum topology [LS21, p. 10], and dimer models [DKS22].

The key insight behind Theorem A is our introduction of a combinatorial framework we call *hourglass plabic graphs*, so named because they allow certain half-twist multi-edges called *hourglasses*. These graphs are an extension of Postnikov’s plabic graphs; while Postnikov’s graphs are governed by a single *trip permutation*, ours crucially involve a tuple trip_\bullet of such permutations. To establish Theorem A, we describe a map \mathcal{T} from move-equivalence classes of certain hourglass plabic graphs to 4-row *fluctuating tableaux* (a class including standard tableaux) and a map \mathcal{G} , based on *growth rules*, in the other direction (see Figure 1 for an example). In [GPPSS24a], we showed that orbits of *promotion* on fluctuating tableaux are tracked by a tuple prom_\bullet of *promotion permutations*.

Theorem B (See Theorem 6.1). *The maps \mathcal{T} and \mathcal{G} are mutually inverse bijections between move-equivalence classes of fully reduced hourglass plabic graphs and 4-row rectangular fluctuating tableaux. Furthermore, this bijection satisfies $\text{trip}_\bullet(G) = \text{prom}_\bullet(\mathcal{T}(G))$ and consequently intertwines promotion of tableaux with rotation of hourglass plabic graphs.*

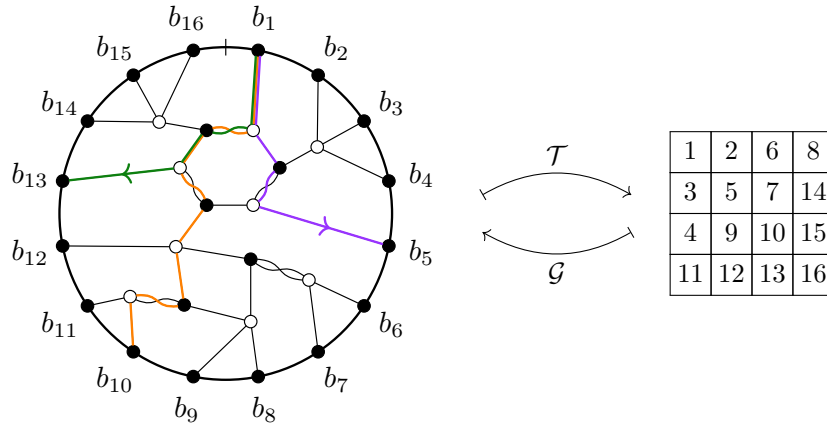


FIGURE 1. A top fully reduced hourglass plabic graph G and its corresponding 4-row rectangular standard tableau $\mathcal{T}(G)$. The purple (■) trip_1 -, orange (■) trip_2 -, and green (■) trip_3 -strands are drawn, showing that $\text{trip}_i(G)(1) = 5, 10, \text{ and } 13$ for $i = 1, 2, \text{ and } 3$, respectively.

The growth algorithm moreover allows us to deduce that the change of basis between \mathcal{B}_q^c from Theorem A and the monomial basis is unitriangular over $\mathbb{Z}[q, q^{-1}]$ (see Theorem 6.3).

This framework unifies the SL_r -web bases for $r \leq 4$, as well as the “2-column” case in arbitrary rank (see Section 9). It is also remarkably rich from a purely combinatorial perspective. For example, two extreme move-equivalence classes for $r = 4$ are naturally identified with the lattices of *alternating sign matrices* and *plane partitions* in a box, respectively (see Section 8).

1.1. Hourglass plabic graphs. Previous efforts to generalize Kuperberg’s work have largely focused on the representation theory of quantum groups (see e.g. [Kim03, Mor07, Hag18]). We instead take a combinatorial approach, which we develop throughout Sections 3 to 5; in Section 6 this combinatorial theory straightforwardly yields our rotation-invariant web basis of $\text{Inv}_{U_q(\mathfrak{sl}_4)}(\bigwedge_q^c V_q)$ from

Theorem A. We now describe the combinatorial ingredients of Theorem B before returning to discussion of web invariants.

Plabic graphs were introduced by Postnikov to study the totally nonnegative Grassmannian [Pos06, Pos18]. These are planar graphs embedded in a disk with interior vertices colored black or white. The *trip permutation* of a plabic graph is the bijection obtained by starting at a boundary vertex and traveling through the graph, taking a left at white vertices and a right at black vertices, until another boundary vertex is reached. Postnikov showed that *reduced* plabic graphs are classified up to *move-equivalence* by their trip permutation.

Building on connections between webs and plabic graphs due to Fraser–Lam–Le [FLL19], Hopkins–Rubey [HR22] recently observed that Kuperberg’s non-elliptic SL_3 basis webs can be interpreted as reduced bipartite plabic graphs. Khovanov–Kuperberg [KK99] introduced a bijection between SL_3 basis webs and *sign and state strings*, which are well-known to correspond to 3-row rectangular tableaux (see, e.g., [PPR09, Pat19]). Petersen–Pylyavskyy–Rhoades [PPR09] showed that this bijection intertwines rotation with tableau promotion in the standard case; Patrias [Pat19] extended this to the (*generalized*) *oscillating* case. The recent work of Hopkins–Rubey [HR22] encodes the structure of tableau promotion in a *promotion permutation* and shows that the Khovanov–Kuperberg bijection carries this permutation to the trip permutation of an SL_3 basis web.

Motivated by results such as [Rho10], combinatorialists have long desired such a planar model encoding promotion of general rectangular tableaux as rotation. In [GPPSS24a], we introduce fluctuating tableaux as a simultaneous generalization of standard, dual-semistandard, and the (*generalized*) oscillating tableaux of Patrias [Pat19]. We also extend the Hopkins–Rubey encoding by associating an r -row rectangular fluctuating tableaux T to a sequence of *promotion permutations* $\text{prom}_\bullet(T) = (\text{prom}_1(T), \dots, \text{prom}_{r-1}(T))$. Theorem B extends this relation to give such a planar model for 4-row fluctuating tableaux.

The key new objects of our combinatorial theory are *hourglass plabic graphs*, as illustrated in Figure 1. These are r -valent properly bicolored graphs embedded in a disk. A special feature are the *hourglass edges*, which are multiple edges twisted so that the clockwise orders of their strands around the two incident vertices are the same. Hourglass plabic graphs come with a tuple $\text{trip}_\bullet(G) = (\text{trip}_1(G), \dots, \text{trip}_{r-1}(G))$ of *trip permutations*, where trip_i is obtained by taking the i -th left at white vertices and the i -th right at black vertices. Here, the twists of the hourglass edges are essential for yielding the desired behavior of $\text{trip}_\bullet(G)$, specifically to give the conclusion from Theorem B that, for each 4-row rectangular tableau T , there is a 4-valent hourglass plabic graph G such that $\text{prom}_\bullet(T) = \text{trip}_\bullet(G)$. Remarkably, the same statement holds for all other known rotation-invariant SL_r web bases: the $r < 4$ cases and Fraser’s [Fra23] 2-column web basis for arbitrary SL_r . (See Section 9 for further discussion.) In future work, we hope to extend our approach to all r .

Hourglass plabic graphs G for $r = 4$ admit a notion of *full reducedness*, defined by forbidding certain faces in graphs equivalent to G under *moves*, most notably *square moves* and *benzene moves* (see Figure 2). Full reducedness is in many ways analogous to the well-studied notion of reducedness on plabic graphs, while moves on hourglass plabic graphs lift moves on plabic graphs. In particular, Theorem B entails that two fully reduced hourglass plabic graphs are move-equivalent if and only if their trip permutations coincide, mirroring Postnikov’s celebrated characterization of move-equivalence for reduced plabic graphs [Pos06, Thm. 13.4]. We moreover establish that full reducedness can be characterized by forbidding certain crossings of trip strands, just as Postnikov demonstrated for reduced plabic graphs [Pos06, Thm. 13.2]; this characterization is critical to many of our arguments.

The definition of full reducedness naturally extends to the $r < 4$ case, forbidding certain uniformly defined face configurations. This definition directly recovers the Temperley–Lieb noncrossing condition when $r = 2$ and Kuperberg’s non-elliptic condition when $r = 3$, giving a uniform description of basis webs in all three settings.

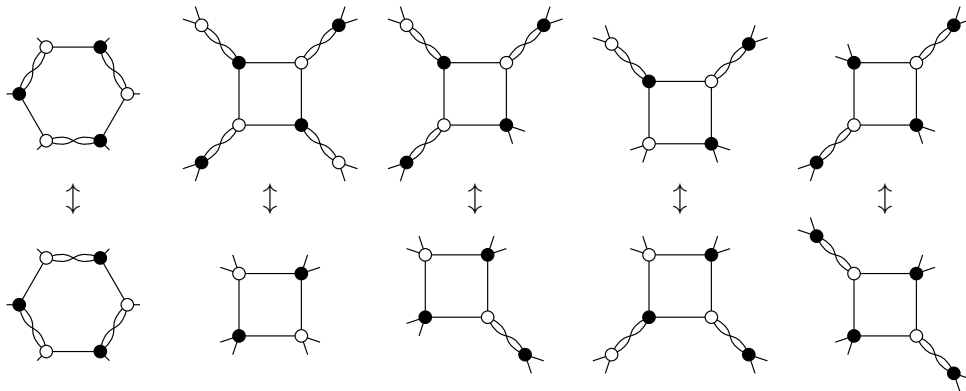


FIGURE 2. A benzene move (leftmost) and the square moves for hourglass plabic graphs. The color reversals of these moves are also allowed.

When $r = 4$, we may transform hourglass plabic graphs into directed graphs that we call *symmetrized six-vertex configurations* (see Section 3.3) and we move back and forth between these realizations as convenient. These configurations appeared independently in Hagemeyer’s thesis [Hag18]. Symmetrized six-vertex configurations are closely related to the usual six-vertex (square ice) model of statistical physics (see e.g. [Bax89]) and we thereby obtain intriguing connections to the combinatorics of *plane partitions* and *alternating sign matrices*; see Sections 8.2 and 8.3.

Our proof of Theorem B involves constructing (Section 4) the map \mathcal{T} from fully reduced hourglass plabic graphs G to fluctuating tableaux. This map involves giving an edge-labeling of G that is obtained from information about the crossings of trip_\bullet -strands. Similar labelings for SL_3 appear in [KK99, BDG⁺22]. In the reverse direction, we give in Section 5 a *growth algorithm* \mathcal{G} , analogous to that of [KK99] for SL_3 , that produces an SL_4 -basis web given the labeling of the boundary edges. The growth algorithm is the most combinatorially intricate part of our work. The proof of correctness relies critically on a novel Kashiwara crystal-theoretic technique that we introduce.

1.2. Bases of tensor invariants. Consider $\mathbf{G} = \text{SL}_r(\mathbb{C})$ with its defining representation $V = \mathbb{C}^r$, its fundamental representations $V^{\omega_k} = \bigwedge^k V$, and their duals, which we write as $\bigwedge^{-k} V := (\bigwedge^k V)^*$. Given any tensor product

$$(1.1) \quad \bigwedge^{\mathbf{e}} V := \bigwedge^{c_1} V \otimes \cdots \otimes \bigwedge^{c_n} V$$

of such representations, the space of linear functionals on $\bigwedge^{\mathbf{e}} V$ also carries a \mathbf{G} -action. It is a classical problem of invariant theory to describe the subspace $\text{Inv}(\bigwedge^{\mathbf{e}} V) := \text{Hom}_{\mathbf{G}}(\bigwedge^{\mathbf{e}} V, \mathbb{C})$ of invariant multilinear forms. It is typical to consider only tensor products of fundamental representations as in (1.1), since the category of all finite-dimensional representations may be recovered from these through the *Karoubi envelope* construction (see e.g. [Mor07, §3.3.1], [CKM14, §3.1]).

Replacing \mathbf{G} with the corresponding quantum group $U_q(\mathfrak{sl}_r)$, we obtain the space $\text{Inv}_{U_q(\mathfrak{sl}_r)}(\bigwedge_q^{\mathbf{e}} V_q)$ of quantum invariants, deforming $\text{Inv}(\bigwedge^{\mathbf{e}} V)$. Such quantum invariants and the associated representation theory of quantum groups give rise to many of the most powerful invariants of knots, links, and tangles (see, for example, [Jon85, Kau87, Tur94, Kho00, Kho04, MN08]).

For many purposes, one needs to have explicit bases for $\text{Inv}(\bigwedge^{\mathbf{e}} V)$ or its quantum deformation. Likely the first such basis to be discovered was the *standard monomial basis* constructed by Hodge [Hod43] and greatly developed by Seshadri and collaborators (e.g., [Ses78, LS78, LMS79a, LMS79b]). While relatively elementary and computable, the standard monomial basis does not enjoy many of the other properties one desires in a basis. As a result, many further authors have developed a panoply of less tractable bases with various assortments of desirable properties. We have, for example, the *dual canonical basis*, developed independently by Lusztig [Lus90] and Kashiwara [Kas91], as well

as the *dual semicanonical basis* of Lusztig [Lus92, Lus00] and the *geometric Satake basis* (see e.g. [Zhu17]). More recently, the theory of cluster algebras has engendered further bases, such as the *theta basis* of Gross, Hacking, Keel, and Kontsevich [GHKK18], in the cases (see [FP16]) where $\text{Inv}(\bigwedge^{\underline{c}} V)$ is known to carry a cluster structure. For a recent survey of cluster algebra bases and their relations, see [Qin21].

There is a natural cyclic shift isomorphism

$$\sqcup : \text{Inv} \left(\bigwedge^{(c_1, \dots, c_n)} V \right) \xrightarrow{\sim} \text{Inv} \left(\bigwedge^{(c_2, \dots, c_n, c_1)} V \right)$$

induced by the natural isomorphism with $\text{Hom}_{\mathbb{G}}(\bigwedge^{(c_2, \dots, c_n)} V, (\bigwedge^{c_1} V)^*)$. Given a choice of basis as above, one might hope that this isomorphism would preserve the basis, mapping basis elements to scalar multiples of basis elements. In such a case, we say the basis is \sqcup -invariant. Indeed, instances of \sqcup -invariance for the dual canonical, geometric Satake, and theta bases have been used to great effect in [Rho10], [FK14], and [SW20], respectively. Unfortunately, these three bases are notoriously difficult for computation. It is much easier to compute with the standard monomial basis; however, the standard monomial basis is far from \sqcup -invariant even in very simple cases and is not well-suited to analysis of quantum link invariants.

1.3. Web bases. *Web bases* are diagrammatic bases for $\text{Inv}(\bigwedge^{\underline{c}} V)$ or its quantum deformation that seek to surmount these challenges. Each basis element $[W]$ is encoded by a planar bipartite graph W embedded in a disk, so that important algebraic operations are realized as simple graph-theoretic manipulations.

When $\mathbb{G} = \text{SL}_2$, the Temperley–Lieb web basis of non-crossing matchings has long been known (see [TL71, KR84, KL94]). When $\mathbb{G} = \text{SL}_3$, Kuperberg [Kup96b] introduced a remarkable web basis involving a non-elliptic condition on trivalent graphs and gave similar constructions for the other simple Lie groups of rank 2. The non-crossing and non-elliptic conditions are clearly rotation-invariant, so the web bases for $U_q(\mathfrak{sl}_2)$ and $U_q(\mathfrak{sl}_3)$ are \sqcup -invariant. While Kuperberg’s SL_3 web basis was primarily introduced as a tool for efficient computation of quantum link invariants, it has since found application in areas as diverse as the geometric Satake correspondence [FKK13, Thm. 1.4], cluster algebras [FP16], and cyclic sieving [PPR09]. Its transition matrices to the bases discussed in Section 1.2 have also been of great recent interest (see [FK97, KK99, Rho19, RT19, HJO22, IZ22, RT22]).

Since Kuperberg’s introduction of rank 2 web bases, a primary focus has been his statement:

“The main open problem related to the combinatorial rank 2 spiders is how to generalize them to higher rank.” –[Kup96b, p. 146]

Kim [Kim03] conjectured web generators and relations for the case of $U_q(\mathfrak{sl}_4)$ and Morrison [Mor07] extended Kim’s conjecture to $U_q(\mathfrak{sl}_r)$. Cautis–Kamnitzer–Morrison [CKM14] later proved these conjectures (with a different proof subsequently given in [FLL19]). While the diagrammatic relations have thus been determined, generalizing Kuperberg’s web basis in a rotation-invariant way has proved difficult.

Several web bases for simple Lie groups of higher rank have appeared in the literature, though none is rotation-invariant. In [Wes12], for $\mathbb{G} = \text{SL}_r$ with representations restricted to $c_i \in \{1, r-1\}$, Westbury gave a recipe to construct a generator with each possible leading term, thereby obtaining a basis of web diagrams. Unfortunately, this basis is not rotation-invariant.¹ Westbury’s basis was extended to products of arbitrary fundamental representations by Fontaine [Fon12]. Fontaine’s basis also is not rotation-invariant; moreover, in general, it involves making arbitrary choices, so is not well-defined in all cases. Elias [Eli15] independently obtained what appear to be the quantum

¹Some brief remarks in [Wes12, p. 94] suggest that Westbury’s basis is rotation-invariant. This is not correct. The smallest example of non-invariance occurs for $r = 4$ and $\underline{c} = (1, 1)$. We thank Bruce Westbury for very helpful correspondence on this point. See also [FLL19, p. 6121] for related discussion.

group deformations of these bases; again, his bases involve arbitrary choices and are not rotation-invariant. A further obstacle to the use of these non-rotation-invariant bases is that there is no known topological or combinatorial property that enables determining whether a given web is a basis element, let alone an efficient method for expressing invariants in the basis. More recently, in his thesis, Hagemeyer gave another family of web bases for $U_q(\mathfrak{sl}_4)$ [Hag18, Thm. 1.8], which, like our basis, are related to the symmetrized six-vertex model. However, he required arbitrary choices and thus did not obtain a rotation-invariant basis.

Previous work has typically focused on trivalent graph models of representation categories of classical or quantum groups (see e.g. [MOY98, KK99, Kim03, Mor07, CKM14]). Intuitively, the trivalent vertices encode multiplication or comultiplication maps in the exterior algebra of V , and webs are formed by composing such maps (along with evaluation and coevaluation morphisms). See [Sel11] for an overview of the graphical calculus of such *pivotal categories*. Our hourglass plabic graphs build instead on [FLL19] by using an r -valent model. (Such r -valent models also appear in the topology literature [Sik05, LS21]; for the connection of that work with [CKM14], see [Pou22].) This r -valent approach is better suited to rotation invariance. For example, under our approach the determinant map corresponds to r simple edges around a single interior vertex, rather than a full binary tree, as in a trivalent model. See Section 2 for details.

Our main algebraic result, Theorem A, gives the first rotation-invariant web basis for SL_4 , and indeed for $U_q(\mathfrak{sl}_4)$. This is the first construction of a rotation-invariant web basis for any simple Lie group of rank greater than 2 (although some apparent web bases for algebras of block-triangular matrices appear in [PPS22]).

The family of basis webs of Theorem A for $r = 4$ is not preserved under reflection, since the *top* condition (see Definition 6.7) requires that benzene rings are oriented as in the upper-left diagram of Figure 2. Reflection interchanges the upper-left and lower-left benzene rings, so one may dually define a *bottom* condition using the lower-left diagram, together with an attendant *bottom basis*. In this way, while we focus in this paper on the top basis, we actually introduce two families of rotation-invariant bases of $\text{Inv}(\bigwedge_q^{\underline{c}} V_q)$, one for the top condition and one for the bottom condition. At $q = 1$, these families are interchanged under reflection, up to reversing the type \underline{c} . In the standard case when $q = 1$, reflection corresponds to the action of the long permutation w_0 . By contrast, the sets of $r = 2$ and $r = 3$ basis webs are both rotation- and reflection-invariant (see [PP23] for discussion). From the behavior of our basis under the action of w_0 , we suspect that our basis differs from all of the bases discussed in Section 1.2. We further suspect the combinatorial top and bottom conditions can be interpreted geometrically in terms of affine A_3 buildings (cf. [FKK13]).

Our results for $\text{Inv}(\bigwedge^{\underline{c}} V)$ can also be extended (see Theorem 9.4) to give a web basis for spaces $\text{Inv}(\text{Sym}^{\underline{\mu}} V)$ of invariants in tensor products of symmetric powers of V . These spaces connect a range of important objects in algebra and geometry. For example, consider a Grassmannian $\text{Gr}_r(\mathbb{C}^n)$ with respect to its Plücker embedding into projective space. We may recover multi-homogeneous parts of the homogeneous coordinate ring of $\text{Gr}_r(\mathbb{C}^n)$ as $\text{Inv}(\text{Sym}^{\underline{\mu}} V)$ for appropriate choices of $\underline{\mu}$. Moreover, certain multi-homogeneous parts of this coordinate ring yield concrete constructions of Schur and Specht modules, irreducible representations of $SL_n(\mathbb{C})$ and the symmetric group \mathfrak{S}_n , respectively. The homogeneous coordinate ring of $\text{Gr}_r(\mathbb{C}^n)$ also carries an important cluster algebra structure [FZ03], conjecturally related to web bases, as do other rings of invariant polynomials [FP16].

1.4. Outline. Section 2 gives preliminaries on webs and their associated quantum invariants and on plabic graphs. We use a less standard presentation of webs—due essentially to [FLL19] in the $q = 1$ case—in which trivalence is not assumed, so even experts may wish to consult this section.

In Section 3, we develop the theory of hourglass plabic graphs and full reducedness. This is applied in Section 4 to define and study the map \mathcal{T} of Theorem B. The growth rules defining the inverse map \mathcal{G} are developed in Section 5; the growth rules also allow for the leading terms of basis elements to be read off. In Section 6, these results are combined to obtain the bijection of Theorem B and subsequently the web basis $\mathcal{B}_q^{\underline{c}}$ of Theorem A.

In Section 7, we show how arbitrary web invariants may be expressed in the basis \mathcal{B}_q^c . These skein relations are of considerable interest in many applications of webs, particularly in relation to quantum link invariants.

Section 8 contains several combinatorial applications of our work to cyclic sieving, alternating sign matrices, and plane partitions.

Finally, in Section 9, we discuss how the previously-known rotation-invariant web bases fit into our unified framework of fully reduced hourglass plabic graphs with $\text{trip}_\bullet = \text{prom}_\bullet$ and how our results allow for the extension of these bases to the semistandard setting.

An extended abstract describing part of this work appears in the proceedings of FPSAC 2023 [GPPSS23].

2. PRELIMINARIES

Let $[r] := \{1, 2, \dots, r\}$, $\overline{[r]} := \{-1, -2, \dots, -r\}$, and $\pm[r] := \{\pm 1, \pm 2, \dots, \pm r\}$. We define \mathcal{A}_r as the collection of subsets of $\pm[r]$ whose elements are all of the same sign. We often write \bar{i} for $-i$.

2.1. Webs and tensor invariants. The quantum group $U_q(\mathfrak{sl}_r)$ is a $\mathbb{C}(q)$ -algebra that arose from the theory of quantum integrable systems; see [Lus93] for a definition by generators and relations. The quantum group $U_q(\mathfrak{sl}_r)$ deforms the universal enveloping algebra $U(\mathfrak{sl}_r)$, so the classical theory of \mathfrak{sl}_r is recovered at $q = 1$. Explicit diagrammatic generators and relations for the category of finite-dimensional $U_q(\mathfrak{sl}_r)$ -modules were obtained in [CKM14, §2, §3] (see also [Kim03, Mor07]), where the generators are drawn as certain trivalent graphs. For our purposes, it is important to use instead an essentially equivalent formulation in terms of *tagged* r -valent graphs, due essentially to [FLL19].

We are primarily interested in the following $U_q(\mathfrak{sl}_r)$ -modules and their tensor products.

- The standard $U_q(\mathfrak{sl}_r)$ -module V_q (deforming the defining representation of \mathfrak{sl}_r) has standard $\mathbb{C}(q)$ -basis v_1, \dots, v_r .
- The *quantum exterior algebra* $\bigwedge_q^\bullet V_q$ (see [BZ08, CKM14]) is a $U_q(\mathfrak{sl}_r)$ -module (deforming the classical exterior algebra). On the generators v_i , the quantum exterior product satisfies the q -commutation relations

$$v_i \wedge_q v_j = \begin{cases} (-q) v_j \wedge_q v_i & \text{if } i < j, \\ 0 & \text{if } i = j. \end{cases}$$

The quantum exterior power $\bigwedge_q^c V_q$ has $\mathbb{C}(q)$ -basis $\{v_I : I \subseteq [r], |I| = c\}$, where we write $v_I := v_{i_1} \wedge_q \dots \wedge_q v_{i_c}$ for $I = \{i_1 > \dots > i_c\}$.

- The linear dual $(\bigwedge_q^c V_q)^*$ is a $U_q(\mathfrak{sl}_r)$ -module with dual basis $\{v_I^*\}$.

As a shorthand, we write $\bigwedge_q^{-c} V_q := (\bigwedge_q^c V_q)^*$. For $I \subseteq [r]$, we write $\bar{I} \in \mathcal{A}_r$ for the corresponding subset of negative numbers and set $v_{\bar{I}} := v_I^*$.

Definition 2.1. Given a *type* $\underline{c} = (c_1, \dots, c_n)$ where each $c_j \in \pm[r]$, let

$$\bigwedge_q^{\underline{c}} V_q := \bigwedge_q^{c_1} V_q \otimes \dots \otimes \bigwedge_q^{c_n} V_q.$$

In this paper, we limit attention to the $U_q(\mathfrak{sl}_r)$ -modules described in Definition 2.1. As the *Karoubi envelope* of the category of such modules recovers the entire category of finite-dimensional representations, this is not a major restriction.

The natural product map $\bigwedge_q^{c_1} V_q \otimes \bigwedge_q^{c_2} V_q \rightarrow \bigwedge_q^{c_1+c_2} V_q$ given by $u \otimes v \mapsto u \wedge_q v$ is $U_q(\mathfrak{sl}_r)$ -equivariant [CKM14, §3.1]. It may be described explicitly by $v_I \wedge_q v_J \mapsto (-q)^{\ell(I,J)} v_{I \cup J}$ when $I \cap J = \emptyset$ and $\ell(I, J) = |\{(i, j) \in I \times J : i < j\}|$. The more general n -ary product map is associative.

Elements of $\mathcal{H} = \text{Hom}_{U_q(\mathfrak{sl}_r)}(\bigwedge_q^{\underline{c}} V_q, \bigwedge_q^{\underline{d}} V_q)$ may be obtained by composition and tensoring from the natural product map as well as natural $U_q(\mathfrak{sl}_r)$ -module maps arising from coproducts, duals, evaluation, coevaluation, and the identity (plus the *pivotal isomorphism* between a representation and its double dual). Each such morphism has explicit transition coefficients which are all integral

powers of q . Webs as in [Mor07, CKM14] are planar graphs between two horizontal lines which are locally given by the building blocks in Figure 3 and which represent elements of \mathcal{H} ; we will call these *CKM-style webs*. The morphism corresponding to a CKM-style web is unchanged under planar isotopies fixing the boundary lines. The domain and codomain types \underline{c} and \underline{d} may be read off from edges incident to the upper and lower horizontal lines, respectively, by reading edge multiplicities from left to right, where upward oriented edges pick up a negative and correspond to dual exterior powers.

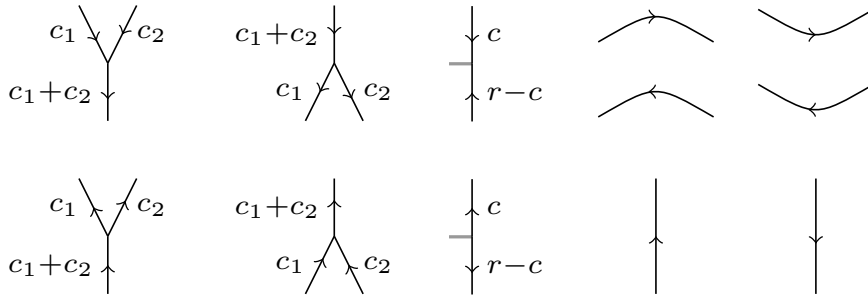


FIGURE 3. Building blocks of CKM-style webs for $U_q(\mathfrak{sl}_r)$ corresponding to products, coproducts, duals, etc. Multiplicities are in $[r]$, and multiplicities on the rightmost diagrams are omitted. Upward arrows indicate duals.

The middle two diagrams in Figure 3 include a short, undirected edge called a *tag*, introduced in [Mor07]. These middle diagrams may be thought of as degenerate cases of the trivalent vertex diagrams where $c_1 + c_2 = r$. When $c = r$, the middle diagrams correspond to the $U_q(\mathfrak{sl}_r)$ -isomorphism $\bigwedge_q^r V_q \cong \mathbb{C}(q)$ and its dual [CKM14, §3.2]. Unlike other edges, tags end as leaves in the middle of the diagram.

As we will see, tags may be moved across an edge of multiplicity c at the cost of multiplying the invariant by $(-1)^{c(r-c)}$. When r is odd, this factor is always 1, and tags may be omitted completely. Tags are hence a comparatively unimportant bookkeeping device and are frequently ignored or de-emphasized. Our web bases for $r = 4$ will come with essentially canonical choices of tags, allowing us to ultimately omit them from our main result.

Remark 2.2. The conventions in [Mor07] and [CKM14] differ in their handling of certain negative signs, and other sources such as [MOY98] differ in their handling of powers of q or other details. We follow the algebraic conventions of [CKM14] throughout. However, for consistency with standard numbering conventions on plabic graphs, we draw CKM-style webs with the domain on top rather than on bottom. That is, our CKM-style webs are obtained by vertically flipping the diagrams from [CKM14].

We now turn to webs as in [FLL19, §6] (where they are referred to as “ r -weblike subgraphs”). While [FLL19] explicitly consider only the case $q = 1$, they note that their diagrammatic construction nonetheless applies over $U_q(\mathfrak{sl}_r)$ using the framework of [CKM14]. For our purposes, it suffices to consider only the (*tensor*) *invariants*

$$[W]_q \in \text{Inv}_{U_q(\mathfrak{sl}_r)} \left(\bigwedge_q^c V_q \right) := \text{Hom}_{U_q(\mathfrak{sl}_r)} \left(\bigwedge_q^c V_q, \mathbb{C}(q) \right),$$

for W a CKM-style web without vertices on the lower horizontal boundary; we draw such webs by closing the upper horizontal boundary to a circle. See Example 2.4.

Definition 2.3. A $U_q(\mathfrak{sl}_r)$ -*web* (or just *web*) is a planar graph W embedded in the disk such that

- W is properly bicolored, with black and white vertices;
- all vertices on the boundary circle have degree 1;

- boundary vertices are labeled b_1, b_2, \dots, b_n in clockwise order;
- all interior vertices have a special “tag” edge, which immediately terminates in the interior and not at a vertex;
- non-tag edges have multiplicities from $[r]$;
- all vertices in the interior of the disk have incident edge multiplicities summing to r .

These webs are defined up to planar isotopy fixing the boundary circle.

Given a $U_q(\mathfrak{sl}_r)$ -web W , the corresponding tensor invariant $[W]_q$ is obtained by converting W to a CKM-style web as in Figure 4. A boundary vertex with edge multiplicity c corresponds to a domain factor $\bigwedge_q^c V_q$ for a black vertex and $\bigwedge_q^{-c} V_q$ for a white vertex. The interior vertices of the $U_q(\mathfrak{sl}_r)$ -web correspond to composites

$$\bigwedge_q^{c_1} V_q \otimes \dots \otimes \bigwedge_q^{c_k} V_q \rightarrow \bigwedge_q^r V_q \rightarrow \mathbb{C}(q).$$

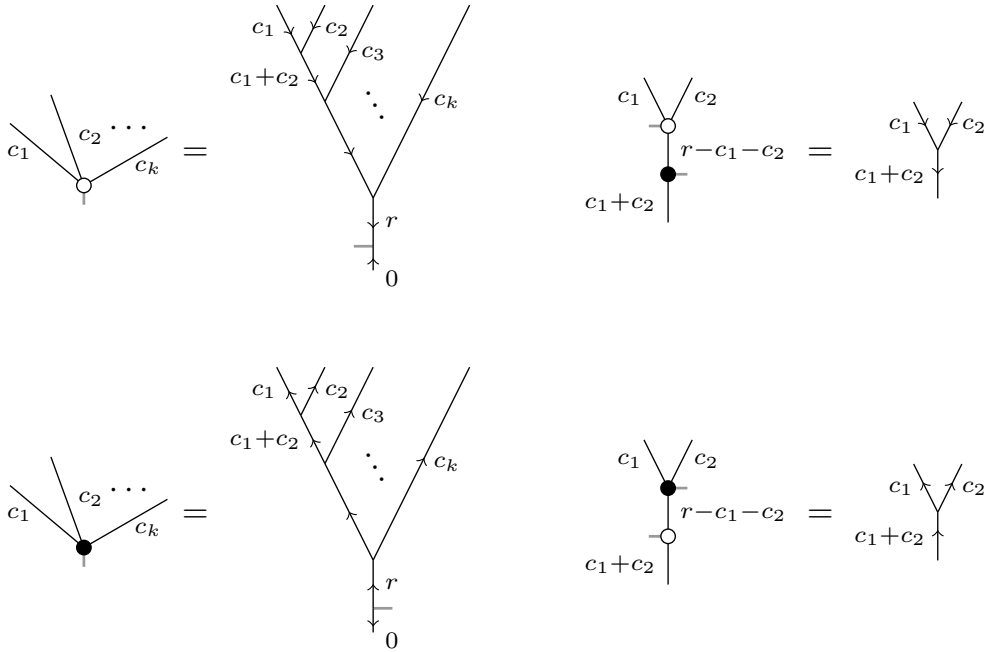
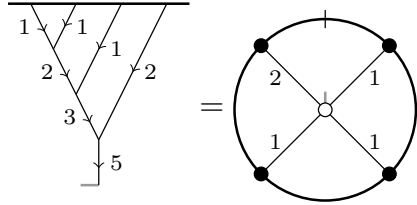


FIGURE 4. Translations between CKM-style webs and $U_q(\mathfrak{sl}_r)$ -webs. Since 0-edges in CKM-style webs correspond to the unit object $\mathbb{C}(q)$, they are typically unwritten.

Example 2.4. Consider the following CKM-style web and the corresponding $U_q(\mathfrak{sl}_r)$ -web.



They represent the same tensor invariant in $\text{Hom}_{U_q(\mathfrak{sl}_5)} \left(V_q \otimes V_q \otimes V_q \otimes \bigwedge_q^2 V_q, \mathbb{C}(q) \right)$, which is similar to a determinant. Boundary vertices in the web on the right are implicitly labeled b_1, b_2, b_3, b_4 like the face of a clock. The “point at infinity” separating vertex b_1 from vertex b_4 is marked on the boundary.

As noted above, the positions of tags around an internal vertex only affect the sign of the corresponding tensor invariant. More precisely, we have the following.

Lemma 2.5. *The relations in Figure 5 hold, as do the those obtained by reversing all arrows or switching all vertex colors.*

Proof. The first relation is [CKM14, (2.3)]. The second is a consequence of [CKM14, (2.3), (2.6), and (2.7)]. \square

FIGURE 5. Tag sign relations for CKM-style webs and $U_q(\mathfrak{sl}_r)$ -webs.

2.2. Polynomial invariants and proper labelings. A $U_q(\mathfrak{sl}_r)$ -web W of type \underline{c} may be considered as a $\mathbb{C}(q)$ -multilinear map

$$\bigwedge_q^{c_1} V_q \times \cdots \times \bigwedge_q^{c_n} V_q \rightarrow \mathbb{C}(q).$$

Write elements in $\bigwedge_q^c V_q$ as $\sum_{|S|=|c|} x_S v_S$ for scalars x_S with $S \in \mathcal{A}_r$. Thus we may interpret the invariant $[W]_q$ as a polynomial

$$[W]_q \in \mathbb{C}(q)[x_{S,i}]$$

where for each i , S ranges over cardinality $|c_i|$ elements of \mathcal{A}_r of the same sign as c_i . The polynomial ring is naturally $\mathbb{Z}_{\geq 0}^n$ -graded where $\deg(x_{S,i}) = \mathbf{e}_i$, and the invariants $[W]_q$ lie in the multilinear component $(1, \dots, 1)$.

Example 2.6. The web in Example 2.4 corresponds to the polynomial

$$\sum_{a,b,c,\{d,e\}} (-q)^{\ell(a,b,c,\{d,e\})} x_{a,1} x_{b,2} x_{c,3} x_{\{d,e\},4}$$

where the sum is over all partitions $\{a\} \sqcup \{b\} \sqcup \{c\} \sqcup \{d,e\} = \{1, \dots, 5\}$ and the exponent ℓ is the number of non-inversions of the permutation (a, b, c, d, e) if we choose $d > e$.

It is difficult to find a precise statement in the literature of a monomial expansion of general $U_q(\mathfrak{sl}_r)$ -web invariants; see [MOY98], [FP16, (4.1)], [FLL19, (5.5)] for certain cases. We next give such a formula which is sufficient for our purposes.

Definition 2.7. A *labeling* ϕ of a $U_q(\mathfrak{sl}_r)$ -web W is an assignment of subsets of $[r]$ to each edge of W , where an edge of multiplicity m is assigned a subset of size m . A labeling is *proper* if the edges incident to each internal vertex partition the set $[r]$.

The *boundary word* $\partial(\phi)$ of a labeling ϕ is the word $w = w_1 \cdots w_n$ in the alphabet \mathcal{A}_r given by reading the labels of the edges adjacent to b_1, b_2, \dots, b_n , where the sign is positive if b_i is black and negative if b_i is white.

Definition 2.8. Given subsets S_1, \dots, S_m of $[r]$, their *coinversion number* is

$$\ell(S_1, \dots, S_m) = |\{(a, b) : a \in S_i, b \in S_j, a \leq b, \text{ and } i < j\}|.$$

Given a $U_q(\mathfrak{sl}_r)$ -web W with a labeling ϕ , the coinversion number of an internal vertex v is $\ell(S_1, \dots, S_n)$ where S_1, \dots, S_n are the labels from ϕ around v read in clockwise order starting from the tag on v . The coinversion number $\ell_W(\phi)$ is the sum of the coinversion numbers of all internal vertices.

Finally, suppose w is a boundary word. Create a word \hat{w} over $[r]$ by replacing each $\overline{S} \subseteq \overline{[r]}$ with $[r] \setminus S$ and then writing the elements of the subsets in w in increasing order. The *coinversion number* $\ell_W(w)$ of w is $\ell_W(\hat{w})$, plus the sum of $\ell(S, [r] \setminus S)$ over all such replaced S .

Theorem 2.9. *Let W be a $U_q(\mathfrak{sl}_r)$ -web. There are statistics $\mathbf{wgt}_W(\phi) \in \mathbb{Z}$ on proper labelings ϕ of W and $\mathbf{sgn}_W(w) \in \{\pm 1\}$ on boundary words w such that*

$$(2.1) \quad \begin{aligned} [W]_q &= \sum_{\phi} (-1)^{\ell_W(\phi)} q^{\mathbf{wgt}_W(\phi)} x_{\partial(\phi)} \\ &= \sum_w \left(\sum_{\phi: \partial(\phi)=w} q^{\mathbf{wgt}_W(\phi)} \right) \mathbf{sgn}_W(w) x_w, \end{aligned}$$

where ϕ ranges over the proper labelings of W , w ranges over the boundary words of proper labelings, and $x_w := x_{w_1,1} \cdots x_{w_n,n}$. Furthermore:

- If ϕ and ϕ' are proper labelings of W with boundary words w and w' , respectively, then

$$(2.2) \quad (-1)^{\ell_W(\phi) - \ell_W(\phi')} = (-1)^{\ell_W(w) - \ell_W(w')}.$$

In particular, $\mathbf{sgn}_W(w) = (-1)^{\ell_W(\phi)}$ for any proper labeling ϕ of W with boundary word w .

- The statistic $\mathbf{wgt}_W(\phi)$ does not depend on the tags of W .

Proof. For the first equality in (2.1), consider the transition coefficients in the v_I and v_I^* bases of morphisms coming from composites of products, duals, evaluations, coevaluations, and pivotal isomorphisms (see p. 7). An edge labeled S corresponds to v_S , and the proper labeling condition precisely ensures the relevant product map around an internal vertex is non-zero. The boundary labeling corresponds to the input variables and hence to the monomial $x_{\partial(\phi)}$. The transition coefficients of these morphisms are of the form $(\pm q)^i$. The negative signs arise only from the product maps around internal vertices, and the overall sign is $(-1)^{\ell_W(\phi)}$. Powers of q without accompanying negative signs arise only when the pivotal isomorphism is used. The first equality in (2.1) now follows.

The second equality in (2.1) asserts that $\ell_W(\phi)$ depends only on $\partial(\phi)$. This is a consequence of (2.2), which is equivalent to [FLL19, Lem. 5.4], in the case that W has type $(1, \dots, 1)$. The general type case follows from this one by ‘‘attaching claws’’ and tracking signs.

Finally, let W' be obtained from W by moving a tag past an edge of multiplicity k . By Lemma 2.5,

$$[W']_q = (-1)^{k(r-k)} [W]_q.$$

If $S_1 \sqcup \cdots \sqcup S_n = [r]$ and $|S_n| = k$, then

$$(-1)^{\ell(S_n, S_1, \dots, S_{n-1})} = (-1)^{k(r-k)} (-1)^{\ell(S_1, \dots, S_n)}.$$

Hence

$$(-1)^{\ell_W(\phi)} = (-1)^{k(r-k)} (-1)^{\ell_{W'}(\phi)}.$$

Applying (2.1) to $[W]_q$ and $[W']_q$ now yields $\mathbf{wgt}_W(\phi) = \mathbf{wgt}_{W'}(\phi)$. \square

Finally, we introduce a term order on $\mathbb{C}(q)[x_{i,S}]$ with respect to which our $U_q(\mathfrak{sl}_4)$ -web bases will be unitriangular.

Definition 2.10. Suppose $w = w_1 \cdots w_n$ is a sequence of elements of $\pm[r]$. Let \tilde{i} be a new symbol representing either i or $r - i + 1$. Let $\tilde{w} = \tilde{w}_1 \cdots \tilde{w}_n$. Define an order $w >_{\text{lex}} w'$ if and only if \tilde{w} is lexicographically greater than \tilde{w}' , where $\tilde{1} < \tilde{2} < \cdots < \tilde{r}$. Extend $\tilde{\bullet}$ and $>_{\text{lex}}$ to sequences $w = w_1 \cdots w_n$ of elements of \mathcal{A}_r , writing subsets in increasing \mathbb{Z} -order. The *total degree* $\deg(w)$ is n , which is also the total degree of x_w .

The *grevlex order* on $\mathbb{C}(q)[x_{i,S}]$ is given by

$$x_w <_{\text{grevlex}} x_{w'} \quad \Leftrightarrow \quad \deg(w) < \deg(w') \text{ or } (\deg(w) = \deg(w') \text{ and } \tilde{w} >_{\text{l}\tilde{\text{e}}\tilde{\text{x}}} \tilde{w}').$$

The tensor invariant associated to a web has grevlex-leading monomial given by proper labelings with the $\text{l}\tilde{\text{e}}\tilde{\text{x}}$ -minimal boundary word. In Section 5, we will show that there is a unique proper labeling with $\text{l}\tilde{\text{e}}\tilde{\text{x}}$ -minimal boundary word associated to each of our $U_q(\mathfrak{sl}_4)$ -basis webs.

2.3. Plabic graphs. A major theme in this work is the view of webs as versions of *plabic graphs*.

Definition 2.11 (Postnikov [Pos06]). A *plabic graph* is a planar undirected graph, embedded in a disk, whose boundary vertices have degree 1 and are labeled b_1, b_2, \dots in clockwise order and whose interior vertices are each colored black or white.

Plabic graphs were introduced by Postnikov [Pos06] in his study of the totally positive Grassmannian, and have since proven to be fundamental objects in the theories of cluster algebras [Sco06] and KP solitons [KW14] and in the physics of scattering amplitudes [ABC⁺16]. See [Pos18] for a recent survey.

Definition 2.12. For each boundary vertex b_i of a plabic graph G , one may obtain another boundary vertex $b_{\pi(i)}$ by beginning a walk on the unique edge incident to b_i and turning left at each white vertex and right at each black vertex, until the boundary is reached. We call the sequence of vertices and edges in such a walk a *trip strand*. The function π is a permutation, called the *trip permutation* of G and denoted $\text{trip}(G)$. The turning rules are called *the rules of the road*.

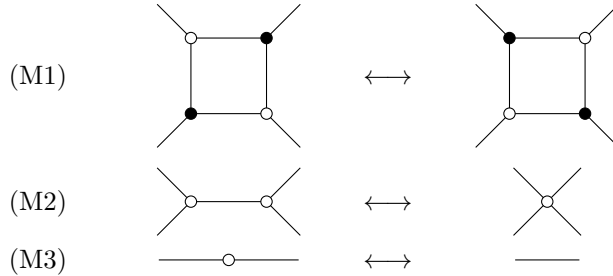


FIGURE 6. The moves for plabic graphs.

Definition 2.13. Two plabic graphs G and G' are *move-equivalent*, denoted $G \sim G'$ if they can be connected by a sequence of the *moves* shown in Figure 6.

It is easily checked that the moves (M1), (M2), (M3) from Figure 6 preserve trip permutations, so if $G \sim G'$, then $\text{trip}(G) = \text{trip}(G')$.

In addition to moves on plabic graphs, the *reduction* (R1), shown in Figure 7, will be important. Unlike moves, reductions do not preserve the trip permutation.

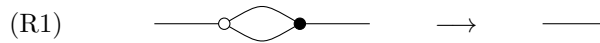


FIGURE 7. The reduction for plabic graphs.

A plabic graph is called *leafless* if it contains no leaves (i.e., vertices of degree 1), other than perhaps leaves incident to the boundary. An *isolated component* is a connected component that is not connected to the boundary.

Definition 2.14. A leafless plabic graph G with no isolated components is called *reduced* if no $G' \sim G$ admits a parallel edge reduction (R1).

Two trip strands $\ell \neq \ell'$ in a plabic graph G are said to have a *bad double crossing* if they traverse some edge e in opposite directions and subsequently (in the forward direction on both strands) traverse another edge e' in opposite directions. A trip strand has an *essential self-intersection* if it traverses some edge in both directions. Finally, G is said to have a *round trip* if following the rules of the road (Definition 2.12) starting from some edge not incident to the boundary produces an infinite walk.

Theorem 2.15 (Postnikov [Pos06]). *A leafless plabic graph G with no isolated components is reduced if and only if all of the following conditions hold:*

- (1) G has no round trips,
- (2) G has no trip strands with essential self-intersections,
- (3) G has no pair of trip strands with a bad double crossing, and
- (4) if $\text{trip}(G)(i) = i$, then G has a leaf attached to the boundary vertex b_i .

The *decorated trip permutation* $\text{trip}'(G)$ of a reduced plabic graph records the extra data of the color of the leaf attached to b_i for all fixed points $\text{trip}(G)(i) = i$.

Theorem 2.16 (Postnikov [Pos06]). *Two reduced plabic graphs G and G' are move-equivalent if and only if $\text{trip}'(G) = \text{trip}'(G')$.*

3. HOURGLASS PLABIC GRAPHS AND SYMMETRIZED SIX-VERTEX CONFIGURATIONS

We now specialize $U_q(\mathfrak{sl}_r)$ to the case $r = 4$ for Sections 3 to 8; see Section 9 for a discussion of how our methods can be adapted to unify the known web bases in other cases.

3.1. Hourglass plabic graphs. An *hourglass graph* G is an underlying planar embedded graph \widehat{G} , together with a positive integer multiplicity $m(e)$ for each edge e . The hourglass graph G is drawn in the plane by replacing each edge e of \widehat{G} with $m(e) > 1$ with $m(e)$ strands, twisted so that the clockwise orders of these strands around the two incident vertices are the same. For $m(e) \geq 2$, we call this twisted edge an $m(e)$ -*hourglass*, and call an edge with $m(e) = 1$ a *simple edge*.

The *degree* $\deg(v)$ of a vertex $v \in G$ is the number of edges incident to v , counted with multiplicity, while its *simple degree* $\widehat{\deg}(v)$ is its degree in the underlying graph \widehat{G} .

Definition 3.1. An *hourglass plabic graph* is a bipartite hourglass graph G , with a fixed proper black-white vertex coloring, embedded in a disk, with all internal vertices of degree 4, and all boundary vertices of simple degree one, labeled clockwise as b_1, b_2, \dots, b_n . See Figure 8 and Figure 23 (lower right) for examples. We consider G up to planar isotopy fixing the boundary circle. We write $\text{col}(v) = 1$ for a black vertex v and $\text{col}(v) = -1$ for a white vertex.

Remark 3.2. In later sections, we will view hourglass plabic graphs as $U_q(\mathfrak{sl}_4)$ -webs, with hourglass multiplicities becoming the web edge multiplicities. However in this section we focus on developing the underlying combinatorics.

Definition 3.3. The *type* \underline{c} of an hourglass plabic graph G is the sequence (c_1, \dots, c_n) where $c_i = \text{col}(b_i) \deg(b_i)$ for $i = 1, \dots, n$. We say the type is *oscillating*² if $|c_i| = 1$ for all i . A type denoted \underline{c} is assumed throughout to be oscillating. For general G , write $\text{osc}(G)$ for the associated hourglass plabic graph of oscillating type obtained from G by replacing each boundary vertex b of degree $d > 1$ (connected by a d -hourglass to an internal vertex v) with d boundary vertices of the same color, each connected to v by a simple edge. (If b is connected instead to another boundary vertex, first subdivide its hourglass by two new vertices using the move of Figure 9.)

²So named because graphs of this type will be seen to correspond to (*generalized*) *oscillating tableaux*.

Note that, for any hourglass plabic graph G , the underlying graph \widehat{G} is a bipartite plabic graph (Definition 2.11) using the vertex colors from G . Unlike plabic graphs, for which a single trip permutation is traditionally considered, we will associate a 3-tuple of trip permutations to each hourglass plabic graph.

Definition 3.4. Let G be an hourglass plabic graph of oscillating type with boundary vertices b_1, \dots, b_n . For $1 \leq a \leq 3$, the a -th trip permutation $\text{trip}_a(G)$ is the permutation of $[n]$ obtained as follows: for each i , begin at b_i and walk along the edges of G , taking the a -th leftmost turn at each white vertex, and a -th rightmost turn at each black vertex, until arriving at a boundary vertex b_j . Then $\text{trip}_a(G)(i) = j$. The walk taken is called the trip_a -strand. See Figure 8 for an example. Note that $\text{trip}_1(G)^{-1} = \text{trip}_3(G)$ and $\text{trip}_2(G)$ is an involution. We write $\text{trip}_\bullet(G)$ for the tuple of these trip permutations. For general G , we define $\text{trip}_\bullet(G) = \text{trip}_\bullet(\text{osc}(G))$.

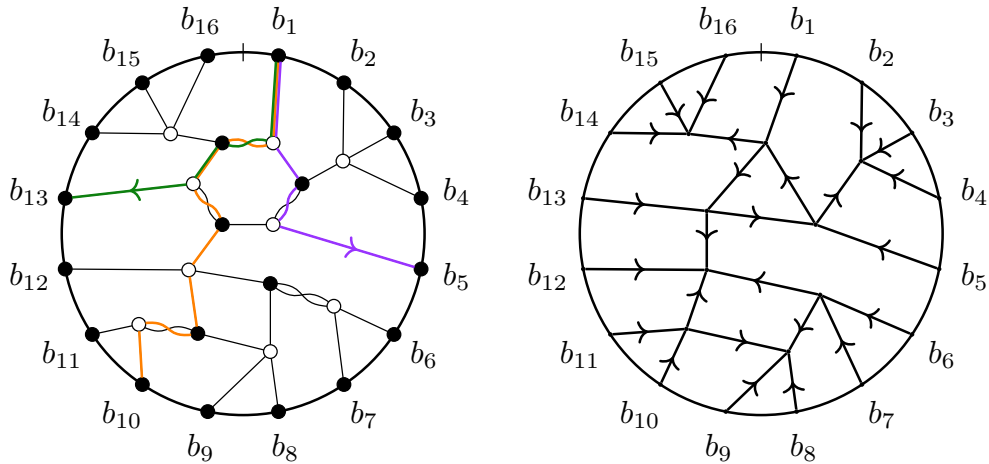


FIGURE 8. Left, an hourglass plabic graph G , with purple (■) trip_1 , orange (■) trip_2 , and green (■) trip_3 strands drawn, showing that $\text{trip}_i(G)(1) = 5, 10,$ and 13 for $i = 1, 2,$ and 3 , respectively. Right, the corresponding six-vertex configuration, as constructed in Definition 3.22.

Proposition 3.5. Suppose G is an hourglass plabic graph of oscillating type. Then the trip_1 -strands of G agree with the trip-strands of \widehat{G} , so in particular $\text{trip}_1(G) = \text{trip}(\widehat{G})$.

Proof. Observe that the sequence of vertices visited by a trip_1 -strand is not affected by the multiplicities of the edges it follows. \square

As for plabic graphs, hourglass plabic graphs admit certain *moves*. These are the *benzene move* and *square moves* shown in Figure 2 and the *contraction moves* shown in Figure 9. None of the vertices appearing in the moves is allowed to be a boundary vertex; hence, moves do not change the type of the hourglass plabic graph.

Definition 3.6. Two hourglass plabic graphs G and G' are *move-equivalent*, written $G \sim G'$, if some sequence of benzene, square, and contraction moves transforms G into G' . An hourglass plabic graph is *contracted* if contraction moves have been applied to convert all subgraphs from the left side of Figure 9 to the corresponding graph from the right side. We write $\text{CG}(\underline{c})$ for the set of contracted hourglass plabic graphs of type \underline{c} . Note that a contracted hourglass plabic graph of oscillating type only contains simple and 2-hourglass edges.

For example, the move equivalence class of the contracted hourglass plabic graph G from Figure 8 contains three other graphs, constructed by applying the benzene move, the square move, or both.

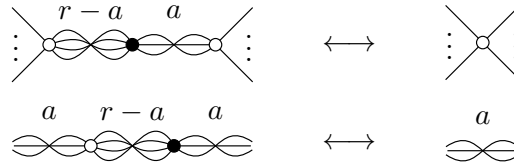


FIGURE 9. The contraction moves for hourglass plabic graphs. The parameter a runs over $0, \dots, r$; we have $r = 4$ except in Section 9. The color reversals of these moves are also allowed.

Proposition 3.7. *Let $G \sim G'$ be move-equivalent hourglass plabic graphs. Then:*

- (a) $\text{trip}_\bullet(G) = \text{trip}_\bullet(G')$, and
- (b) the underlying plabic graphs \widehat{G} and \widehat{G}' are move-equivalent.

Proof. Part (a) is easily checked by observing that the benzene, square, and contraction moves all locally preserve trip_\bullet . For part (b), notice that each of the moves for hourglass plabic graphs is a composite of the plabic graph moves from Figure 6. For example, after passing to \widehat{G} , the hourglass square moves correspond to expanding the corners of the square with (M2) if necessary, applying the plabic square move (M1), and then contracting the remaining corners with another application of (M2). \square

Remark 3.8. As noted in the proof of Proposition 3.7, the hourglass square moves and contraction moves are lifts to G of (composites of) usual plabic moves on \widehat{G} . The benzene move, on the other hand, is trivial on the level of \widehat{G} .

Compositions of benzene moves on an hourglass plabic graph can be seen as a transformation on a *dimer cover* (perfect matching) of the subgraph of vertices of simple degree 3, where the hourglass edges correspond to the included edges of the dimer cover. For hexagonal lattices, this transformation is well-known to correspond to adding and removing boxes from an associated *plane partition* (see e.g. [KO05]). This is discussed further in Section 8.3.

3.2. Fully reduced hourglass plabic graphs. The following definition is central to this work, and should be compared to the notion of reduced plabic graph (Definition 2.14).

Definition 3.9. An hourglass plabic graph G with no isolated components is called *fully reduced* if no $G' \sim G$ has a 4-cycle containing an hourglass (a *forbidden 4-cycle*). We write $\text{RG}(\underline{c})$ for the set of fully reduced hourglass plabic graphs of type \underline{c} . We write $\text{CRG}(\underline{c})$ for the set of these which are contracted (as in Definition 3.6).

Remark 3.10. Theorem 3.25 and Corollary 3.33 provide alternative characterizations of fully reduced graphs which avoid the (*a priori* infinite) move-equivalence class exploration in Definition 3.9.

Remark 3.11. Definition 3.9 implies, in particular, that a fully reduced hourglass plabic graph G does not have two or more distinct edges connecting a pair of vertices u, v ; otherwise one of the edges could be expanded using a contraction move, creating a forbidden 4-cycle.

The following proposition partially justifies the use of “reduced” in “fully reduced”. Note that the converse is not true: G being fully reduced is a stronger condition than \widehat{G} being reduced.

Proposition 3.12. *Let G be a fully reduced hourglass plabic graph. Then the underlying plabic graph \widehat{G} is reduced.*

Proposition 3.12 is key to the proof of Theorem 3.13, which is an analogue of Theorem 2.16 for hourglass plabic graphs, and is a fundamental ingredient in the construction of our web basis.

Theorem 3.13. *Two fully reduced hourglass plabic graphs G_1 and G_2 of the same type are move-equivalent if and only if $\text{trip}_\bullet(G_1) = \text{trip}_\bullet(G_2)$.*

We now transform contracted fully reduced hourglass plabic graphs to another form which will be useful in the proofs of Proposition 3.12 and Theorem 3.13. These proofs appear in Section 3.6.

3.3. Symmetrized six-vertex configurations. In this subsection, we define certain six-vertex configurations on 4-valent graphs embedded in a disk and show these configurations are in bijection with contracted hourglass plabic graphs. The *well oriented* configurations (Definition 3.19) correspond under this bijection to the fully reduced hourglass plabic graphs (Theorem 3.25). In the later sections, we convert freely between these objects, as convenient.

Definition 3.14. Let G be a planar graph embedded in a disk, with all internal vertices of degree 4 and all boundary vertices of degree 1 labeled clockwise as b_1, \dots, b_n . A *symmetrized six-vertex configuration* D on G is a directed graph with underlying undirected graph G such that the orientation of edges around each vertex is any rotation of:



These are *sources*, *sinks*, and *transmitting vertices*, respectively; note that there are six possibilities for the orientation around a single vertex. We write $\text{SSV}(G)$ for the set of symmetrized six-vertex configurations on G .

Remark 3.15. Symmetrized six-vertex configurations can be seen as a symmetrized version of the well-studied *six-vertex model* (see e.g. [Bax89]), a model equivalent to ours by reversing the direction of all vertical edges in the allowed vertex configurations. On a square grid, six-vertex configurations with domain wall boundary conditions (in our convention, corresponding to all boundary edges oriented inward) are well-known to correspond to *alternating sign matrices*, matrices whose entries are in $\{0, \pm 1\}$, whose rows and columns sum to 1, and whose nonzero entries alternate in sign along each row and column (see e.g. [Kup96a, Pro01]). On our graphs, sinks correspond to 1, sources to -1 , and transmitting vertices to 0. See Section 8.2 for further discussion.

Like (hourglass) plabic graphs, symmetrized six-vertex configurations have a notion of trip permutation.

Definition 3.16. Let $D \in \text{SSV}(G)$. Define $\text{trip}_2(D)$ as the permutation of $[n]$ obtained as follows: for each i , begin at b_i and walk along the edges of G , going straight across each vertex to the opposite edge, until arriving at a boundary vertex b_j . Then $\text{trip}_2(D)(i) = j$ and each walk constructed by this rule is called a trip_2 -strand.

We define $\text{trip}_1(D)$ as the permutation of $[n]$ obtained as follows: for each i , begin at b_i and walk along the edges of D , turning as indicated in Figure 10 until arriving at a boundary vertex b_j . Then $\text{trip}_1(D)(i) = j$ and each such walk is called a trip_1 -strand. Define $\text{trip}_3(D)$ via reversal of the trip_1 -strands. Note that $\text{trip}_1(D)^{-1} = \text{trip}_3(D)$ and $\text{trip}_2(D)$ is an involution.

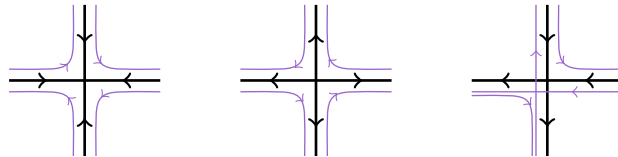


FIGURE 10. The behavior of trip_1 -strands in the symmetrized six-vertex model.

As with (hourglass) plabic graphs, we consider an equivalence relation on symmetrized six-vertex configurations generated by *moves*. These are the *Yang-Baxter* and *ASM* moves shown in Figure 11.

Remark 3.17. The moves of Figure 11 are so named because of their correlation to studied moves on six-vertex configurations and alternating sign matrices. The Yang–Baxter move corresponds to the *star-triangle relation* associated to the *Yang–Baxter equation* [Bax89], while the ASM move may be seen as a *fiber toggle* in the alternating sign matrix tetrahedral poset [Str15] or as travelling along an edge of the *alternating sign matrix polytope* [Str09]. Appropriate compositions of these toggles produce the well-studied *gyration* action of [Wie00] on *fully-packed loops*, objects in bijection with alternating sign matrices. Fully-packed loops on generalized domains (such as ours) were considered by Cantini and Sportiello in their proof of the *Razumov–Stroganov conjecture* [CS14] and relate to *chained alternating sign matrices* [HMN⁺17].

Definition 3.18. Two symmetrized six-vertex configurations D and D' are *move-equivalent*, written $D \sim D'$, if some sequence of Yang–Baxter and ASM moves transforms D into D' .

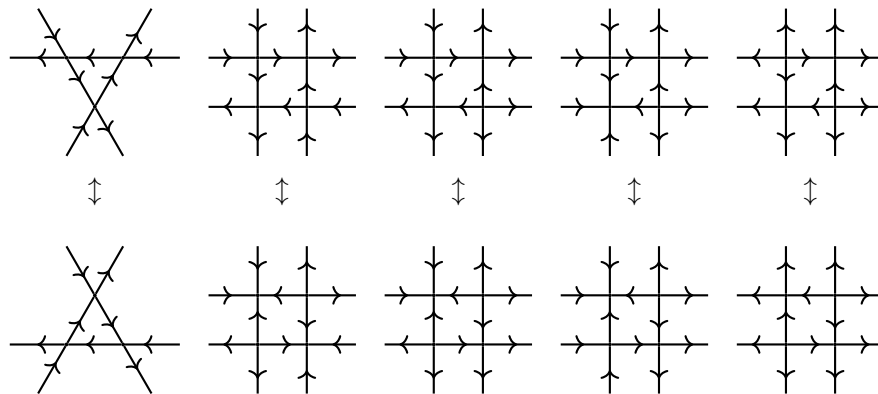


FIGURE 11. The Yang–Baxter move (leftmost) and the ASM moves for symmetrized six-vertex configurations. The edge reversals of these ASM moves are also allowed.

Definition 3.19. A symmetrized six-vertex configuration D with no isolated components is *well oriented* if for every D' with $D \sim D'$, the underlying undirected graph of D' is simple (no loops and no 2-cycles) and every 3-cycle of D' is (cyclically) oriented. We write $\text{WSSV}(G)$ for the set of well oriented configurations D from $\text{SSV}(G)$.

Consider the following properties that $D \in \text{SSV}(G)$ may have:

- (P1) The trip_2 -strands of D do not double-cross or self-intersect.
- (P2) The segments between the three intersection points of three pairwise crossing trip_2 -strands are oriented (*big triangles* are oriented).
- (P3) Among any four trip_2 -strands, there is a pair of strands which do not cross.

Theorem 3.25 shows that well oriented symmetrized six-vertex configurations are in bijection with contracted fully reduced hourglass plabic graphs. The conditions of Definition 3.19 parallel those for full-reducedness. However, Proposition 3.21 gives an effective way to determine whether a symmetrized six-vertex configuration is well oriented by checking (P1) and (P2).

Lemma 3.20. *If $D \in \text{SSV}(G)$ satisfies (P1) and (P2), then it satisfies (P3).*

Proof. If four trip_2 -strands in D are pairwise crossing, then by (P1) these strands form $\binom{4}{3}$ big triangles, but there is no way to consistently direct the edges of these triangles satisfying (P2). \square

Proposition 3.21. *A configuration $D \in \text{SSV}(G)$ is well oriented if and only if (P1) and (P2) hold.*

Proof. Suppose $D \in \text{SSV}(G)$ satisfies (P1) and (P2) and $D' \sim D$. Yang–Baxter and ASM moves do not change the multiplicity of intersection of any pair of trip_2 -strands. Since trip_2 -strands in D do not double-cross or self-intersect, the same is true for D' , and in particular D' has no loops or 2-cycles. We now argue that D' has oriented 3-cycles. We may assume without loss of generality that D' differs from D by a single move. An ASM move applied to a face F of D cannot create an unoriented 3-cycle, for such a cycle would need to contain an edge bordering F , in which case D would contain an unoriented big triangle ($\triangle \ell_1 \ell_2 \ell_4$ on the left side of Figure 12), violating (P2). A Yang–Baxter move applied to D cannot create an unoriented 3-cycle either, for the new 3-cycles in D' (see the right side of Figure 12) are forced to be oriented by property (P2) of D . Thus D' has oriented 3-cycles and D is well oriented.

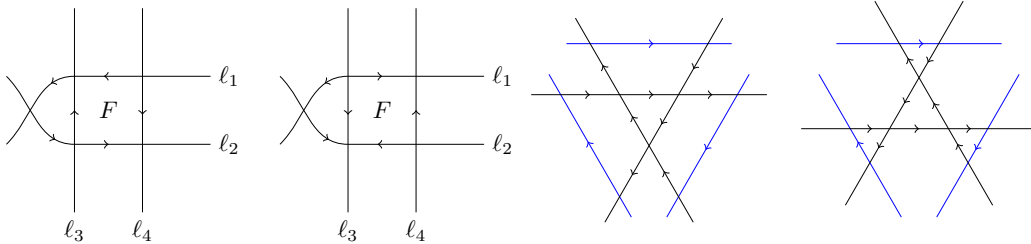


FIGURE 12. Left: a 3-cycle adjacent to the face F in D and in D' from the proof of Proposition 3.21. Right: the 3-cycles potentially created by a Yang–Baxter move applied to D .

Now suppose that D is well oriented; we show that (P1) and (P2) must hold. We begin by proving (P2) in the case that D satisfies (P1). Under this assumption, if ℓ_1, ℓ_2, ℓ_3 are three pairwise crossing trip_2 -strands, let $T = \triangle \ell_1 \ell_2 \ell_3$ denote the big triangle they form. We prove that the boundary of T is oriented by induction on the number of vertices inside T , inclusive of the boundary. As a base case, if T is a 3-cycle, it must be oriented, since D is well oriented. Otherwise, some strand must cross through T . Let v be any vertex on the boundary of T , but not a corner of T . The strand passing into T at v forms a smaller big triangle T' with the boundary of T . By induction T' is oriented, so v is a transmitting vertex. Thus the edge directions along any side of T all agree (otherwise some v along the side would be a source or sink). Since T' is oriented, the orientations of the sides it crosses, say ℓ_1 and ℓ_2 , must agree. If T is not oriented, it then follows that the remaining side ℓ_3 has a single edge in T . In this case, all strands crossing through T must cross ℓ_1 and ℓ_2 and not cross each other, forming a nested set of triangles sharing vertex $\ell_1 \cap \ell_2$ and sharing a common orientation. By a sequence of Yang–Baxter moves at $\ell_1 \cap \ell_2$, we may remove these strands from T . Since D is well oriented, the resulting D' has oriented 3-cycles; in particular, ℓ_3 is oriented compatibly with ℓ_1 and ℓ_2 . Thus T is oriented.

Finally, we prove (P1). Suppose D has a double-crossing or self-intersection in its trip_2 -strands and let R denote the region of the graph this bounds. Suppose also that R contains the minimal number of vertices among all such regions in all move-equivalent configurations. In particular, there are no double-crossings or self-intersections inside R . If R were bounded by a self-intersection, any other trip_2 -strand crossing into R would create a smaller double-crossing, so we may assume that R is bounded by a double-crossing between trip_2 -strands ℓ_1 and ℓ_2 . Therefore, viewing the interior of R as a well oriented symmetrized six-vertex configuration D'' with ℓ_1 and ℓ_2 forming the boundary circle, (P1) is satisfied. By the above argument, so is (P2), and by Lemma 3.20, D'' satisfies (P3). Since D is well oriented, there must be a pair of strands intersecting inside R . Choose such a pair a and b so that the number of vertices in $\triangle ab \ell_1$ is minimized (see Figure 13). All strands cutting through this triangle must cross both a and b , and they may not cross each other by (P3). Thus a sequence of Yang–Baxter moves may be applied at $a \cap b$ to remove these strands from the triangle.

Finally, a Yang–Baxter move may be applied to $\triangle ab\ell_1$ to obtain a smaller region bounded by a double-crossing, contradicting the minimality of R . This completes the proof of (P1). \square

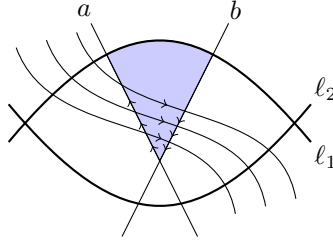


FIGURE 13. The diagram described in the final paragraph of the proof of Proposition 3.21.

The numbers $\underline{o} = (o_1, \dots, o_n)$ where $o_i = 1$ (resp. $o_i = -1$) if the edge incident to b_i is directed inwards (resp. outwards) form the *boundary conditions* of a symmetrized six-vertex configuration. We write $\text{SSV}(\underline{o})$ (and $\text{WSSV}(\underline{o})$) for the (well oriented) symmetrized six-vertex configurations with boundary conditions \underline{o} .

We now define the correspondence φ between contracted hourglass plabic graphs and symmetrized six-vertex configurations.

Definition 3.22. Given $G \in \text{CG}(\underline{o})$, $\varphi(G)$ is the symmetrized six-vertex configuration formed from G by orienting all simple edges from black vertex to white, removing the vertex coloring, and contracting each 2-hourglass and incident vertices to a single 4-valent vertex. Figure 8 shows an example of an hourglass plabic graph and its image under φ .

Proposition 3.23. For $G \in \text{CG}(\underline{o})$, we have $\varphi(G) \in \text{SSV}(\underline{o})$.

Proof. Let $D = \varphi(G)$. When a 2-hourglass in G is collapsed to a vertex in D , the resulting vertex is still 4-valent. Every white vertex in G incident to no hourglass becomes a sink in D . Every black vertex in G incident to no hourglass becomes a source in D . Each contracted hourglass results in a transmitting vertex. The map φ converts boundary colors to edge orientations, so $\varphi(G)$ has boundary conditions \underline{o} . \square

The following notion will be used in Section 5.6.

Definition 3.24. For $D \in \text{SSV}(\underline{o})$, a *proper labeling* is a labeling of the edges by elements of $\{1, 2, 3, 4\}$ such that the labels adjacent to each source or sink are distinct and each transmitting vertex has its two incoming edges labeled $a \neq b$, and its two outgoing edges labeled a and b .

Theorem 3.25. The map $\varphi : \text{CG}(\underline{o}) \rightarrow \text{SSV}(\underline{o})$ is a bijection intertwining benzene moves with Yang–Baxter moves, intertwining square moves with ASM moves, and preserving trip permutations and proper labelings. Moreover, G is fully reduced if and only if $\varphi(G)$ is well oriented.

Proof. The map φ has an inverse which colors sinks white, sources black, and expands each transmitting vertex to an hourglass from a black to a white vertex in the direction of transmission. The output of φ^{-1} is contracted, since this procedure does not produce 3- or 4-hourglasses or adjacent pairs of 2-hourglasses.

The Yang–Baxter move of Figure 11, is the image under φ of the benzene move of Figure 2. The ASM moves of Figure 11, are the images under φ of the corresponding square moves of Figure 2. The preservation of trip permutations and proper labelings is by construction. The behavior in Figure 10 was chosen to reflect the rules of the road after applying φ , while the labelings of Definition 3.24 correspond under φ^{-1} to proper labelings in the usual sense of hourglass plabic graphs (by labeling hourglass edges with the complement in $\{1, 2, 3, 4\}$ of the labels that appear on adjacent edges).

Suppose $G \in \text{CRG}(\varrho)$. Then G has no isolated components and no $G' \sim G$ has a 4-cycle containing an hourglass. An unoriented 3-cycle, a 2-cycle, or a loop corresponds under φ^{-1} to a 4-cycle containing an hourglass. Thus D has no isolated components and no $D' \sim D = \varphi(G)$ contains an unoriented 3-cycle, a 2-cycle, or a loop. By definition, this means D is well oriented. The converse works similarly. \square

3.4. Matching diagrams. In this subsection, we establish Proposition 3.26, which will be used in the proof of Theorem 3.13.

A *matching diagram* M is the underlying graph of some well oriented symmetrized six-vertex configuration D (with edge directions forgotten). The *matching* of M is $\text{trip}_2(D)$, viewed as a matching of the boundary vertices b_1, \dots, b_n . By Lemma 3.20 and Proposition 3.21, among any four strands in a matching diagram M , there is a pair which does not cross (that is, M has no *4-crossings*). We may apply Yang–Baxter moves to matching diagrams as to symmetrized six-vertex configurations, but without remembering the edge orientations.

The following is closely related to the Tits–Matsumoto theorem (see, e.g., [BB05, Thm. 3.3.1]) on reduced words of permutations.

Proposition 3.26. *Any matching diagrams for the same matching are connected by Yang–Baxter moves.*

Proof. We will show that all matching diagrams with a fixed matching m are move-equivalent by constructing a canonical matching diagram \tilde{M} with matching m to which all diagrams are connected.

We denote a strand in a matching diagram with endpoints b_i and b_j with $i < j$ by ℓ_i . The region of the disk bounded by ℓ_i and the boundary segments connecting b_i, b_{i+1}, \dots, b_j is called the *inside* of ℓ_i and the remainder of the disk, bounded by ℓ_i and the boundary segments connecting $b_j, b_{j+1}, \dots, b_n, b_1, \dots, b_i$ is the *outside*.

The matching diagram \tilde{M} is uniquely characterized by the following property (the *abc-property*): if $a < b < c$ and strands ℓ_a, ℓ_b, ℓ_c all cross each other, then ℓ_b and ℓ_c cross on the outside of ℓ_a . The abc-property is simultaneously achievable for all $a < b < c$ since \tilde{M} may be drawn according to the following recipe: Cut the boundary of the disk between b_n and b_1 and unfold the boundary onto a line; then, for each $i = 1, 2, \dots$ in order, draw ℓ_i with an initial vertical segment, during which it crosses exactly those previously drawn strands ℓ_j such that ℓ_i, ℓ_j are required to cross in m ; finish drawing ℓ_i with a horizontal segment followed by a vertical segment, during which it does not cross any previously drawn strands. See Figure 14 for an example. Furthermore the abc-property uniquely specifies the matching diagram \tilde{M} , since it determines the relative positions of the crossings in every 3-crossing ℓ_a, ℓ_b, ℓ_c .

Suppose that M is a matching diagram with matching m having some number $d > 0$ of triples $a < b < c$ which violate the abc-property. Among these violations, choose the one with a maximal, b minimal with respect to a , and c maximal with respect to a, b . By assumption, ℓ_b and ℓ_c cross on the inside of ℓ_a . If no strands enter the region bounded by ℓ_a, ℓ_b, ℓ_c , then we may immediately apply a Yang–Baxter move to eliminate this violation. Otherwise there is some strand entering this region which crosses exactly two of ℓ_a, ℓ_b, ℓ_c , since a 4-crossing is impossible by Proposition 3.21; see Figure 14. But in any case, the new strand $\ell_{a'}, \ell_{b'}$, or $\ell_{c'}$ creates a new violation $\{\ell_{a'}, \ell_b, \ell_c\}$, $\{\ell_a, \ell_{b'}, \ell_c\}$, or $\{\ell_a, \ell_b, \ell_{c'}\}$ of the abc-property which contradicts the minimality and maximality assumptions imposed on a, b, c . Thus we can reduce the number of violations of the abc-property using the Yang–Baxter move, and we see by induction that $M \sim \tilde{M}$. \square

3.5. Well oriented configurations and monotonicity. We now establish a key trip_\bullet -theoretic property of well oriented configurations and fully reduced hourglass plabic graphs.

Definition 3.27. A symmetrized six-vertex configuration D is *monotonic* if trip_2 -strands do not revisit vertices or double cross, and if for every trip_1 -strand ℓ_1 , passing through vertices U_1 , and every trip_2 -strand ℓ_2 , passing through vertices U_2 , the vertices in the intersection $U_1 \cap U_2$ are consecutive

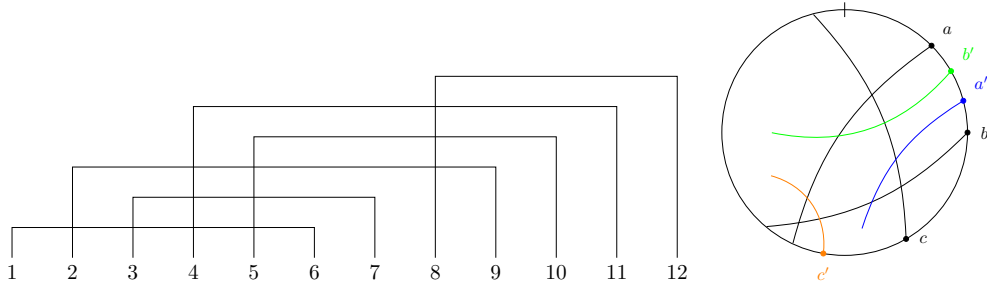


FIGURE 14. Left: the drawing of \tilde{M} for $m = (16)(29)(37)(411)(510)(812)$. Right: the violation of the abc-property discussed in the proof of Proposition 3.26.

along both ℓ_1 and ℓ_2 . Note that we could equivalently impose this condition for trip_3 -strands instead of trip_1 -strands.

Theorem 3.28. *Let D be a well oriented symmetrized six-vertex configuration, then D is monotonic.*

We use the following lemma in the proof of Theorem 3.28.

Lemma 3.29. *Let ℓ be a trip_1 -strand in a symmetrized six-vertex configuration D . Then the following hold.*

- (a) *Suppose ℓ passes through edges $e = uv$ and $e' = vw$. Then ℓ turns left at v if e, e' are oriented toward v , turns right if e, e' are oriented away from v , and goes straight through v otherwise.*
- (b) *The turns of ℓ alternate between left and right.*

Proof. A simple inspection of the turning rules for trip_1 yields part (a). For part (b), note that if ℓ has just turned right at v , then the orientation of ℓ agrees with the orientation of the edge it is traversing, and this will continue to be the case as ℓ passes straight through any vertices. While this condition is satisfied, ℓ cannot turn right by part (a). Thus ℓ must take a left turn between any two right turns, and, symmetrically, must take a right turn between any two left turns. \square

Proof of Theorem 3.28. Let D be a well oriented symmetrized six-vertex configuration. By Proposition 3.21, trip_2 -strands do not revisit vertices or double cross. Suppose that D is not monotonic, with some trip_1 -strand ℓ_1 intersecting a trip_2 -strand ℓ_2 , separating from it after some vertex v , and then re-intersecting at some vertex v' (see Figure 15).

Let v_1, \dots, v_k be the vertices between v, v' along ℓ_1 at which ℓ_1 turns, and write $v = v_0, v' = v_{k+1}$ for convenience. By Lemma 3.29, these turns alternate between left and right, with inward pointing edges at left turns and outward pointing edges at right turns, and with orientations not changing along the intervening segments on which ℓ_1 goes straight.

If $k = 1$, then ℓ_2 and the trip_2 -strands s, s' , passing through $\{v, v_1\}$ and $\{v_1, v'\}$, respectively, form an unoriented triangle, contradicting the fact that D is well oriented.

Thus we have $k \geq 2$. The polygon with vertices v, v', v_1, \dots, v_k has two trip_2 -strands entering the interior of the polygon at v_2 ; these strands s and s' must recross the boundary of the polygon elsewhere. Let s be the strand passing through v_1 and v_2 .

The strand s may not exit the polygon through any of the segments $\overline{vv_1}, \overline{v_1v_2}, \overline{v_2v_3}$, or $\overline{vv'}$, lest it create an unoriented triangle or double crossing of trip_2 -strands. Thus s exits the polygon at some vertex u , further along ℓ_1 . But then, replacing ℓ_2 by s , v by v_2 , and v' by u , we have a smaller instance of trip_1 - and trip_2 -strands intersecting, separating, and re-intersecting; by induction on k this is impossible. \square

Definition 3.30 (cf. Definition 3.27). An hourglass plabic graph G is *monotonic* if trip_2 -strands do not revisit vertices or double cross, and if for every trip_1 -strand ℓ_1 , passing through vertices

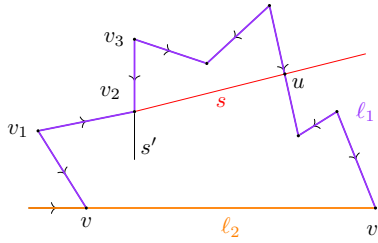


FIGURE 15. The strands discussed in the proof of Theorem 3.28.

U_1 , and every trip_2 -strand ℓ_2 , passing through vertices U_2 , the vertices in the intersection $U_1 \cap U_2$ are consecutive along both ℓ_1 and ℓ_2 . Note that we could equivalently impose this condition for trip_3 -strands instead of trip_1 -strands.

Proposition 3.31 is immediate from the definition of φ (Definition 3.22).

Proposition 3.31. *A symmetrized six-vertex configuration D is monotonic if and only if the contracted hourglass plabic graph $\varphi^{-1}(D)$ is.*

Proposition 3.32. *An hourglass plabic graph G is fully reduced if and only if $\text{osc}(G)$ is fully reduced.*

Proof. A sequence of moves on $\text{osc}(G)$ produces a forbidden 4-cycle if and only if the same sequence of moves applied to G does. □

Corollary 3.33. *An hourglass plabic graph G is fully reduced if and only if it is monotonic.*

Proof. First, suppose G is fully reduced. We may assume without loss of generality that G is contracted, since contraction moves do not affect monotonicity.

Suppose moreover that G is of oscillating type. Then by Theorem 3.25, $D = \varphi(G)$ is well oriented, and thus by Theorem 3.28 D is monotonic. By Proposition 3.31, we conclude that G is monotonic.

If G is of general type, Proposition 3.32 implies that $\text{osc}(G)$ is fully reduced, and so by the above argument $\text{osc}(G)$ is monotonic. It is clear then by construction that G must also be monotonic.

For the converse, Figure 16 demonstrates that each of the forbidden 4-cycles fails to be monotonic. Furthermore, the moves for hourglass plabic graphs preserve monotonicity. Thus monotonic graphs are fully reduced. □

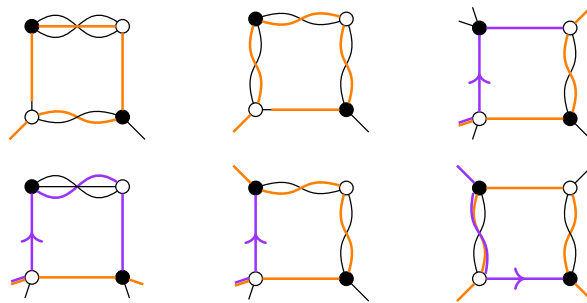


FIGURE 16. The 4-cycles forbidden in a fully reduced hourglass plabic graph. The trip_2 -strands, drawn in orange (■), and trip_1 -strands, drawn in purple (■), demonstrate the failure of monotonicity in each case.

3.6. Move equivalence and trip permutations. We now give some final trip_\bullet -theoretic lemmas and the proofs of Proposition 3.12 and Theorem 3.13.

Lemma 3.34. *Let $G \in \text{CRG}(\underline{o})$, and let ℓ_1 and ℓ_2 be trip_1 - and trip_2 -strands, respectively. Let v_1, \dots, v_k be the vertices shared by ℓ_1 and ℓ_2 , ordered according to the direction of ℓ_1 . For $i = 1, \dots, k-1$, let e_i be the edge between v_i and v_{i+1} . Then:*

- (a) *The multiplicities $m(e_i)$ alternate between 1 and 2.*
- (b) *If $m(e_1) = 2$ then $k = 2$.*
- (c) *k is even, so $\text{col}(v_k) \neq \text{col}(v_1)$; thus if v_1 and v_k are not boundary vertices, ℓ_1 ends on the opposite side of ℓ_2 from which it started.*
- (d) *If $m(e_i) = 1$, then $\text{col}(v_i) = \text{col}(v_1)$.*

Proof. Since G is contracted and of oscillating type, it has no edges of multiplicity greater than two, and no pair of consecutive 2-hourglasses. The case $m(e_i) = m(e_{i+1}) = 1$ is impossible, since ℓ_1 and ℓ_2 could not share both edges; this establishes (a).

If $m(e_1) = 2$, then ℓ_1 and ℓ_2 must enter v_1 on different simple edges, share e_1 , and then leave v_2 on different simple edges, so $k = 2$.

A simple case check shows that if ℓ_1 and ℓ_2 share at least one vertex, then they share an edge, so $k = 0$ or $k \geq 2$. If $k > 2$, then by parts (a) and (b), we know $m(e_1) = m(e_3) = \dots = 1$ and $m(e_2) = m(e_4) = \dots = 2$. If $m(e_{k-1}) = 2$, then letting ℓ_3 be the trip_3 -strand obtained by reversing ℓ_1 , the same arguments as above would require $k = 2$. Thus we must have $m(e_{k-1}) = 1$ and k is even, proving (c). Finally, if $m(e_i) = 1$, then $k > 2$, so $m(e_1) = 1$; then (d) follows from (a) and the bipartiteness of G . \square

Lemma 3.35. *Let $G \in \text{RG}(\underline{c})$, let ℓ be a trip_1 -strand in G , and let v be an interior vertex. Then ℓ visits v at most once.*

Proof. By Corollary 3.33, G is monotonic. Suppose ℓ visits v twice, enclosing a polygon with vertices $v = v_0, v_1, \dots, v_k$. Since G is bipartite, this polygon has a vertex, say v_i , at which some trip_2 -strand ℓ_2 enters the interior of the polygon. Now, ℓ_2 must also exit the polygon at some vertex v_j . Since G is fully reduced, ℓ_2 may not have a self intersection, so $v_i \neq v_j$. The only other possibility consistent with the monotonicity of the pair ℓ_1, ℓ_2 is $v_j = v_{i+1}$. But then G must contain two separate edges between v_i and v_{i+1} (the edges traversed by ℓ_1 and ℓ_2), impossible in a fully reduced graph. \square

Proof of Proposition 3.12. Let $G \in \text{RG}(\underline{c})$ have underlying plabic graph \widehat{G} . We wish to show that \widehat{G} is reduced, which we will do by verifying that the conditions of Theorem 2.15 are satisfied.

First, \widehat{G} is leafless, since any vertex v with $\widehat{\text{deg}}(v) = 1$ must be incident in G to a 4-hourglass. Since all vertices of G have degree 4, the endpoints of e would form an isolated component in G , violating full reducedness. This also implies that \widehat{G} has no isolated components.

Assume now that G is of oscillating type. Proposition 3.5 and Lemma 3.35 ensure that \widehat{G} satisfies conditions (1),(2), and (4) of Theorem 2.15, so it remains to check that \widehat{G} has no bad double crossings.

Suppose that two trip_1 -strands ℓ_1 and ℓ'_1 cross; then in G , we have one of the local configurations shown in Figure 17. In each case, trip_2 -strands ℓ_2 and ℓ'_2 are indicated. By Lemma 3.34, the trip_1 -strands diverge from the trip_2 -strands as indicated in the figure. In particular, after the crossing, ℓ_2 and ℓ'_2 lie between ℓ_1 and ℓ'_1 . Since G is fully reduced, it is monotonic by Corollary 3.33. Since each of ℓ_1, ℓ'_1 has already shared vertices with both ℓ_2 and ℓ'_2 , neither can retouch these strands, and thus ℓ_1, ℓ'_1 cannot recross in the forward direction.

If G is not of oscillating type, the above argument implies that $\widehat{\text{osc}}(\widehat{G})$ is reduced. It then follows that \widehat{G} is likewise reduced. \square

Lemma 3.36. *Let $G_1, G_2 \in \text{RG}(\underline{o})$, and suppose $\widehat{G}_1 = \widehat{G}_2 = P$ and that the symmetrized six-vertex configurations $\varphi(G_1)$ and $\varphi(G_2)$ have the same underlying matching diagram M . Then $G_1 = G_2$.*

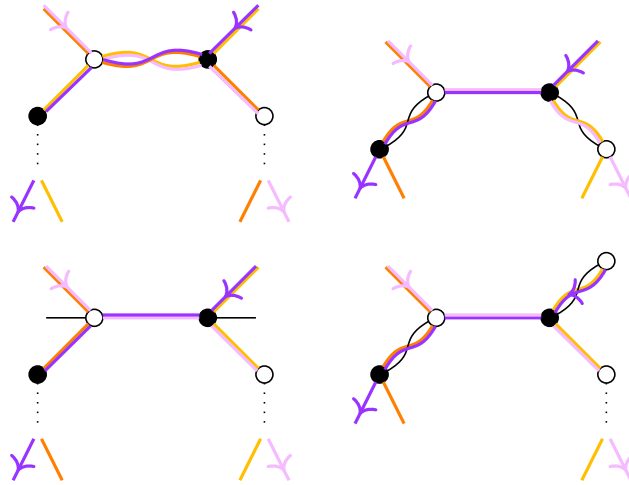


FIGURE 17. The possibilities for the local configuration of a pair of crossing trip_1 -strands ℓ_1 (light purple \blacksquare) and ℓ'_1 (dark purple \blacksquare). In each case a pair ℓ_2 (orange \blacksquare) and ℓ'_2 (yellow \blacksquare) of trip_2 -strands prevents ℓ_1 and ℓ'_1 from crossing again, by monotonicity.

Proof. We show, by induction on the number of vertices, how to uniquely recover G from P and M .

If M contains some trip_2 -strand that does not intersect any other trip_2 -strand, then both M and P may be split in two pieces, taking that strand as part of the boundary of the pieces, giving smaller pairs of plabic graphs and matching diagrams which, by induction, may each be uniquely lifted to reconstruct G . Thus we may assume that M contains no such strand.

In this case, there exists some consecutive boundary vertices b and b' which are both adjacent in M to the same internal vertex v . The possible neighborhoods of b, b' in P are shown in Figure 18. In the latter two cases, the edge e must come from a 2-hourglass in G , allowing us to uniquely reconstruct this neighborhood of G . After doing so, we can replace the boundary segment surrounding b, b' with the dashed line shown in the figure, to obtain a smaller matching diagram M_1 and plabic graph P_1 . By induction, that information allows us to uniquely reconstruct the remainder of G . \square

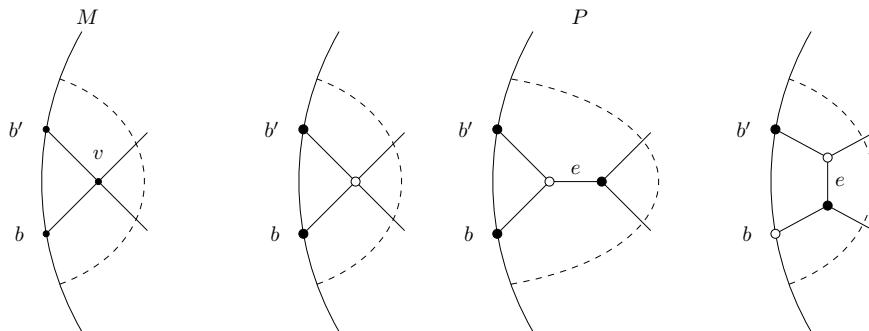


FIGURE 18. Consecutive boundary vertices with a common neighbor in a matching diagram M (left) and the three possible corresponding configurations in the plabic graph P (right). See the proof of Lemma 3.36.

Proof of Theorem 3.13. Let $G_1, G_2 \in \text{RG}(\underline{c})$. If $G_1 \sim G_2$, then $\text{trip}_\bullet(G_1) = \text{trip}_\bullet(G_2)$ by Proposition 3.7(a).

Conversely, suppose $\text{trip}_\bullet(G_1) = \text{trip}_\bullet(G_2)$. Since any hourglass plabic graph is move-equivalent to a unique contracted graph, we may also assume without loss of generality that G_1, G_2 are contracted.

Suppose first that G_1, G_2 are of oscillating type. By Proposition 3.12, the underlying plabic graphs $P_1 = \widehat{G}_1$ and $P_2 = \widehat{G}_2$ are reduced and by Proposition 3.5, we have $\text{trip}(P_1) = \text{trip}_1(G_1) = \text{trip}_1(G_2) = \text{trip}(P_2)$. Thus, by Theorem 2.16, P_1 and P_2 are equivalent under the moves from Figure 6. Consider a sequence of moves transforming P_1 into P_2 that minimizes the number s of times that the square move (M1) is applied, and also such that the only moves occurring before the first square move are those necessary to make the square move applicable. Let F be the face on which the first square move acts. Since G_1 is bipartite, so is P_1 , and since G_1 is contracted with all internal vertices of degree 4, P_1 has all internal vertices of degree 3 or 4. Since P_1 is reduced, it has no 2-gonal faces. From this we conclude that F is already a bipartite square face of P_1 , so the only moves occurring before the square move at F are the expansions of any degree-4 corners of F into two degree-3 vertices. Let P_1^\dagger be the plabic graph obtained by applying these expansion moves, then the square move at F , and then contracting with their unique neighbors outside of F all those corners of F that were not expanded. Then $P_1^\dagger = \widehat{G}_1^\dagger$, where G_1^\dagger is obtained from G_1 by applying the appropriate square move from Figure 2. Furthermore, P_1^\dagger can be transformed into P_2 by $s - 1$ square moves. Hence, by induction on s , there exists a contracted fully reduced hourglass plabic graph G'_1 with $G_1 \sim G'_1$ and $\widehat{G}'_1 = P_2$.

It remains to show that G'_1 may be transformed into G_2 by a sequence of benzene moves. Let φ be the bijection from Definition 3.22 and define $D'_1 = \varphi(G'_1)$ and $D_2 = \varphi(G_2)$. The symmetrized six-vertex configurations D'_1, D_2 are well oriented by Theorem 3.25 and satisfy $\text{trip}_2(D'_1) = \text{trip}_2(D_2)$. Thus, by Proposition 3.26, the matching diagram M'_1 for D'_1 can be transformed into the matching diagram M_2 for D_2 by a sequence of Yang–Baxter moves. Consider the hourglass plabic graph G''_1 obtained by transporting these Yang–Baxter moves to benzene moves on G'_1 via φ^{-1} . Since benzene moves do not change the underlying plabic graph, we have $\widehat{G}''_1 = \widehat{G}'_1 = P_2 = \widehat{G}_2$, and by construction the matching diagram for $\varphi(G''_1)$ is equal to the matching diagram M_2 for $\varphi(G_2)$. By Lemma 3.36 we conclude that in fact $G''_1 = G_2$, as desired.

If G_1, G_2 are not of oscillating type, we oscillize to $\text{osc}(G_1), \text{osc}(G_2)$, which are fully reduced by Proposition 3.32. Indeed, these still satisfy $\text{trip}_\bullet(\text{osc}(G_1)) = \text{trip}_\bullet(\text{osc}(G_2))$, so by the previous argument, $\text{osc}(G_1) \sim \text{osc}(G_2)$. Since benzene and square moves cannot be applied to boundary faces, the sequence of moves yielding this move equivalence can also be applied to yield $G_1 \sim G_2$. \square

The following useful fact is immediate from the preceding proof.

Corollary 3.37. *Suppose that $G, G' \in \text{CRG}(\underline{c})$ are move-equivalent. Then they may be connected by a sequence of benzene moves followed by a sequence of square moves, or vice versa.*

4. FLUCTUATING TABLEAUX AND SEPARATION LABELINGS

In this section, we recall the notion of *fluctuating tableaux* of r rows from [GPPSS24a]. For $r = 4$, we establish a map (shown later, in Theorem 6.1, to be a bijection) between move-equivalence classes of fully reduced hourglass plabic graphs and rectangular fluctuating tableaux. See Section 9 for related constructions outside the $r = 4$ setting.

4.1. Fluctuating tableaux and promotion permutations. In this subsection, we recall needed material from the companion paper [GPPSS24a].

A *generalized partition* with r rows is a tuple $\lambda = (\lambda_1, \dots, \lambda_r) \in \mathbb{Z}^r$ where $\lambda_1 \geq \dots \geq \lambda_r$. We visualize generalized partitions as *diagrams*, which are semi-infinite collections of *cells*.

We write \mathbf{e}_i for the i -th standard basis vector of \mathbb{Z}^r . If $S \in \mathcal{A}_r$ is a positive subset of $\{\pm 1, \dots, \pm r\}$, we define $\mathbf{e}_S = \sum_{i \in S} \mathbf{e}_i$, while if S is a negative subset, we define $\mathbf{e}_S = -\sum_{i \in S} \mathbf{e}_{-i}$. We say two

r -row generalized partitions λ, μ *differ by a skew column* if $\lambda = \mu + \mathbf{e}_S$ for some $S \in \mathcal{A}_r$. For $c \geq 0$, we furthermore write $\mu \xrightarrow{c} \lambda$ if λ is obtained from μ by adding a skew column of c boxes and $\mu \xrightarrow{-c} \lambda$ if λ is obtained from μ by removing a skew column of c boxes.

Definition 4.1. An r -row *fluctuating tableau* of length n is a sequence

$$T = (\mathbf{0} = \lambda^0 \xrightarrow{c_1} \lambda^1 \xrightarrow{c_2} \dots \xrightarrow{c_n} \lambda^n)$$

of r -row generalized partitions such that λ^{i-1} and λ^i differ by a skew column obtained by adding c_i or removing $-c_i$ cells for all $1 \leq i \leq n$. The partition λ^n is called the *shape* of T . The sequence $\underline{c} = (c_1, \dots, c_n) \in \{0, \pm 1, \dots, \pm r\}^n$ is the *type* of T . Let $\text{FT}(r, \lambda, \underline{c})$ be the set of fluctuating tableaux with r rows, shape λ , and type \underline{c} . We will drop some parameters from $\text{FT}(r, \lambda, \underline{c})$ as convenient. In particular, unless otherwise specified, we assume $r = 4$ in the remainder of the paper.

An r -row fluctuating tableau is *rectangular* if its shape λ satisfies $\lambda_1 = \dots = \lambda_r$. In this case λ is called a *generalized rectangle*. We write $\text{RFT}(\underline{c})$ for the set of rectangular fluctuating tableau of type \underline{c} , where no $c_j = 0$. We say a fluctuating tableau is of *oscillating type* if each $c_j \in \{\pm 1\}$.

Building on work of Patrias [Pat19] in the oscillating case, we visualize fluctuating tableaux by writing i in the added cells of $\lambda^i - \lambda^{i-1}$ or \bar{i} in the removed cells of $\lambda^{i-1} - \lambda^i$; see Figure 19 for an example.

Fluctuating tableaux interest us because of the following fact.

Proposition 4.2 (see [GPPSS24a, Prop. 2.10]). *For any type \underline{c} , we have*

$$(4.1) \quad |\text{RFT}(\underline{c})| = \dim_{\mathbb{C}} \text{Inv}_{\text{SL}_r} \left(\bigwedge^{\underline{c}} V \right) = \dim_{\mathbb{C}(q)} \text{Inv}_{U_q(\mathfrak{sl}_r)} \left(\bigwedge_q^{\underline{c}} V_q \right).$$

The *lattice word* associated to a fluctuating tableau $T \in \text{FT}(\underline{c})$ is the word $L = L(T) = w_1 \dots w_n$ on \mathcal{A}_r , where $\lambda^i = \lambda^{i-1} + \mathbf{e}_{w_i}$. We may recover T from $L(T)$, so we sometimes identify T and $L(T)$.

A word w is a lattice word of a fluctuating tableau if and only if for every prefix $w_1 \dots w_k$ and every $1 \leq a \leq b \leq r$,

$$(4.2) \quad (\mathbf{e}_{w_1} + \dots + \mathbf{e}_{w_k})_a \geq (\mathbf{e}_{w_1} + \dots + \mathbf{e}_{w_k})_b,$$

where $\mathbf{e}_{\bar{a}} = -\mathbf{e}_a$. More concretely, in each prefix we require the number of a 's minus the number of \bar{a} 's to be weakly greater than the number of b 's minus the number of \bar{b} 's. A fluctuating tableau is rectangular if and only if equality holds when $k = n$, in which case we call L *balanced*.

Definition 4.3. Consider a word $L = w_1 \dots w_n$ in the alphabet \mathcal{A}_r . Define

- (i) $\tau(L) = \overline{w_n} \dots \overline{w_1}$;
- (ii) $\varpi(L) = \varpi(w_1) \dots \varpi(w_n)$, where $\varpi(w)$ replaces each element i in w with $-\text{sgn}(i)(r - |i| + 1)$;
and
- (iii) $\varepsilon(L) = \varepsilon(w_n) \dots \varepsilon(w_1)$, where $\varepsilon(w)$ replaces each element i in w with $\text{sgn}(i)(r - |i| + 1)$.

Consider $\mu \xrightarrow{c} \lambda$. Let $\lambda = \mu + \mathbf{e}_{\{i_1 < \dots < i_c\}}$. The *oscillization* of $\mu \xrightarrow{c} \lambda$ is the sequence

$$\text{osc}(\mu \xrightarrow{c} \lambda) := \mu \rightarrow \mu^1 \rightarrow \dots \rightarrow \mu^{|c|-1} \rightarrow \lambda,$$

where

$$\mu^j = \mu^{j-1} + \mathbf{e}_{i_j}$$

with $\mu^0 := \mu$ and $\mu^{|c|} = \lambda$. Given a fluctuating tableau $T = (\mathbf{0} = \lambda^0 \xrightarrow{c_1} \lambda^1 \xrightarrow{c_2} \dots \xrightarrow{c_n} \lambda^n)$, let $\text{osc}(T)$ be the concatenation of $\text{osc}(\lambda^{i-1} \rightarrow \lambda^i)$ for $1 \leq i \leq n$. A fluctuating tableau is in the image of oscillization if and only if it is of oscillating type. Oscillization may be described easily in terms of lattice words. To compute $L(\text{osc}(T))$, we simply erase the braces from $L(T)$, where elements of each letter are written in increasing order, keeping the same initial and final shape.

We now define promotion on fluctuating tableaux; see [GPPSS24a, §4.2, §4.4] for detailed examples and further discussion.

Definition 4.4. Fix $1 \leq i \leq n - 1$. Let $T \in \text{FT}(\underline{c})$ be a fluctuating tableau whose diagram is labeled by $1 < 2 < \dots < i - 1 < \bullet < i < \dots$ and their negatives. If $c_i \cdot c_{i+1} \leq 0$, for each row R which does not contain any of i, \bullet, \bar{i} , or $\bar{\bullet}$, we identify a cell \mathbf{b}_R in R and call it *open*. Let j be the largest absolute value of an entry in R less than i , if any exist.

- If $c_i \geq 0$, let \mathbf{b}_R be the cell immediately right of the cell containing j , or the cell containing \bar{j} , or if j does not exist then let \mathbf{b}_R be first cell of row R .
- If $c_i \leq 0$, let \mathbf{b}_R be the cell containing j , or the cell immediately left of the cell containing \bar{j} , or otherwise the first negative cell of R .

The *jeu de taquin slides* for jdt_{i-1} are the following. See [GPPSS24a, Figure 6] for schematic diagrams.

- 's first move right by swapping places with i 's, then move down as far as possible by swapping places with i 's.
- 's first move left by swapping places with \bar{i} 's, then move up as far as possible by swapping places with \bar{i} 's.
- \bar{i} pairs move down as far as possible into open cells, and then they move left one column.
- $\bar{\bullet}i$ pairs move up as far as possible into open cells, and then move right one column.

All other entries are left unchanged. This results in a fluctuating tableau whose diagram is labeled by $1 < 2 < \dots < i < \bullet < i + 1 < \dots$ and their negatives.

Definition 4.5. Let T be a length n fluctuating tableau.

- The *promotion* $\mathcal{P}(T)$ is the result of replacing ± 1 's with $\pm \bullet$'s, sequentially applying jeu de taquin slides $\text{jdt}_1, \dots, \text{jdt}_{n-1}$, replacing $\pm \bullet$'s with $\pm(n+1)$'s, and subtracting 1 from each entry's absolute value.
- The *evacuation* $\mathcal{E}(T)$ is the result of first replacing ± 1 's with $\pm \bullet_n$'s, sliding them past $\pm n$'s, replacing ± 2 's with $\pm \bullet_{n-1}$'s, sliding them past $\pm n$'s, etc., and finally replacing $\pm \bullet_i$'s with $\pm i$'s.
- The *dual evacuation* $\mathcal{E}^*(T)$ is the result of first replacing $\pm n$'s with $\pm \bullet_1$'s, sliding backward past ± 1 's, replacing $\pm(n-1)$'s with $\pm \bullet_2$'s, sliding backward past ± 1 's, etc., and finally replacing $\pm \bullet_i$'s with $\pm i$'s.

We define *promotion permutations* as follows. See [GPPSS24a, §6] for a more general construction and further details.

Definition 4.6. Let $T \in \text{FT}(r, \underline{c})$ be a fluctuating tableau and $1 \leq i \leq r - 1$. Then the i -th *promotion permutation* $\text{prom}_i(T)(b) \equiv |a| + b - 1 \pmod{n}$ if and only if a is the unique value that crosses the boundary between rows i and $i + 1$ in the application of promotion to $\mathcal{P}^{b-1}(\text{osc}(T))$. We write $\text{prom}_\bullet(T)$ for the tuple of these promotion permutations.

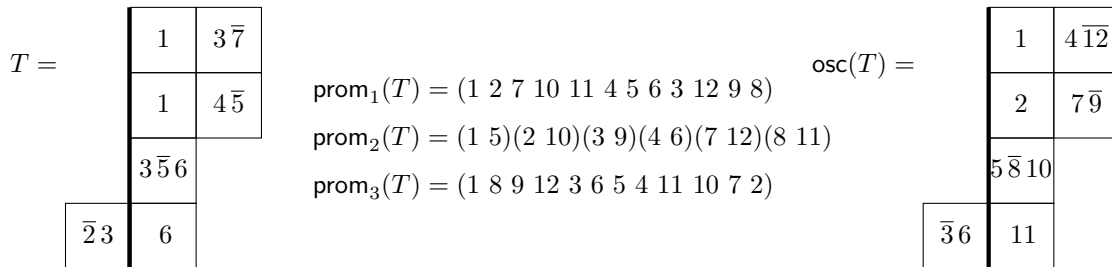


FIGURE 19. An example visual depiction of a rectangular fluctuating tableau T with $n = 7$ and $\underline{c} = (2, \bar{1}, 2, 1, \bar{2}, 2, \bar{1})$, together with its promotion permutations in cycle notation. For the full promotion orbit of $\text{osc}(T)$, see [GPPSS24a, Fig. 7].

Let $\sigma = (12 \cdots N)$ be the long cycle and let $w_0 = (1, N)(2, N-1) \cdots$ be the longest element in the symmetric group \mathfrak{S}_N . The following collects the key results we need on promotion permutations.

Theorem 4.7 ([GPPSS24a, Thm. 6.7]). *Let $T \in \text{FT}(r, \underline{c})$, where $|c_1| + \cdots + |c_n| = N$. Then for all $1 \leq i \leq r-1$:*

- (i) $\text{prom}_i(T)$ is a permutation in \mathfrak{S}_N ,
- (ii) $\text{prom}_i(T) = \text{prom}_{r-i}(T)^{-1}$,
- (iii) $\text{prom}_i(\mathcal{P}(T)) = \sigma^{-|c_1|} \text{prom}_i(T) \sigma^{|c_1|}$,
- (iv) $\text{prom}_i(\mathcal{E}(T)) = w_0 \text{prom}_i(T) w_0$.

4.2. The separation labeling. To connect to fluctuating tableaux, we now define an intrinsic labeling of contracted fully reduced hourglass plabic graphs.

Recall from Definition 2.7 the notion of a (proper) labeling, which we now apply to hourglass plabic graphs rather than webs. A labeling assigns to each m -hourglass an m -subset of $\{1, 2, 3, 4\}$.

Definition 4.8. Let $G \in \text{CRG}(\underline{c})$. The *base face* of G is the face F_0 incident to the boundary segment between b_n and b_1 . We define the *separation labeling* sep of G as follows:

- For e a simple edge of G , let $F(e)$ be the face incident to e which is on the right when traversing e from the black vertex to the white vertex, and let ℓ_1, ℓ_2, ℓ_3 be, respectively, the trip_1 -, trip_2 -, and trip_3 -strands traversing e in this direction. If exactly a of ℓ_1, ℓ_2, ℓ_3 separate $F(e)$ from F_0 , then set $\text{sep}(e) = \{a+1\}$. We often omit braces when writing singleton sets.
- For an hourglass e , let v be either endpoint, and define

$$(4.3) \quad \text{sep}(e) = \{1, 2, 3, 4\} \setminus \bigcup_{\substack{e' \ni v \\ e' \neq e}} \text{sep}(e').$$

See Figure 21 for an example.

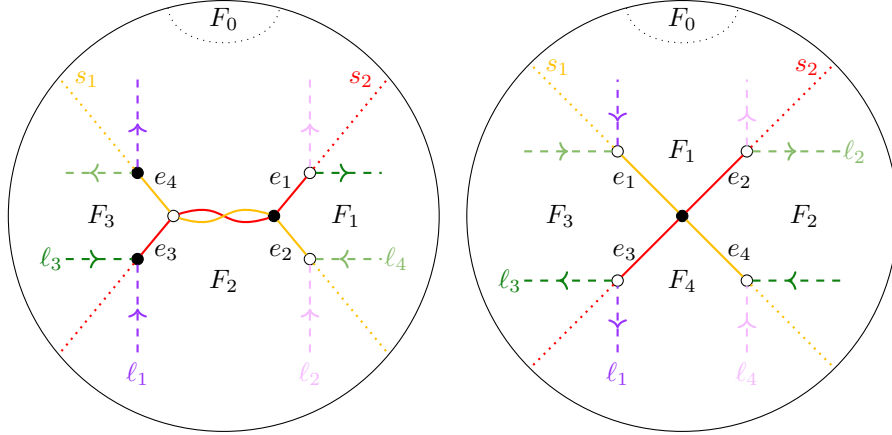


FIGURE 20. The trip_1 / trip_3 -strands ℓ_i and trip_2 -strands s_i passing through the simple edges surrounding an hourglass (left) or a simple vertex (right). See the proof of Proposition 4.9.

Proposition 4.9. *Let $G \in \text{CRG}(\underline{c})$. Then the separation labeling is well defined and proper.*

Proof. The separation labeling is clearly well defined on simple edges, so it suffices to show that (4.3) does not depend on the choice of v .

Consider the four simple edges e_1, e_2, e_3, e_4 adjacent to the two endpoints of an hourglass; see the left side of Figure 20 for notation we will use. To compute $\text{sep}(e_1)$, we must determine which of

s_2, ℓ_2, ℓ_3 separate the face F_1 from the base face F_0 . Since G is fully reduced, and hence monotonic by Corollary 3.33, the trip_2 -strands s_1, s_2 do not recross, nor do any trip_1 -strands retouch either trip_2 -strand. Thus we see that s_2, ℓ_3 separate F_1 from F_0 , and that ℓ_2 separates the two faces if and only if it reaches the boundary to the right of F_0 . Similarly, computing $\text{sep}(e_2)$, we see that s_1, ℓ_4 separate F_2 from F_0 , and that ℓ_2 does so if and only if it ends to the left of F_0 . Thus we conclude that $\{\text{sep}(e_1), \text{sep}(e_2)\} = \{3, 4\}$. A similar analysis shows $\{\text{sep}(e_3), \text{sep}(e_4)\} = \{3, 4\}$, so that the hourglass may be consistently labeled by $\{1, 2\}$; moreover, the resulting labeling is proper around these vertices. The cases differing from Figure 20 by a color reversal or the relative location of F_0 are analogous.

It remains to verify that sep gives a proper labeling around each simple vertex; see the right side of Figure 20. It is easy to see that F_2 and F_0 are separated by s_2, ℓ_2 and that F_4 and F_0 are separated by s_1, ℓ_3 . Furthermore, exactly one of F_2, F_4 is separated from F_0 by ℓ_4 . Similarly, exactly one of F_1, F_3 is separated from F_0 by ℓ_1 . Thus $\{\text{sep}(e_1), \dots, \text{sep}(e_4)\} = \{1, 2, 3, 4\}$ and sep is a proper labeling. \square

4.3. From labelings to lattice words. We now show that the separation labeling of a contracted fully reduced hourglass plabic graph gives rise to a rectangular fluctuating tableau.

Definition 4.10. Given $G \in \text{CRG}(\underline{c})$, with boundary vertices b_1, \dots, b_n , incident to edges e_1, \dots, e_n , respectively, the *separation word* $\mathbf{w}(G) = w_1 \dots w_n$ is the word of type \underline{c} given by setting $w_i = \text{col}(b_i) \text{sep}(e_i)$ for $i = 1, \dots, n$. That is, $\mathbf{w}(G) = \partial(\text{sep})$.

For $\pi \in \mathfrak{S}_n$, let $\text{Aexc}(\pi) := \{i : \pi^{-1}(i) > i\}$ denote the set of *antirecedances* of π .

Proposition 4.11. *Let $G \in \text{CRG}(\underline{a})$. Then:*

$$\text{sep}(e_i) = \begin{cases} 1 + |\{a : i \notin \text{Aexc}(\text{trip}_a(G))\}|, & \text{if } b_i \text{ is black;} \\ 1 + |\{a : i \in \text{Aexc}(\text{trip}_a(G))\}|, & \text{if } b_i \text{ is white.} \end{cases}$$

Proof. If b_i is black, then the $\text{trip}_{4-a}(G)(i)$ -strand separates $F(e_i)$ and F_0 when $\text{trip}_{4-a}(G)(i) < i$. This is equivalent to $i \notin \text{Aexc}(\text{trip}_a(G))$. The other case is similar. \square

Lemma 4.12. *Let $G \in \text{CRG}(\underline{a})$. If b_i is black (resp. white), then $b_i, \text{trip}_1(b_i), \text{trip}_2(b_i)$, and $\text{trip}_3(b_i)$ appear in clockwise (resp. counterclockwise) order. Some of these vertices may coincide.*

Proof. This claim follows by using Lemma 3.34 to track the colors of the vertices at which the other strands diverge from the $\text{trip}_2(b_i)$ -strand. \square

Theorem 4.13. *Let $G \in \text{CRG}(\underline{c})$. Then $\mathbf{w}(G)$ is the lattice word of a rectangular fluctuating tableau $\mathcal{T}(G) \in \text{RFT}(\underline{c})$.*

Proof. We may assume without loss of generality that \underline{c} is oscillating, since $\mathbf{w}(\text{osc}(G))$ being a lattice word implies the same for $\mathbf{w}(G)$. By Proposition 4.9, sep is a proper labeling, so $\mathbf{w}(G)$ is balanced.

We proceed by induction on the number v of internal vertices in G , the theorem being true if $v = 0$ since in that case $\mathbf{w}(G)$ is an appropriately nested collection of pairs of 1 and $\bar{1}$ and of $\bar{4}$ and 4, by Proposition 4.11.

If $v > 0$, let ℓ denote the trip_2 -strand incident to b_1 , and suppose $\text{col}(b_1) = 1$; otherwise we may reverse all colors, which has the affect of applying the involution ϖ to $\mathbf{w}(G)$, preserving lattice words. We divide G into smaller hourglass plabic graphs C_1, C_2, C_3 by drawing contours $\mathbf{c}_1, \mathbf{c}_2, \mathbf{c}_3$, which form the boundaries of the C_i , as follows (see Figure 21):

- (1) \mathbf{c}_1 starts in the boundary face between b_1 and b_2 and includes all internal vertices to the right of ℓ ;
- (2) \mathbf{c}_2 starts in the base face and includes the internal vertices of G which lie on ℓ ;
- (3) \mathbf{c}_3 starts in the base face and includes the internal vertices of G which lie to the left of ℓ .

Each C_i has boundary vertices on the cut edges of \mathbf{c}_i , whose color is determined by bipartiteness. These boundary vertices are numbered so that the starting point of \mathbf{c}_i is taken as the base face of C_i .

If all internal vertices of G lie on ℓ , we call G a *backbone*; this case is treated separately in Lemma 4.14. Otherwise, by induction, we know that $\mathbf{w}(C_i)$ is a balanced lattice word for $i = 1, 2, 3$.

Write $\mathbf{w}'(C_i)$ for the balanced separation word obtained by using the separation edge labels of G , rather than the intrinsic separation labels used to compute $\mathbf{w}(C_i)$. Since G is fully reduced and therefore monotonic by Corollary 3.33, and since C_2 and C_3 have the same base face as G , it follows by Lemma 3.34 and Proposition 4.11 that $\mathbf{w}'(C_2) = \mathbf{w}(C_2)$ and $\mathbf{w}'(C_3) = \mathbf{w}(C_3)$, the key point being that trip_i -strands do not reenter any of the contours after having left. Write $\mathbf{w}'(C_1) = u'_1 \dots u'_m$ and $\mathbf{w}(C_1) = u_1 \dots u_m$. In the same way, we see that $u'_i = u_i$ except when $i = j, k$ where $j = \text{trip}_1(G)(b_1)$ and k is the boundary edge of C_1 through which the $\text{trip}_1(G)(b_1)$ -strand passes.

By Proposition 4.11 and Lemma 4.12, we have $u'_j = 2$ or $\bar{1}$ (according to $\text{col}(b_j)$) while $u_j = 1$ or $\bar{2}$ and $u'_k = \bar{2}$ while $u_k = \bar{1}$. Note that we have $w_1 = 1$, since $\text{col}(b_1) = 1$. Consider the word

$$z = 1 \circ \mathbf{w}'(C_1) \circ \bar{1} \circ \mathbf{w}(C_2) \circ \mathbf{w}(C_3),$$

where \circ denotes concatenation. In the example of Figure 21, we have

$$z = 1(123212134\bar{1}4\bar{2})\bar{1}(12\bar{4}1\bar{4}3444\bar{1})(1\bar{4}\bar{4}\bar{4}444234).$$

Since $\mathbf{w}(C_1)$ is a balanced lattice word by induction, so is $1 \circ \mathbf{w}'(C_1) \circ \bar{1}$. Thus, since concatenation preserves lattice words, z is also a balanced lattice word. By construction, we may re-parenthesize z as

$$z = 112321213(4\bar{1}4\bar{2}\bar{1}12\bar{4}1\bar{4})3(444\bar{1}1\bar{4}\bar{4}\bar{4})444234,$$

grouping together the reversed and sign-reversed substrings coming from the overlaps (with reversed orientations) of \mathbf{c}_1 and \mathbf{c}_2 and of \mathbf{c}_2 and \mathbf{c}_3 . We may remove such consecutive balanced substrings from a lattice word and obtain another lattice word $z' = 1123212133444234$. By construction, we have $z' = \mathbf{w}(G)$, so $\mathbf{w}(G)$ is a balanced lattice word, as desired. \square

Lemma 4.14. *Suppose $G \in \text{CRG}(\varrho)$ is a backbone (as in the proof of Theorem 4.13). Then $\mathbf{w}(G)$ is a lattice word.*

Proof. Suppose that $\text{col}(b_1) = 1$; otherwise apply ϖ . Let $i_a = \text{trip}_a(G)(1)$ for $a = 1, 2, 3$. By Lemma 3.34, we have $\text{col}(b_{i_a}) = 1$ for $a = 1, 2, 3$ and by Proposition 4.11 and Lemma 4.12 we have $\text{sep}(b_{i_a}) = a + 1$ for $a = 1, 2, 3$.

Let ℓ denote the trip_2 -strand through b_1 . It is easy to see that all edges e incident to white boundary vertices on the right of ℓ have $\text{sep}(e) = 4$, while those incident to black vertices have $\text{sep}(e) = 1$. Those on the left side of ℓ incident to white (resp. black) boundary vertices have $\text{sep}(e) = 1$ (resp. $\text{sep}(e) = 4$). Let \mathbf{w}' be the word obtained from $\mathbf{w}(G)$ by deleting w_1, w_{i_1}, w_{i_2} , and w_{i_3} (equal to 1, 2, 3 and 4, respectively). Then \mathbf{w}' is a sequence of 1's and $\bar{4}$'s followed by a sequence of $\bar{1}$'s and 4's, and is balanced; any such word is a lattice word. It follows that $\mathbf{w}(G)$ is also a lattice word. \square

4.4. Separation words, promotion, and evacuation. We are now able to relate promotion and evacuation of fluctuating tableaux to rotation and reflection of hourglass plabic graphs.

Definition 4.15. Given an hourglass plabic graph G , let $\text{rot}(G)$ be the graph obtained by rotating G one step counterclockwise with respect to the labeling b_1, \dots, b_n of the boundary. Let $\text{refl}(G)$ denote the graph obtained by reflecting G with respect to the diameter of the boundary circle passing between b_n and b_1 .

Recall that we often identify a fluctuating tableau T with its lattice word $L(T)$. In particular, we write $\mathcal{P}(L(T))$ for $L(\mathcal{P}(T))$, and likewise for \mathcal{E} .

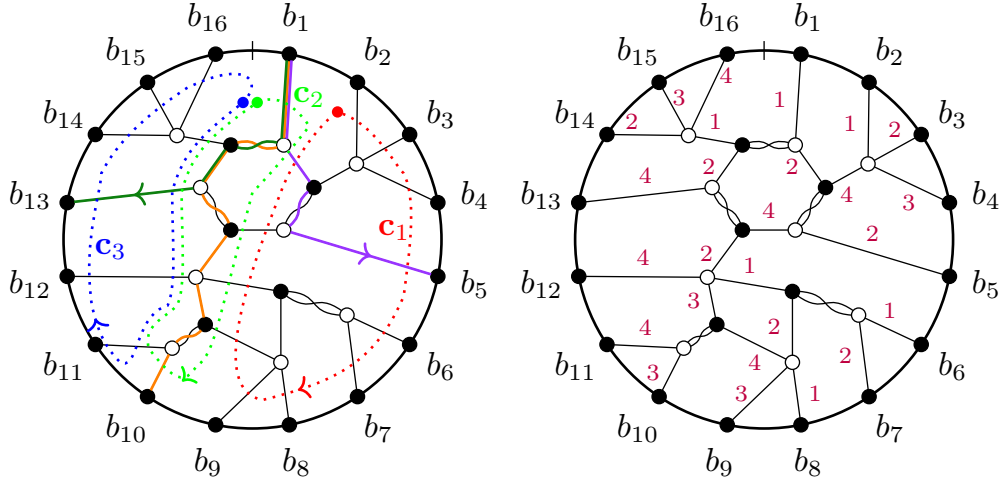


FIGURE 21. Left: the contours discussed in the proof of Theorem 4.13. Right: the separation labeling of the same graph, where the labels on 2-hourglass edges are omitted for visual clarity.

Theorem 4.16. *Let $G \in \text{CRG}(\underline{c})$. Then:*

$$\begin{aligned} \mathcal{P}(\mathbf{w}(G)) &= \mathbf{w}(\text{rot}(G)), \\ \mathcal{E}(\mathbf{w}(G)) &= \mathbf{w}(\text{refl}(G)). \end{aligned}$$

Proof. Let $\mathbf{w}(G) = w_1 \dots w_n$ be the separation word of G . The claim for \mathcal{E} is straightforward: evacuation [GPPSS24a, Thm. 6.5] and reflection both have the affect of applying the involution ε to $\mathbf{w}(G)$.

For $a = 1, 2, 3$, let $i_a = \text{trip}_a(G)(1)$. Since trip_i -strands rotate along with the graph, it is clear by Proposition 4.11 that $\mathbf{w}(\text{rot}(G))_{j-1} = \mathbf{w}(G)_j$ (with indices taken modulo n) unless $j \in \{1, i_1, i_2, i_3\}$. Thus, by the first balance point characterization of promotion [GPPSS24a, Prop. 8.22], we need to show that i_a is the smallest index weakly greater than i_{a-1} such that $w_1 \dots w_{i_a}$ has balanced a 's and $a+1$'s.

We prove the case $a = 1$, the others being similar. Let C_0 denote the hourglass plabic graph inside the contour c_0 encircling all interior vertices of G that lie to the left of the trip_1 -strand ℓ starting at b_1 (with respect to its orientation), with base face taken to be the boundary face between b_1 and b_2 . Let $\mathbf{w}(C_0) = u_1 \dots u_m$; we wish to compare $w_2 \dots w_{i_1-1}$ with $u_1 \dots u_{i_1-2}$.

First, notice that for $j > i_1 - 2$, we have $|u_j| \in \{3, 4\}$, since these are obtained from the separation labeling of the boundary edges e' of C_0 that are incident to ℓ . The corresponding boundary vertices b' of C_0 are black, as otherwise ℓ would have turned left to follow e' . Furthermore, since G (and so C_0) is fully reduced, the trip_2 -strand passing through e' must end at one of the genuine boundary vertices b_2, \dots, b_{i_1-1} , which have a smaller index in C_0 . Thus, by Proposition 4.11 and Lemma 4.12, we have $\text{sep}_{C_0}(e') \geq 3$. This implies that, since $\mathbf{w}(C_0)$ is balanced, the prefix $u_1 \dots u_{i_1-2}$ must have balanced 1's and 2's.

Now, let b_j be among b_2, \dots, b_{i_1-1} with incident edge e_j . Since G is fully reduced and therefore monotonic by Corollary 3.33, the trip_2 -strand through b_j may not exit and reenter the subgraph C_0 . This implies $\text{sep}_{C_0}(b_j) \in \{1, 2\}$ if and only if $\text{sep}_G(b_j) \in \{1, 2\}$. Together with the fact that $u_1 \dots u_{i_1-2}$ has balanced 1's and 2's, this implies that $w_2 \dots w_{i_1-1}$, and therefore also $w_1 \dots w_{i_1}$, has balanced 1's and 2's. If $\mathbf{w}(G)$ had balanced 1's and 2's for some shorter prefix, this would contradict the fact that $\mathbf{w}(C_1)$, analyzed in the proof of Theorem 4.13, is a lattice word. \square

In Sections 3 and 4, we have developed the theory of fully reduced hourglass plabic graphs in order to define the map $\mathcal{T} : \text{CRG}(\underline{c})/\sim \rightarrow \text{RFT}(\underline{c})$ (Theorem 4.13) and show (Theorem 4.16) that it intertwines rotation with promotion. Our web basis \mathcal{B}_q^c for $\text{Inv}_{U_q(\mathfrak{sl}_4)}(\bigwedge_q^c V_q)$ will consist of a special representative W from each equivalence class in $\text{CRG}(\underline{c})/\sim$. In Section 5, we develop *growth rules* in order to show that the invariants $[W]_q$ are linearly independent and to define a map $\mathcal{G} : \text{RFT}(\underline{c}) \rightarrow \text{CRG}(\underline{c})/\sim$. In Section 6, we show that \mathcal{T} and \mathcal{G} are mutually inverse bijections and therefore (by Proposition 4.2) that \mathcal{B}_q^c is the desired basis.

5. GROWTH RULES FROM CRYSTALS

5.1. The growth algorithm. We now give an algorithm which takes as input the lattice word of a rectangular fluctuating tableau with $r = 4$ and constructs a corresponding fully reduced hourglass plabic graph; see Theorem 5.3. While there are 14 growth rules in the $r = 3$ case in [KK99], our $r = 4$ algorithm involves 88 *short* growth rules of length 2 or 3 (falling into 10 families), with 2 of those families extending to *long* growth rules of arbitrary length; see Figure 22. Our proof primarily involves carefully tracking trip and promotion permutations simultaneously by using a novel crystal-theoretic algorithm, which we introduce; see Theorem 5.11.

Algorithm 5.1 (GROWTH ALGORITHM). Let $T \in \text{RFT}(\underline{c})$ and $w = L(T)$ with $r = 4$.

- (G1) Make a horizontal line of boundary vertices and downward dangling strands for each letter in $\text{osc}(w)$. Orient strands down for positive letters and up for negative letters.
- (G2) Apply the growth rules from Figure 22 by crossing dangling strands or applying end caps until there are no dangling strands.
- (G3) Convert the resulting symmetrized six-vertex configuration to an hourglass plabic graph and de-oscillize boundary vertices by combining into hourglasses.

RETURN the resulting hourglass plabic graph $\mathcal{G}(T)$.

For $G = \mathcal{G}(T)$, the *growth labeling* $\Gamma(G)$ is the proper labeling of G obtained by applying the growth rules and ignoring bars on the labels. Note that $\partial(\Gamma(G)) = w$.

At each application of (G2), reading the remaining dangling strands from left to right gives a balanced lattice word w . The algorithm proceeds by selecting certain subwords $w_{j+1} \cdots w_{j+p}$ of w and creating either a new oriented “X” or a “U” (an *end cap*) by, respectively, crossing or joining two adjacent strands; all other strands are extended further down without other modification. This process results in a new dangling lattice word w' obtained from w by substituting a subword $w'_{j+1} \cdots w'_{j+q}$ for $w_{j+1} \cdots w_{j+p}$.

Example 5.2. Let $w = 1\bar{1}\bar{4}2\bar{1}\bar{3}\{\bar{4}, \bar{3}, \bar{2}, \bar{1}\}3\bar{1}\bar{1}\{\bar{2}, \bar{1}\}4$. Begin with dangling strands labeled by $\text{osc}(w)$. First apply growth rule $3\bar{2}\bar{1} \rightarrow 4\bar{1}\bar{1}$, then apply $\bar{4}\bar{4} \rightarrow \emptyset$ and $1\bar{1} \rightarrow \emptyset$, etc. See Figure 23 for the resulting symmetrized six-vertex configuration and the final fully reduced hourglass plabic graph G , with its growth labeling.

The following is the main result of this section.

Theorem 5.3. *Applying the growth algorithm (Algorithm 5.1) to $T \in \text{RFT}(\underline{c})$ always terminates in finitely many steps at an hourglass plabic graph $G = \mathcal{G}(T) \in \text{CRG}(\underline{c})$. Moreover,*

- (i) G is fully reduced,
- (ii) $\text{trip}_\bullet(G) = \text{prom}_\bullet(T)$,
- (iii) $\Gamma(G)$ is the unique proper labeling of G with boundary $w = L(T)$,
- (iv) all other proper labelings ϕ of G have $\partial(\phi) >_{\text{lex}} w$, and
- (v) $i \in \text{Des}(w)$ (see Definition 5.30) if and only if boundary vertices b_i and b_{i+1} of G are connected to the same vertex.

Remark 5.4. While any sequence of choices in Algorithm 5.1 eventually results in some hourglass plabic graph G , in contrast to the growth rules in [KK99] for the case $r = 3$, the resulting G

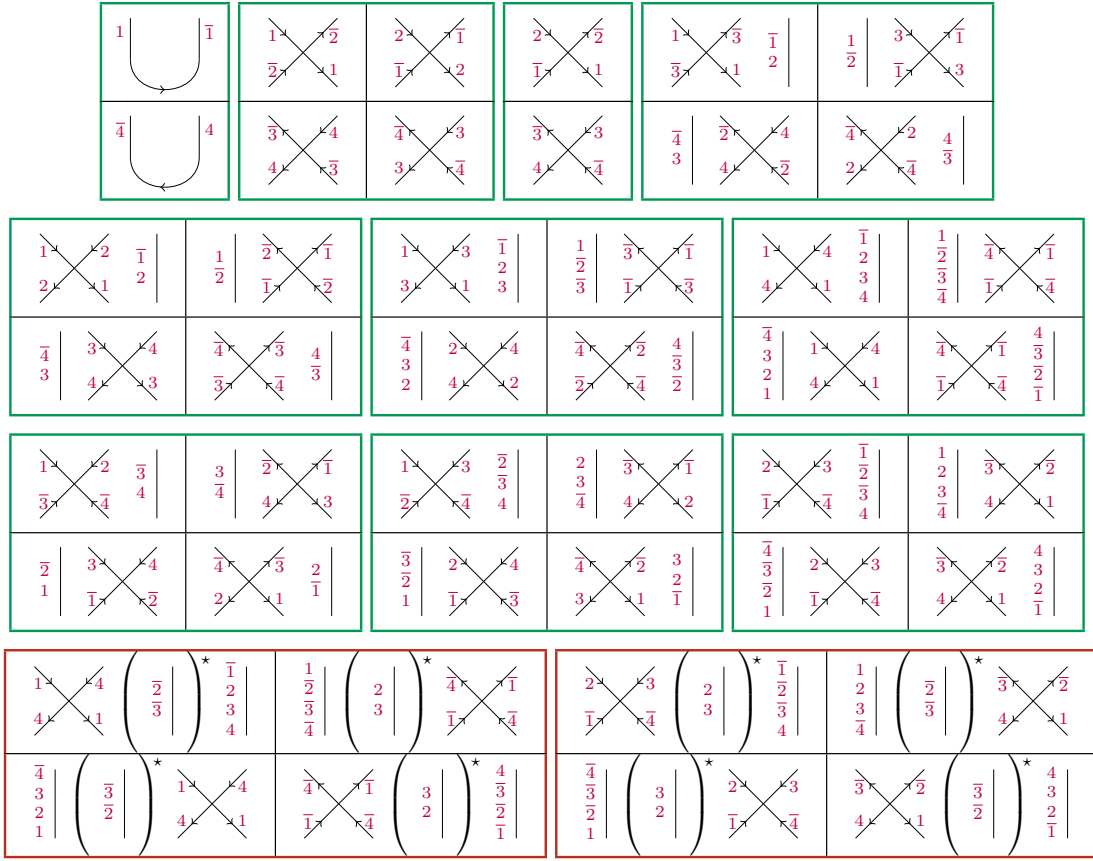


FIGURE 22. The growth rules of Algorithm 5.1. The 88 short rules of length 2 or 3 are boxed in green (■) and fall into 10 families. Vertical lines with multiple labels indicate that a *witness* with one of these labels must be present. Two additional families of long rules extend two of the short families and are boxed in red (■). Each of these long rules includes a witness in parentheses with a \star beside it; this means multiple such witnesses (or none) may appear.

is not independent of the choices made. However, by Theorem 3.13 and Theorem 5.3(i)–(ii), all choices produce hourglass plabic graphs in the same move-equivalence class. We will later see in Theorem 6.1 that every move-equivalence class of $\text{CRG}(\underline{c})$ has an element produced by the growth algorithm. Furthermore, every element of this move-equivalence class has a unique $\tilde{\text{lex}}$ -minimal proper labeling with boundary w . The rules presented here do not in general produce all elements of all move-equivalence classes, though they always produce at least one.

The proof of Theorem 5.3 occupies the remainder of Section 5. It may be skipped by a reader willing to accept Theorem 5.3 as a black box; however, we believe the crystal-theoretic techniques developed here may be of independent interest.

5.2. Plumbings, promotion appliances, and good degenerations. We use the notions in Definition 5.5 to track partially defined trip and promotion permutations through each step of the growth algorithm. See Figure 24 for an example.

Definition 5.5. A *plumbing* from set B' to set B is a tuple $\pi_\bullet = (\pi_1, \dots, \pi_{r-1})$ of bijections $\pi_i: B' \sqcup B \rightarrow B' \sqcup B$, such that $\pi_s^{-1} = \pi_{r-s}$ for all $s \in [r-1]$. The *transpose* π_\bullet^\top of π_\bullet is the plumbing defined by $\pi_s^\top = \pi_{r-s}$. The *composite* of plumbings σ_\bullet from B'' to B' and π_\bullet from B' to

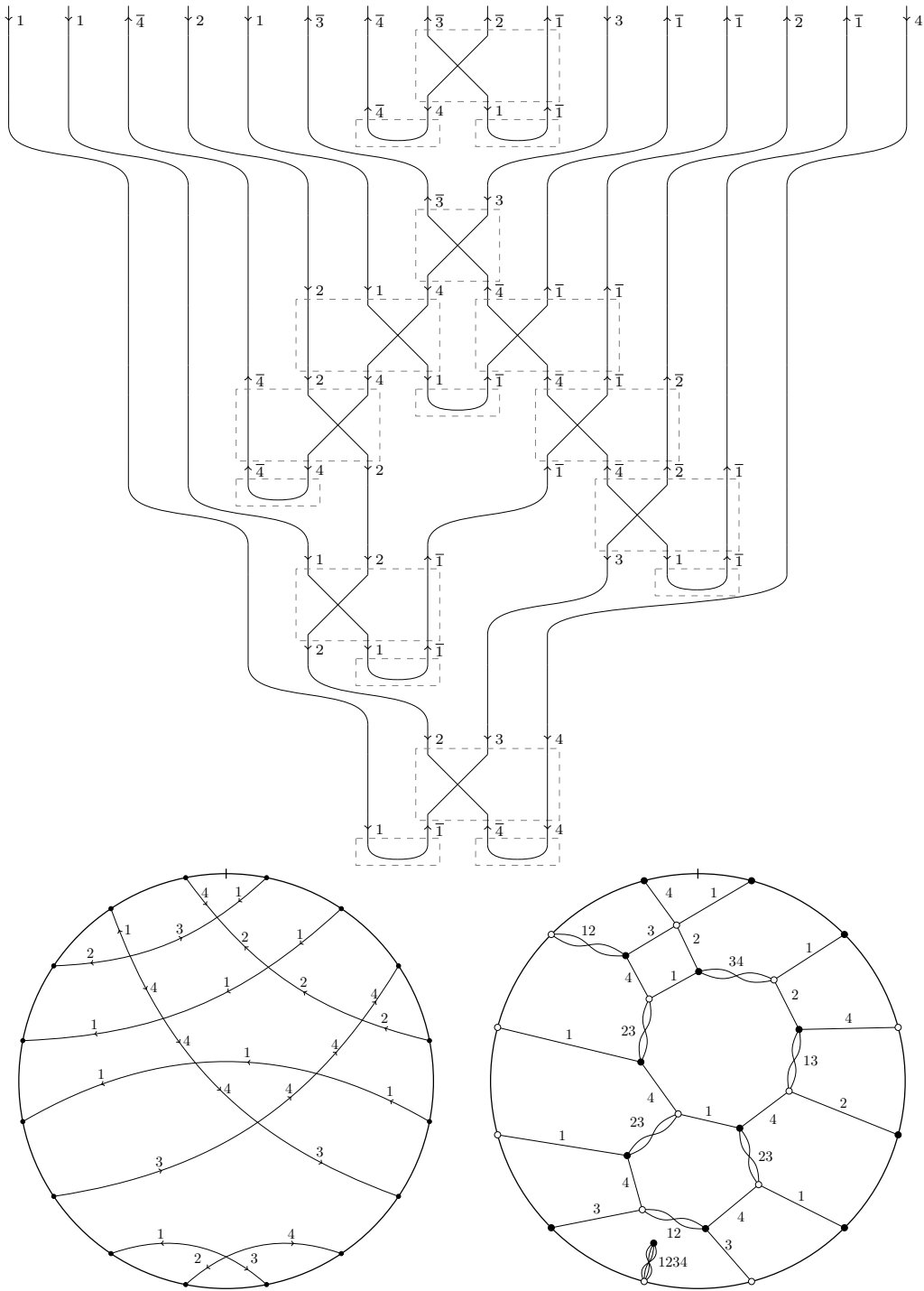


FIGURE 23. An example of the growth algorithm, Algorithm 5.1. The top diagram illustrates the process of applying the growth rules of Figure 22; the lower left diagram is a resulting symmetrized six-vertex configuration; and the lower right diagram is the resulting fully reduced hourglass plabic graph G , together with its growth labeling. The $|$ on each circle marks the location of the base face. See Example 5.2 for discussion.

B is the plumbing $\pi_\bullet \circ \sigma_\bullet$ from B'' to B where $(\pi_\bullet \circ \sigma_\bullet)_s: B'' \sqcup B \rightarrow B'' \sqcup B$ sends each $i \in B$ to the first value of $\cdots \circ \pi_s \circ \sigma_s \circ \pi_s(i)$ that is in $B'' \sqcup B$ and sends each $i \in B''$ to the first value of $\cdots \circ \sigma_s \circ \pi_s \circ \sigma_s(i)$ that is in $B'' \sqcup B$.

An *appliance* $g_\bullet = (g_1, \dots, g_{r-1})$ on $A \sqcup B \sqcup C$ is a tuple of functions $g_i: B \rightarrow A \sqcup B \sqcup C$, such that $g_s(i) = j \Leftrightarrow g_{r-s}(j) = i$ for all $s \in [r-1]$ and $i, j \in B$. The transpose g_\bullet^\top of g_\bullet is the appliance defined by $g_s^\top = g_{r-s}$. A plumbing π_\bullet from B' to B acts on an appliance g_\bullet on $A \sqcup B \sqcup C$ on the right and results in an appliance $g_\bullet \cdot \pi_\bullet$ on $A \sqcup B' \sqcup C$ where $(g_\bullet \cdot \pi_\bullet)_s$ sends each $i \in B'$ to the first value of $\cdots \circ \pi_s \circ g_s \circ \pi_s(i)$ that is in $A \sqcup B' \sqcup C$.

Finally, if $h: A \sqcup C \rightarrow A' \sqcup C'$ is any function, then $h \cdot g_\bullet$ is the appliance on $A' \sqcup B \sqcup C'$ where $(h \cdot g_\bullet)_s = \check{h} \circ g_s$ where $\check{h}: A \sqcup B \sqcup C \rightarrow A' \sqcup B \sqcup C'$ is the extension of h which fixes B .

We visualize a plumbing π_\bullet from B' to B as a network of connections from a line of nodes B' at the top to nodes B at the bottom as in Figure 24. We think of inputs i to π_s as inputs to the network, initially headed downward for $i \in B'$ and upward for $i \in B$. Outputs i of π_s are outputs of the network, headed upward for $i \in B'$ and downward for $i \in B$. Plumblings are composed by concatenating networks. An appliance g_\bullet on $A \sqcup B \sqcup C$ is visualized as a line of nodes from A, B, C . Inputs $i \in B$ to g_s initially head downward through a network and finish by heading upward into A, B , or C . Plumblings act on appliances also by concatenation. The actions satisfy $g_\bullet \cdot (\pi_\bullet \circ \sigma_\bullet) = (g_\bullet \cdot \pi_\bullet) \cdot \sigma_\bullet$ and $(h \cdot g_\bullet) \cdot \pi_\bullet = h \cdot (g_\bullet \cdot \pi_\bullet)$.

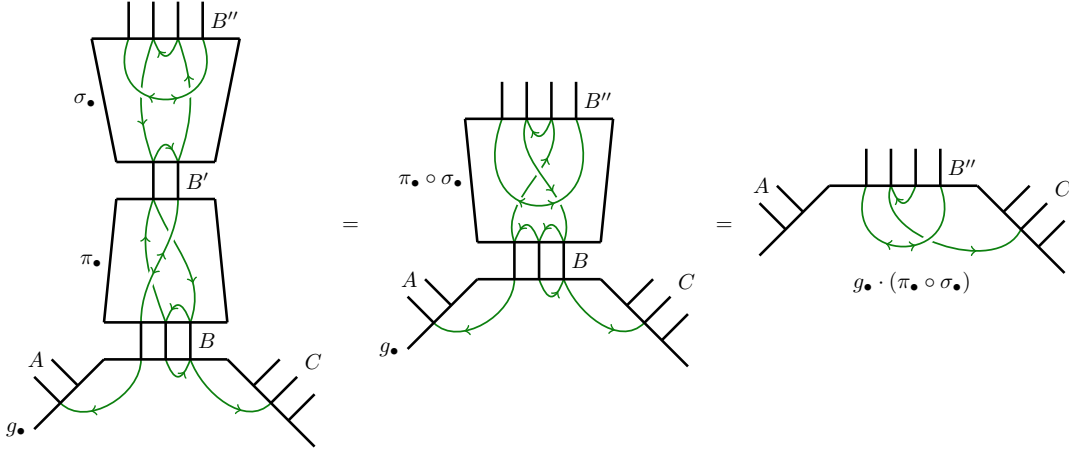


FIGURE 24. Graphical representations of plumblings and appliances.

A plumbing that arises from the trip permutations of a portion of an hourglass plabic graph (or a symmetrized six-vertex configuration) is *realizable*. A plumbing without such a realization is called *virtual*. There are natural notions of the *identity* plumbing id and of the *product* of two plumblings, which is given by horizontal concatenation and denoted by \times . For a rectangular fluctuating tableau T or an hourglass plabic graph G , $\text{prom}_\bullet(T)$ and $\text{trip}_\bullet(G)$ can be thought of as appliances from $[n]$ to $\emptyset \sqcup [n] \sqcup \emptyset$.

The substitutions allowed in the growth algorithm are of the following sort. The growth rules in Figure 22 will be our main examples.

Definition 5.6. A *good degeneration* is a substitution $v_1 \cdots v_p \rightarrow v'_1 \cdots v'_q$ where $v_i, v'_i \in \mathcal{A}_r$, together with a plumbing π_\bullet from $[p]$ to $[q]$, such that the following hold for every balanced lattice word $w = w_1 \cdots w_n$:

- (i) Replacing a consecutive substring $v_1 \cdots v_p$ in w with $v'_1 \cdots v'_q$ results in a new balanced lattice word $w' = w_1 \cdots w_j v'_1 \cdots v'_q w_{j+p+1} \cdots w_n$.

(ii) We have

$$(5.1) \quad \mathbf{prom}_\bullet(w) = \mathbf{prom}_\bullet(w') \cdot \check{\pi}_\bullet,$$

where the plumbing $\check{\pi}_\bullet = \text{id}^j \times \pi_\bullet \times \text{id}^{n-j-p}$ corresponds to the replacement $w \rightarrow w'$.

Good degenerations have a natural 4-fold symmetry. Recall the operations on words τ, ϖ, ϵ from Definition 4.3. These operations are applied to hourglass plabic graphs or a realizable plumbings as follows: ϖ acts by inverting the color of all vertices; ϵ acts by reflection through the vertical axis; and τ acts by both inversion and reflection. The following is a simple consequence of the interaction between these involutions and $\mathbf{prom}_\bullet(T)$ using [GPPSS24a, Lem. 5.12].

Lemma 5.7. *Suppose $v \rightarrow v'$ is a good degeneration with (realizable) plumbing π_\bullet . Then $\iota(v) \rightarrow \iota(v')$ is a good degeneration with (realizable) plumbing $\iota(\pi_\bullet)$ for all $\iota \in \{\tau, \varpi, \epsilon\}$.*

The 10 families of growth rules in Figure 22 are orbits under this 4-fold symmetry, where the left/right symmetry is τ , the top/bottom symmetry is ϵ , and the diagonal symmetry is ϖ . The 14 growth rules in [KK99] can similarly be grouped into 5 families, two of size 4 and three of size 2.

5.3. A crystal-theoretic good degeneration algorithm. We now provide an algorithm for establishing that a given substitution satisfies (5.1). Our proof relies on Kashiwara's theory of crystals [Kas90]. See [GPPSS24a, §8] for background and conventions; our conventions mostly match those of the textbook [BS17], except that we follow [Kas90] in using the original tensor product convention, which is opposite to that of [BS17].

Definition 5.8. Suppose that v is a word on \mathcal{A}_r and that uvw is a balanced lattice word. The *promotion appliance* associated to the inclusion $v \rightarrow uvw$ is the appliance $\rho_\bullet(u, v, w)$ on $A \sqcup B \sqcup C = \{1, \dots, |u|\} \sqcup \{|u| + 1, \dots, |u| + |v|\} \sqcup \{|u| + |v| + 1, \dots, |u| + |v| + |w|\}$ defined by

$$\rho_s(u, v, w)(i) = \mathbf{prom}_s(uvw)(i) \quad \text{for } i \in B.$$

The appliance $\rho_\bullet(u, v, w)$ encodes the rows of the *promotion matrix* $\mathbf{M}(uvw)$ (defined as in [GPPSS24a, Def. 5.14]) corresponding to entries from v . We will see that the following crystal-theoretic construction is well-defined and corresponds to the columns of $\mathbf{M}(uvw)$ with entries from v . Let $\mathcal{B}(\Lambda^{\underline{c}}V)$ be the $U_q(\mathfrak{sl}_r)$ -crystal of words associated to the representation $\Lambda^{\underline{c}}V$. The highest-weight elements of $\mathcal{B}(\Lambda^{\underline{c}}V)$ are the lattice words of type \underline{c} and the balanced lattice words are the highest-weight elements of weight zero. All crystals we consider will consist of unions of connected components of such crystals.

Definition 5.9. Let v be a word in a connected crystal with highest-weight element v^\uparrow , lowest-weight element v^\downarrow , and $|v| = b$. Fix an increasing and a decreasing path

$$\text{osc}(v) = v^0 \xrightarrow{e_{s_1}} v^1 \xrightarrow{e_{s_2}} \dots \xrightarrow{e_{s_a}} v^a = \text{osc}(v^\uparrow),$$

$$\text{osc}(v) = u^c \xrightarrow{f_{t_c}} u^{c-1} \xrightarrow{f_{t_{c-1}}} \dots \xrightarrow{f_{t_1}} u^0 = \text{osc}(v^\downarrow).$$

Let $\vec{e} = (s_1, \dots, s_a)$, $\vec{f} = (t_c, \dots, t_1)$. The *crystal appliance* associated to these paths is the appliance $\rho_\bullet(\vec{e}, v, \vec{f})$ on $\{1, \dots, a\} \sqcup \{a + 1, \dots, a + b\} \sqcup \{a + b + 1, \dots, a + b + c\}$ defined as follows:

- If $v^i = e_s(v^{i-1})$ is applied at the j -th letter, set $\rho_s(a + j) = i$.
- If $u^{i-1} = f_s(u^i)$ is applied at the j -th letter, set $\rho_s(a + j) = a + b + i$.
- If $\mathbf{prom}_s(v^\uparrow \epsilon(v^\downarrow))(j) = i$ where $1 \leq i, j \leq b$, set $\rho_s(a + j) = a + i$.

Lemma 5.10. *Let uvw be a balanced lattice word. Then there exist \vec{e}, \vec{f} , and h such that*

$$(5.2) \quad \rho_\bullet(u, v, w)^\top = h \cdot \rho_\bullet(\vec{e}, v, \vec{f}).$$

Here $|u| = a$, $|v| = b$, $|w| = c$, $\vec{e} \in [r-1]^{a'}$, $\vec{f} \in [r-1]^{c'}$, and $h: \{1, \dots, a'\} \sqcup \{a' + b + 1, \dots, a' + b + c'\} \rightarrow \{1, \dots, a\} \sqcup \{a + b + 1, \dots, a + b + c\}$ is the disjoint union of two weakly increasing functions.

Proof. Since $\mathbf{prom}_s(uvw) = \mathbf{prom}_{r-s}(uvw)^{-1}$, $\rho_\bullet(u, v, w)^\top$ corresponds to the columns of v in $\mathbf{M}(uvw)$. These columns may be computed crystal-theoretically as follows. The crystal raising algorithm (see [GPPSS24a, Prop. 8.20]) computes $\mathcal{P}(\mathbf{osc}(uvw))$ by cutting off the first letter, applying raising operators to reach the highest weight element, and appending the unique letter which yields the original weight. By [GPPSS24a, Thm. 8.24], $\mathbf{M}(uvw)_{i,i+j}$ contains s if and only if the raising operator e_s is applied at index j when applying \mathcal{P} to $\mathcal{P}^{i-1}(\mathbf{osc}(uvw))$, where $i+j$ is taken modulo $|uvw|$. Equivalently, $\mathbf{prom}_s(uvw)(i) = i+j$. We illustrate phases of this operation in Figure 25.

During the raising algorithm, the subword corresponding to $\mathbf{osc}(v)$ shifts leftward as initial letters are repeatedly cut off. After the initial phase I consisting of a promotion steps, this subword has shifted to the beginning and has become a highest-weight word. Each promotion step computes one row of $\mathbf{M}(uvw)$. Raising operators applied outside of the subword do not appear in the columns of v in $\mathbf{M}(uvw)$ and may be ignored. If a' raising operators are applied to the subword during phase I, we have a path $\mathbf{osc}(v) \rightarrow \mathbf{osc}(v^\uparrow)$ in the connected crystal of $\mathbf{osc}(v)$ with a' steps, by the associativity of the crystal tensor product. If e_s is applied at the j -th letter of the subword during step i' of the crystal path, then e_s is applied at the $(a+j)$ -th letter of the original word when computing some row i of $\mathbf{M}(uvw)$. In this case, $\rho_s(a+j) = i'$ and $\mathbf{prom}_s(uvw)(i) = a+j$. The function $i' \mapsto i$ is weakly increasing and fulfills (5.2) for these values.

After phase I, the next phase II consists of b promotion steps. It computes the upper triangle of the rows and columns of v in $\mathbf{M}(uvw)$. This calculation depends only on the initial b letters, namely $\mathbf{osc}(v^\uparrow)$. Hence $\mathbf{prom}_s(uvw)(a+i) = a+j$ if and only if $\mathbf{prom}_s(v^\uparrow v')(i) = j$ for $1 \leq i < j \leq b$, where v' is any word such that $v^\uparrow v'$ is balanced, so in particular for $v' = \varepsilon(v^\uparrow)$. Thus (5.2) also holds for these values. Note that when any particular letter of $\mathbf{osc}(v)$ reaches the beginning of the lattice word in phase II, it has been transformed into 1 or \bar{r} .

Phases III and IV, as illustrated in Figure 25, determine the other half of the columns of v in $\mathbf{M}(uvw)$. We may imagine the promotion algorithm is applied in reverse from the bottom up since $\mathcal{P}^n(uvw) = uvw$, in which case phase III produces a decreasing path $\mathbf{osc}(v) \rightarrow \mathbf{osc}(v^\downarrow)$ of length c' . During phase IV, the relevant lower triangle of $\mathbf{M}(v^\uparrow \varepsilon(v^\uparrow))$ agrees with that of $\mathbf{M}(uvw)$ by [GPPSS24a, Thm. 8.25]. Thus (5.2) holds.

Note that if we track the letters in a particular column of v in $\mathbf{M}(uvw)$ through this process from phase II to I to III to IV, we have $1 \rightarrow \dots \rightarrow r$ or $\bar{r} \rightarrow \dots \rightarrow \bar{1}$, so $\rho_\bullet(\vec{e}, v, \vec{f})$ is indeed well-defined. The same argument applies even if \vec{e} and \vec{f} have not necessarily come from some uvw , so crystal appliances are well-defined in general. \square

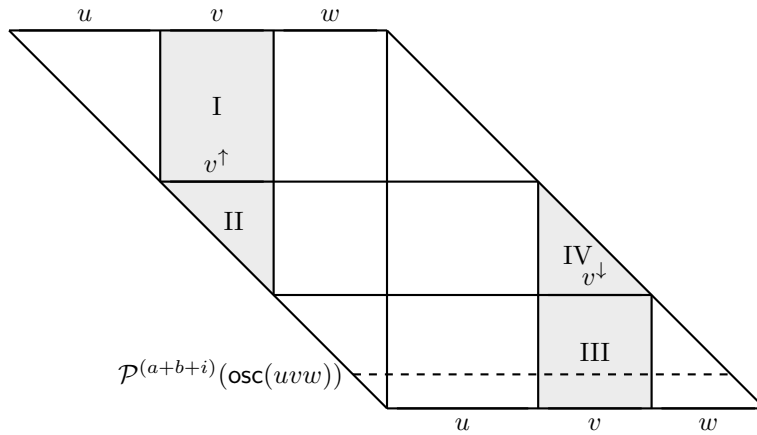


FIGURE 25. Phases of the crystal raising algorithm to compute $\mathbf{M}(uvw)$.

The following result is our main tool for proving that a particular substitution is a good degeneration and, in turn, for proving the validity of the growth rules. Our setup applies for general r and in particular can be used to easily re-verify the $r = 3$ growth rules of Khovanov–Kuperberg [KK99]. In this paper we focus on the case $r = 4$, but we aim in future work to apply these techniques for higher r (and in other Lie types).

Theorem 5.11. *Let v, v' be words on \mathcal{A}_r with $B \sqcup B' = \{1, \dots, |v|\} \sqcup \{|v|+1, \dots, |v|+|v'|\}$. Suppose there is an $U_q(\mathfrak{sl}_r)$ -crystal isomorphism sending v to v' . If there is a plumbing π_\bullet from B to B' such that*

$$(5.3) \quad \rho_\bullet(\vec{e}, v, \vec{f})^\top = \rho_\bullet(\vec{e}, v', \vec{f})^\top \cdot \pi_\bullet$$

for all \vec{e}, \vec{f} , then $v \rightarrow v'$ with plumbing π_\bullet is a good degeneration.

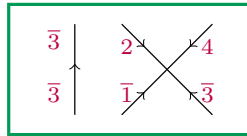
Proof. Suppose uvw is a balanced lattice word. Since v and v' are corresponding vertices in isomorphic crystal graphs, $uv'w$ is a balanced lattice word. Moreover, from the proof of Lemma 5.10 and Figure 25, the portions of $\mathbf{M}(uvw)$ and $\mathbf{M}(uv'w)$ corresponding to rows or columns from u or w are the same. Hence (5.1) holds here directly. By symmetry, it now suffices to consider only the rows corresponding to v .

Let $\text{prom}_\bullet(uvw)|_v$ denote the appliance restricting the domain to entries corresponding to v . By Lemma 5.10 and (5.3),

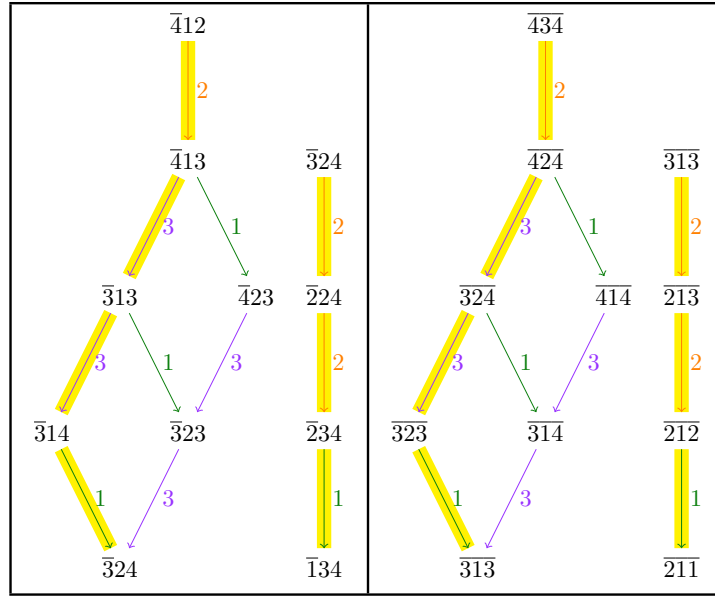
$$\begin{aligned} \text{prom}_\bullet(uv'w)|_{v'} \cdot \pi_\bullet &= \rho_\bullet(u, v', w) \cdot \pi_\bullet = h \cdot \rho_\bullet(\vec{e}, v', \vec{f})^\top \cdot \pi_\bullet \\ &= h \cdot \rho_\bullet(\vec{e}, v, \vec{f})^\top = \rho_\bullet(u, v, w) \\ &= \text{prom}_\bullet(uvw)|_v. \end{aligned}$$

Here the fact that there is a crystal isomorphism sending v to v' implies that \vec{e}, \vec{f} , and h from Lemma 5.10 are the same. We now have (5.1). \square

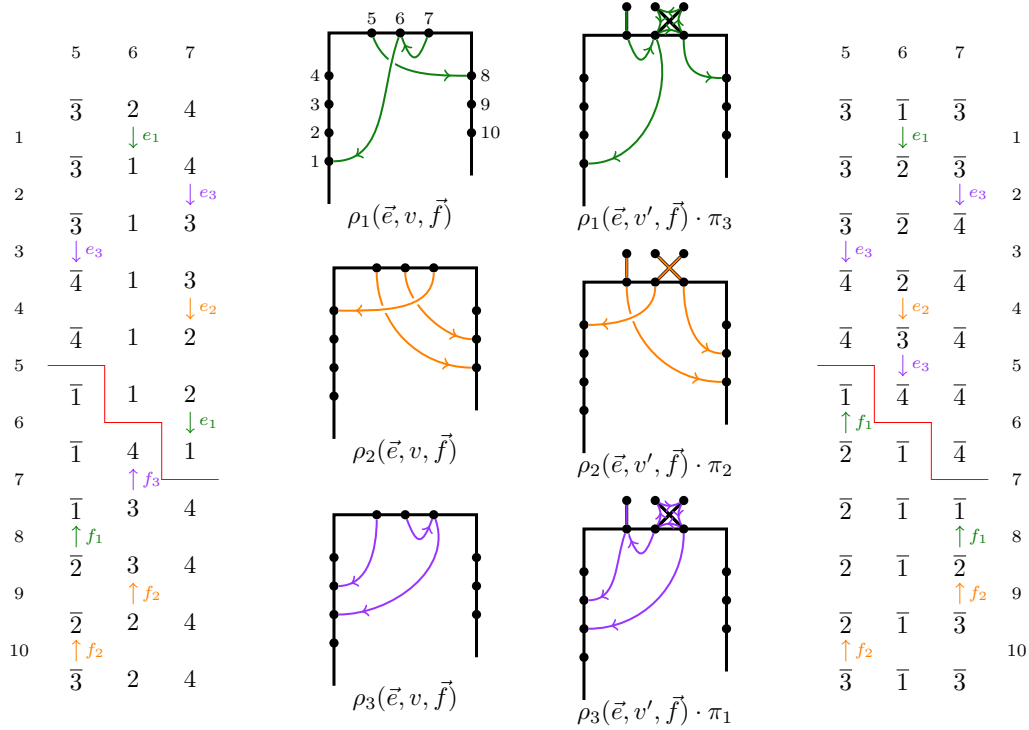
Example 5.12. For any proposed substitution $v \rightarrow v'$, Theorem 5.11 reduces the *a priori* infinite list of conditions in (5.1) to a finite calculation. We summarize part of this calculation for the good degeneration $\overline{3}24 \rightarrow \overline{3}1\overline{3}$ with the following realizable plumbing:



First, we compute the portions of the crystals above and below $\overline{3}24$ and $\overline{3}1\overline{3}$ and pick corresponding paths to the highest and lowest weight elements:



Each path yields a possible column in $\mathbf{M}(uvw)$. We then compute the crystal appliances and verify that applying π_\bullet to $\rho_\bullet(\vec{e}, v', \vec{f})^\top$ yields $\rho_\bullet(\vec{e}, v, \vec{f})^\top$:



Proposition 5.13. *The 88 short rules of length 2 or 3 in Figure 22 are good degenerations.*

Proof. In each case, the result follows from Theorem 5.11 exactly as in Example 5.12. The calculations are lengthy, routine, and omitted. Using Lemma 5.7 reduces the labor considerably. \square

5.4. Long good degenerations. We now prove that the two families of long growth rules in Figure 22 are also good degenerations. Our argument will involve the plumbings in Figure 26.

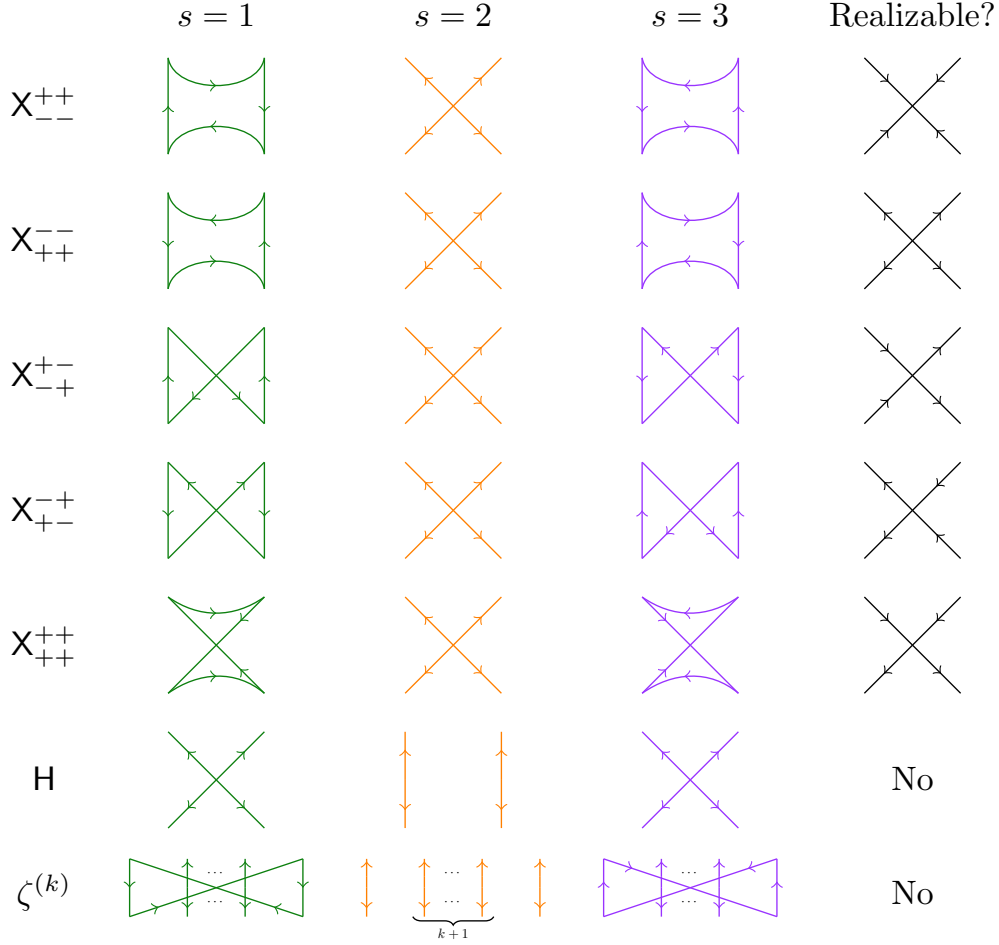


FIGURE 26. Some realizable and virtual plumbings needed to establish the long growth rules of Figure 22.

Lemma 5.14. *The following are good degenerations, which are their own inverses.*

- (i) For plumbing H: $\bar{3}2 \leftrightarrow 2\bar{3}$, $\bar{2}2 \leftrightarrow 3\bar{3}$, $\bar{2}3 \leftrightarrow 3\bar{2}$, $\bar{3}1 \leftrightarrow 24$, $\bar{2}1 \leftrightarrow 34$, $\bar{3}2 \leftrightarrow 14$, $\bar{4}2 \leftrightarrow 13$, $\bar{4}3 \leftrightarrow 12$.
- (ii) For plumbing X_{-+}^{+-} : $\bar{1}2 \leftrightarrow \bar{2}1$, $\bar{2}1 \leftrightarrow \bar{1}2$, $\bar{2}2 \leftrightarrow \bar{1}1$.
- (iii) For plumbing X_{+-}^{-+} : $\bar{3}4 \leftrightarrow \bar{4}3$, $\bar{4}3 \leftrightarrow \bar{3}4$, $\bar{3}3 \leftrightarrow \bar{4}4$.

Proof. This is a direct verification using Theorem 5.11. □

Remark 5.15. Strictly speaking, the plumbings in Lemma 5.14(ii) and (iii) are only realizable in one direction. For instance, the substitution $\bar{2}1 \rightarrow \bar{1}2$ would normally expect to be associated to the plumbing X_{-+}^{+-} in order for the six-vertex edge directions to be consistent with the label signs, though this is not in fact a good degeneration. Good degenerations are typically not invertible, since plumbings do not in general possess inverses; however, these good degenerations are invertible.

Lemma 5.16. *The following are good degenerations, for all $k \in \mathbb{Z}_{\geq 0}$.*

- (i) For plumbing $X_{++}^{--} \times \text{id}^{k+1}$: $\bar{3}2\bar{2}^k 4 \rightarrow 4\bar{1}2^k 4$.
- (ii) For plumbing $X_{++}^{++} \times \text{id}^{k+1}$: $14\bar{2}^k 4 \rightarrow 4\bar{1}2^k 4$.
- (iii) For plumbing $X_{--}^{++} \times \text{id}^{k+1}$: $23\bar{2}^k 4 \rightarrow \bar{1}4\bar{2}^k 4$.

(iv) For plumbing $\zeta^{(k)}: 4\overline{12}^k 4 \rightarrow \overline{322}^k 4$.

Moreover, the composite $\zeta^{(k)} \circ (X_{++}^- \times \text{id}^{k+1})$ acts as the identity on the appliance $\rho_\bullet(\vec{e}, \overline{322}^k 4, \vec{f})^\top$.

Proof. Consider (i). In Figure 27, we depict finite state machines representing all elements reachable from $\overline{322}^k 4$ by e_i 's or by f_i 's, together with information equivalent to $\text{prom}_\bullet(v^\uparrow \varepsilon(v^\uparrow))$. One may check the correctness of Figure 27 directly, by using the bracketing rule for the action of crystal raising and lowering operators. Likewise, Figure 28 depicts equivalent information for the word $4\overline{12}^k 4$. We may read off promotion appliances from this data as in Figure 29. Thus (5.3) holds in this case. The claim about the composite may also be verified directly from Figures 26 and 29.

The other verifications are virtually identical and the details are omitted. In each case the finite state machines from Figures 27 and 28 are the same as for $14\overline{2}^k 4$, $23\overline{2}^k 4$, and $\overline{142}^k 4$ aside from the first two and final letters, which may be read off from the $k = 0$ case. \square

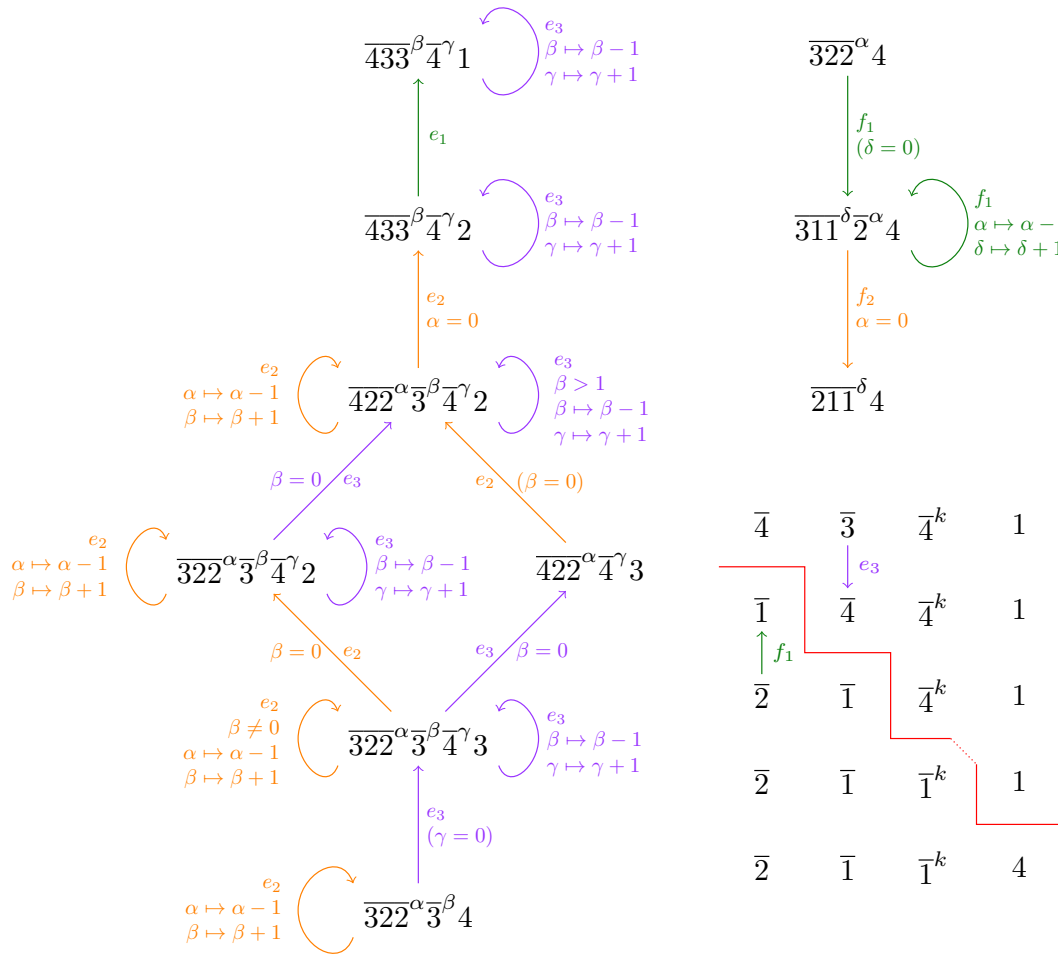


FIGURE 27. Finite state machines for $\overline{322}^k 4$. Here $\alpha + \beta + \gamma + \delta = k$.

Theorem 5.17. *The growth rules in Figure 22 are all good degenerations.*

Proof. The short rules were handled in Proposition 5.13. It remains to consider the two families of long rules in Figure 22. For these, we induct on length; the length-3 base cases are contained among

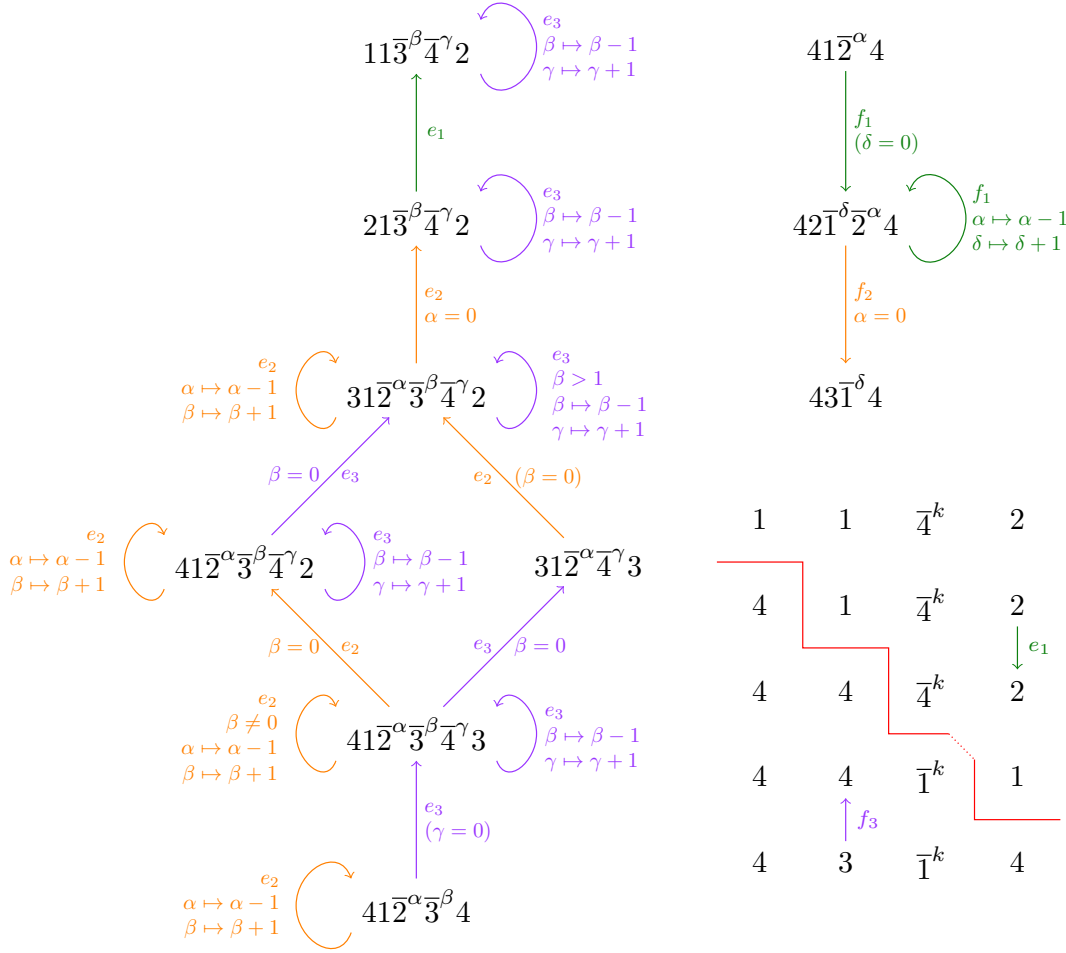


FIGURE 28. Finite state machines for $41\bar{2}^k 4$.

the short rules. We focus on $14wx$ where $w \in \{\bar{3}, \bar{2}\}^*$ and $x \in \{2, 3, 4, \bar{1}\}$; the argument for $23wx$ is identical. First suppose $x = 2$.

- If $w = \dots \bar{2}$, apply $14 \dots \bar{2}2 \rightarrow 14 \dots \bar{3}\bar{3} \rightarrow 41 \dots \bar{3}\bar{3} \rightarrow 41 \dots \bar{2}2$. The first and third steps use the plumbings in Lemma 5.14(i) and the second step uses induction. The first and third plumbings cancel each other.
- If $w = \dots \bar{3}$, apply $14 \dots \bar{3}2 \rightarrow 14 \dots \bar{2}\bar{3} \rightarrow 41 \dots \bar{2}\bar{3} \rightarrow 41 \dots \bar{3}2$ likewise.

The $x = 3$ and $x = \bar{1}$ cases are extremely similar and are omitted.

Now suppose $x = 4$. If $w = \dots \bar{3}$, the above argument again applies, so take $w = \dots \bar{2}$. If w contains no $\bar{3}$, the result is Lemma 5.16(ii). Otherwise, $w = \dots \bar{3}\bar{2}\bar{2}^k$ for some $k \in \mathbb{Z}_{\geq 0}$. Now apply the substitutions $14 \dots \bar{3}\bar{2}\bar{2}^k 4 \rightarrow 14 \dots 41\bar{2}^k 4 \rightarrow 41 \dots 41\bar{2}^k 4 \rightarrow 41 \dots \bar{3}\bar{2}\bar{2}^k 4$, where the first and third steps use Lemma 5.16 and the second step uses induction. While the plumbings from the two applications of Lemma 5.16 do not cancel, nonetheless their composite acts as the identity on the promotion appliances of $\bar{3}\bar{2}\bar{2}^k 4$. Hence we may remove their composite from the structure entirely, completing the induction and proof. \square

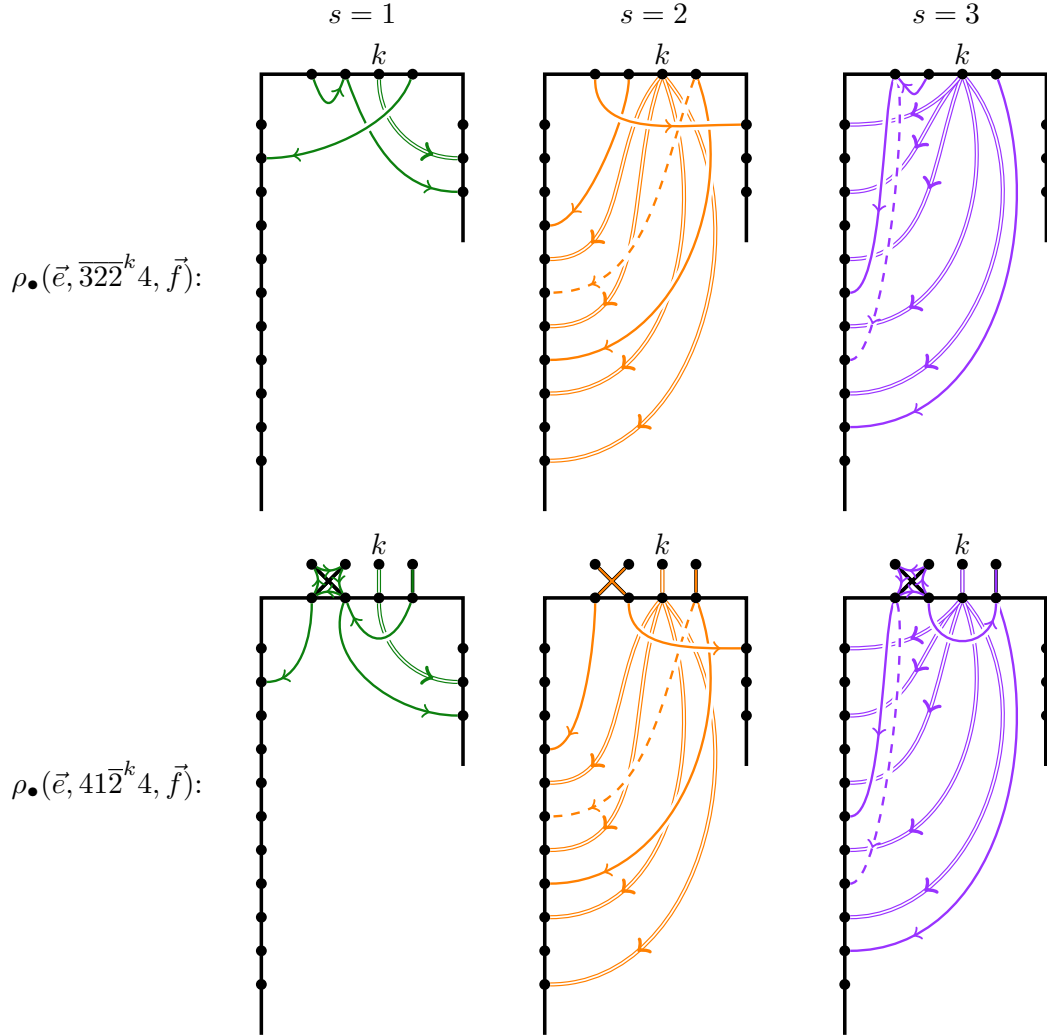


FIGURE 29. Promotion appliances for $\overline{322^k 4}$ and $412^k 4$. The plumbing in this case involves the source X_{++}^- .

5.5. Completeness of the growth rules. We now show that any balanced lattice word w of oscillating type with $r = 4$ has at least one applicable growth rule. Recall the notation \tilde{i} from Definition 2.10, which represents either i or $\overline{r-i+1}$. Note that the involutions τ and ε act on \tilde{w} by reversing and performing substitutions $\tilde{1} \leftrightarrow \tilde{4}$, $\tilde{2} \leftrightarrow \tilde{3}$. The composite ϖ fixes \tilde{w} . By inspecting Figure 22, we have the following.

Lemma 5.18. *At least one of the short growth rules in Figure 22 applies whenever any of the following patterns appears in \tilde{w} :*

$$\tilde{1}\tilde{1}\tilde{4}, \tilde{1}\tilde{2}\tilde{3}, \tilde{1}\tilde{2}\tilde{4}, \tilde{1}\tilde{3}\tilde{2}, \tilde{1}\tilde{3}\tilde{3}, \tilde{1}\tilde{3}\tilde{4}, \tilde{1}\tilde{4}\tilde{4}, \tilde{2}\tilde{2}\tilde{4}, \tilde{2}\tilde{3}\tilde{4}, \tilde{3}\tilde{2}\tilde{4}.$$

Lemma 5.19. *At least one of the growth rules in Figure 22 applies whenever any of the following patterns appears in \tilde{w} :*

$$\tilde{1}\tilde{4}x\tilde{4}, \tilde{1}x\tilde{1}\tilde{4}, \tilde{2}\tilde{3}x\tilde{4}, \tilde{1}x\tilde{2}\tilde{3},$$

where x is a word consisting entirely of $\tilde{2}$'s and $\tilde{3}$'s.

Proof. The first two patterns and last two patterns are equivalent under τ . For $\tilde{1}\tilde{4}x\tilde{4}$, apply ϖ to consider $1\tilde{4}x\tilde{4}$. A rule applies to $1\tilde{1}$, so we have $14x\tilde{4}$. If x contains a 2 or 3, a long growth rule applies to the prefix ending at the leftmost 2 or 3 in x . Otherwise, a long growth rule still applies. The argument for $\tilde{2}\tilde{3}x\tilde{4}$ is essentially identical. \square

Lemma 5.20. *At least one of the growth rules in Figure 22 applies to any non-empty balanced lattice word w .*

Proof. Consider \tilde{w} , which must begin with $\tilde{1}$ and which must end with $\tilde{4}$. Consider the rightmost $\tilde{1}$. It is followed by a letter other than $\tilde{1}$, so we consider the following three cases.

- $\cdots \tilde{1}\tilde{2}\cdots$: this must be $\cdots \tilde{1}\tilde{2}\tilde{2}^k\tilde{3}\cdots$ or $\cdots \tilde{1}\tilde{2}\tilde{2}^k\tilde{4}\cdots$. In the first case, apply Lemma 5.19. In the second case, we have $\cdots \tilde{1}\tilde{2}\tilde{4}\cdots$ or $\cdots \tilde{2}\tilde{2}\tilde{4}$, so apply Lemma 5.18.
- $\cdots \tilde{1}\tilde{3}\cdots$: this must be $\cdots \tilde{1}\tilde{3}\tilde{2}\cdots$, $\cdots \tilde{1}\tilde{3}\tilde{3}\cdots$, or $\tilde{1}\tilde{3}\tilde{4}\cdots$, so apply Lemma 5.18.
- $\cdots \tilde{1}\tilde{4}\cdots$: since w is reverse lattice, \tilde{w} cannot end in $\tilde{1}\tilde{4}$, so we have $\cdots \tilde{1}\tilde{4}w\tilde{4}\cdots$ where w consists entirely of $\tilde{2}$'s and $\tilde{3}$'s, so apply Lemma 5.19. \square

5.6. Linearized diagrams, nice labelings, and unitriangularity. Recall the $\tilde{\text{lex}}$ -order from Definition 2.10. Our next goal is to show that the growth labeling $\Gamma(G)$ yields the unique grevlex-maximal monomial in $[G]_q$. We will work in somewhat more generality so that our results will apply to all $G \in \text{CRG}(\underline{c})$, rather than just those produced by the growth algorithm. We begin by considering diagrams similar to those appearing at the top of Figure 23.

Definition 5.21. A *linearized diagram* is a symmetrized six-vertex configuration obtained by beginning with a row of directed dangling strands and at each step either (i) combining an adjacent pair of strands in an X, or (ii) combining an adjacent pair in a \cup , with all other strands extended directly down in either case, until there are no more dangling strands.

A *signed proper labeling* ϕ of a linearized diagram is a labeling of the edges by $\pm\{1, \dots, 4\}$ whose absolute value is a proper labeling (see Definition 3.24) and where the sign is positive for downward-pointing arrows and negative for upward-pointing arrows. The boundary $\partial(\phi)$ of ϕ is the word of oscillating type obtained by reading off the topmost labels from left to right.

A *nice labeling* of a linearized diagram is a signed proper labeling where the labels on the X's and \cup 's are those that appear in the X's and \cup 's of the growth rules in Figure 22, plus those appearing in Figure 30.

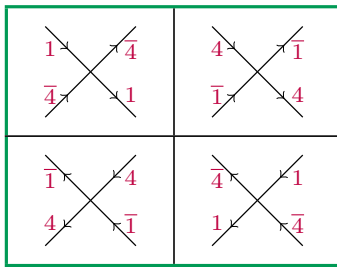


FIGURE 30. The additional directed X label configurations allowed in nice labelings.

Remark 5.22. The output G of the growth algorithm can be seen as a linearized diagram. The growth labeling $\Gamma(G)$ is a nice labeling without the configurations appearing in Figure 30. Strictly speaking, G also includes witness information, though linearized diagrams are more flexible and do not insist upon having witnesses. The additional configurations in Figure 30 do not correspond to good degenerations, though we will find that they arise when applying Yang–Baxter moves to such G . Despite ignoring witnesses, linearized diagrams with nice labelings track more information

than circular diagrams (such as in the lower-left of Figure 23), since they give a consistent set of orientations for each X and \cup .

The collection of possible nice labelings of X 's possesses the following properties.

Lemma 5.23. *Suppose $ab \rightarrow cd$ is the portion of a good degeneration from the growth rules in Figure 22 corresponding to the X , or similarly one of the additional labelings in Figure 30. Then the following hold:*

- (i) *Either $\tilde{a} = \tilde{b} = \tilde{c} = \tilde{d}$, or $\tilde{a} < \tilde{c}$ and $cd >_{1\tilde{e}\tilde{x}} ab$.*
- (ii) *Fixing labels ab at the top of the X and assigning labels cd at the bottom is the $1\tilde{e}\tilde{x}$ -maximal way to create a signed proper labeling at these vertices.*
- (iii) *Given an X properly labeled by pq at the top and ts at the bottom, if $ts \geq_{1\tilde{e}\tilde{x}} cd$, then $pq \geq_{1\tilde{e}\tilde{x}} ab$.*
- (iv) *If u, v are words of oscillating type where $ucdv$ is a lattice word, then $uabv$ is a lattice word with the same weight.*

Proof. All properties may be checked case-by-case. For example, consider $ab = 2\bar{2} \rightarrow \bar{1}1 = cd$. For (i), $\tilde{a} = \tilde{2} < 4 = \tilde{c}$. For (ii), expanding the X in this case yields two internal vertices connected horizontally by an hourglass. Labeling the top strands with 2's forces any proper labeling to label both bottom strands with the same number. The $1\tilde{e}\tilde{x}$ -maximal way of doing so uses 1's at the bottom, as in the growth rule. For (iii), we must consider $t = \bar{1}$, $s = 1, 2, 3, 4$. Using $s = 1$, proper labelings can have $pq = 2\bar{2}, 3\bar{3}, 4\bar{4}$. Each of these satisfies $pq \geq_{1\tilde{e}\tilde{x}} 2\bar{2}$. All other cases are similar. For (iv), the mixed-sign cases like $2\bar{2} \rightarrow \bar{1}1$ in fact involve a pair of vertices that correspond under a crystal isomorphism. For the remaining cases like $12 \rightarrow 21$, the direction in (iv) matters. \square

Equality in Lemma 5.23(i) occurs precisely for the additional labelings in Figure 30, which do not occur in growth labelings. The following important fact is then immediate.

Corollary 5.24. *If $w \rightarrow w'$ is obtained by applying a growth rule, then either w' is shorter than w , or $w' >_{1\tilde{e}\tilde{x}} w$. In particular, the growth algorithm cannot enter an infinite loop.*

Linearized diagrams with nice labelings have the following key property. Note that it applies to the output $\mathcal{G}(T)$ of the growth algorithm using the growth labeling.

Theorem 5.25. *Let G be a linearized diagram with a given nice labeling ψ and suppose ϕ is a (signed) proper labeling of G . Then:*

- (i) $\partial(\phi) \geq_{1\tilde{e}\tilde{x}} \partial(\psi)$,
- (ii) if $\partial(\phi) = \partial(\psi)$, then $\phi = \psi$, and
- (iii) $\partial(\psi)$ is a balanced lattice word.

In particular, linearized diagrams have at most one nice labeling.

Proof. We induct on the number of steps in the linearized diagram. The base case is trivial. If an end cap is the topmost step in G , the result is obvious by induction. If instead an X is the topmost step in G , let G' be the subgraph of G without this X and let ψ', ϕ' be the proper sub-labelings of ψ and ϕ restricted to G' . Since ψ' is a nice labeling, induction gives $\partial(\phi') \geq_{1\tilde{e}\tilde{x}} \partial(\psi')$. By Lemma 5.23(a), $\partial(\psi') \geq_{1\tilde{e}\tilde{x}} \partial(\psi)$, hence $\partial(\phi') \geq_{1\tilde{e}\tilde{x}} \partial(\psi)$. Note that $\partial(\psi), \partial(\psi')$ and $\partial(\phi), \partial(\phi')$ differ only at the positions of the X . Suppose that the X in ψ is labeled by ab at the top and cd at the bottom. Further suppose that the X in ϕ is labeled by pq at the top and ts at the bottom, so that the corresponding portion of $\partial(\phi')$ is ts and $\partial(\phi)$ is pq . If $\partial(\phi')$ does not agree with $\partial(\psi)$ up until the X , then $\partial(\phi') \geq_{1\tilde{e}\tilde{x}} \partial(\psi)$ implies $\partial(\phi) >_{1\tilde{e}\tilde{x}} \partial(\psi)$ and we are done. So, suppose $\partial(\phi')$ agrees with $\partial(\psi)$ at least until the X . Since $\partial(\phi') \geq_{1\tilde{e}\tilde{x}} \partial(\psi')$, we have $ts \geq_{1\tilde{e}\tilde{x}} cd$. By Lemma 5.23(iii), we have $pq \geq_{1\tilde{e}\tilde{x}} ab$. If $pq \neq ab$, then $\partial(\phi) >_{1\tilde{e}\tilde{x}} \partial(\psi)$, and (i) holds. If $pq = ab$, then by Lemma 5.23(ii), $cd \geq_{1\tilde{e}\tilde{x}} ts$, so $cd = ts$. Now $\partial(\phi')$ and $\partial(\psi')$ agree through at least the X , so $\partial(\phi') \geq_{1\tilde{e}\tilde{x}} \partial(\psi')$ implies $\partial(\phi) \geq_{1\tilde{e}\tilde{x}} \partial(\psi)$, giving (i).

Now suppose $\partial(\phi) = \partial(\psi)$. In the notation above, this gives $ab = pq$ and so, as before, $cd = ts$. Thus $\partial(\phi') = \partial(\psi')$, so $\phi' = \psi'$ by induction, and hence $\phi = \psi$, giving (ii).

For (iii), $\partial(\psi)$ is a balanced lattice word by Lemma 5.23(iv) and induction. \square

Our next goal is to show that one may apply Yang–Baxter moves to linearized diagrams in such a way that nice labelings are preserved.

Lemma 5.26. *The possible oriented triangles in linearized diagrams are those configurations depicted in Figure 31.*

Proof. The argument involves a straightforward though tedious case-by-case check. The details are omitted. \square

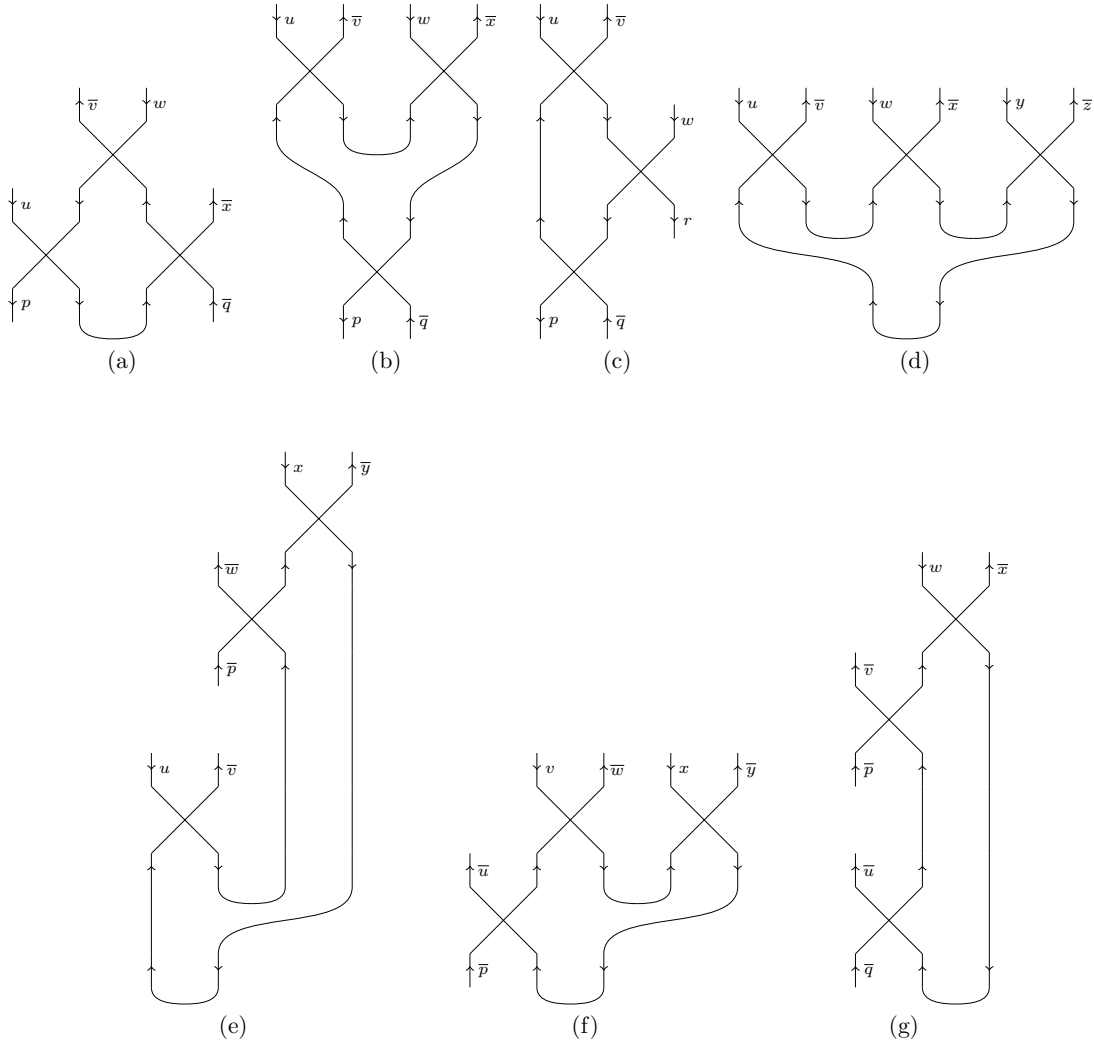


FIGURE 31. Configurations of oriented triangles in linearized diagrams. Those configurations obtained by reflecting through the vertical axis, reversing arrows, or both are also allowed, as are configurations obtained by shifting X 's while preserving the linearized structure and \cup 's.

Lemma 5.27. *Suppose one of the oriented triangles in Figure 31 appears in a nice labeling of a linearized diagram. The complete list of possible boundary conditions is in Table 1.*

Case(s)	Orientation(s)	u, v, \dots to p, q, \dots boundary conditions
(a), (b)	CCW, CW	$\overline{133\bar{1}} \rightarrow \overline{4\bar{4}} \quad \overline{142\bar{1}} \rightarrow \overline{2\bar{4}} \quad \overline{143\bar{1}} \rightarrow \overline{3\bar{4}} \quad \overline{134\bar{1}} \rightarrow \overline{4\bar{3}} \quad \overline{124\bar{1}} \rightarrow \overline{4\bar{2}}$ $\overline{422\bar{4}} \rightarrow \overline{1\bar{1}} \quad \overline{413\bar{4}} \rightarrow \overline{3\bar{1}} \quad \overline{412\bar{4}} \rightarrow \overline{2\bar{1}} \quad \overline{421\bar{4}} \rightarrow \overline{1\bar{2}} \quad \overline{431\bar{4}} \rightarrow \overline{1\bar{3}}$
(b)	CCW	$\overline{331\bar{4}} \rightarrow \overline{1\bar{4}} \quad \overline{413\bar{3}} \rightarrow \overline{4\bar{1}}$
	CW	$\overline{224\bar{1}} \rightarrow \overline{4\bar{1}} \quad \overline{142\bar{2}} \rightarrow \overline{1\bar{4}}$
(c)	CCW, CW	$\overline{43\bar{1}} \rightarrow \overline{1\bar{3}\bar{4}} \quad \overline{34\bar{1}} \rightarrow \overline{1\bar{4}\bar{3}} \quad \overline{33\bar{1}} \rightarrow \overline{1\bar{4}\bar{4}} \quad \overline{42\bar{1}} \rightarrow \overline{1\bar{2}\bar{4}}$
		$\overline{13\bar{4}} \rightarrow \overline{4\bar{3}\bar{1}} \quad \overline{14\bar{3}} \rightarrow \overline{3\bar{4}\bar{1}} \quad \overline{13\bar{3}} \rightarrow \overline{4\bar{4}\bar{1}} \quad \overline{12\bar{4}} \rightarrow \overline{4\bar{2}\bar{1}}$
		$\overline{42\bar{2}} \rightarrow \overline{1\bar{1}\bar{4}} \quad \overline{24\bar{1}} \rightarrow \overline{1\bar{4}\bar{2}} \quad \overline{41\bar{3}} \rightarrow \overline{3\bar{1}\bar{4}} \quad \overline{41\bar{2}} \rightarrow \overline{2\bar{1}\bar{4}}$
		$\overline{22\bar{4}} \rightarrow \overline{4\bar{1}\bar{1}} \quad \overline{14\bar{2}} \rightarrow \overline{2\bar{4}\bar{1}} \quad \overline{31\bar{4}} \rightarrow \overline{4\bar{1}\bar{3}} \quad \overline{21\bar{4}} \rightarrow \overline{4\bar{1}\bar{2}}$
(d)	CCW	$\overline{41331\bar{4}} \rightarrow \emptyset$
	CW	$\overline{14224\bar{1}} \rightarrow \emptyset$
(e)		(None)
(f)	CCW, CW	$\overline{4124\bar{1}} \rightarrow \overline{2} \quad \overline{4134\bar{1}} \rightarrow \overline{3}$ $\overline{1431\bar{4}} \rightarrow \overline{3} \quad \overline{1421\bar{4}} \rightarrow \overline{2}$
	CCW	$\overline{14224} \rightarrow \overline{1}$ $\overline{41331} \rightarrow \overline{4}$
(f)	CW	$\overline{4224\bar{1}} \rightarrow \overline{1}$ $\overline{1331\bar{4}} \rightarrow \overline{4}$
	(g)	CCW
CW		$\overline{4241} \rightarrow \overline{12} \quad \overline{4341} \rightarrow \overline{13}$ $\overline{1314} \rightarrow \overline{43} \quad \overline{1214} \rightarrow \overline{42}$

TABLE 1. Possible boundary conditions of nice labelings of oriented triangles in Figure 31.

Proof. Consider configuration (a) in Figure 31, with boundary conditions $u\bar{v}w\bar{x} \rightarrow p\bar{q}$. To be a fragment of a nice labeling, the \cup must be labeled 1. Examining the allowed \times nice labelings, we find $u = 1 = x$, the uppermost vertex is $\bar{v}w \rightarrow p\bar{q}$, and at least one of p or q is 4. If $p = q = 4$, we must have $v = w = 3$, so $\overline{133\bar{1}} \rightarrow \overline{4\bar{4}}$ is a valid nice labeling boundary condition this counterclockwise-oriented type (a) triangle. All other cases are similar and are omitted. The fundamental involutions provide symmetries which simplify the argument. Specifically, ε, ϖ interchange clockwise and counterclockwise orientations by reflecting or reversing arrows, respectively, and their composite τ fixes clockwise and counterclockwise orientations. \square

Remark 5.28. The counterclockwise boundary condition $\overline{142\bar{1}} \rightarrow \overline{2\bar{4}}$ involves only labelings coming from growth rules and not the additional nice labelings from Figure 30. The clockwise version of the same boundary condition does however involve the additional nice labelings, which is conceptually where the additional nice labelings arise.

Lemma 5.29. *Suppose G and G' are symmetrized six-vertex configurations related by a Yang–Baxter move. If G can be written as a linearized diagram with a nice labeling, then the same is true of G' . Moreover, the nice labelings of G and G' are the same except inside the triangle at which the move was applied.*

Proof. By Lemma 5.26, every oriented triangle in a linearized diagram looks locally like one of the configurations in Figure 31. It suffices to show that every such local configuration can be replaced by one with the same boundary conditions and opposite orientation. Most of the possible boundary conditions listed in Table 1 are symmetric in this way. A sample exception is the clockwise-oriented configuration $1\bar{4}2\bar{2}4\bar{1} \rightarrow \emptyset$ of type (d). This may be replaced by the counterclockwise-oriented configuration on the left in Figure 32, which arises from appending end caps to a configuration of type (c). Exceptions of type (a)/(b) and (f) may be handled similarly using this type (c) configuration but using only the right-most end cap or the left and right end caps, respectively. Exceptions of type (g) may be handled with the configuration on the right in Figure 32. \square

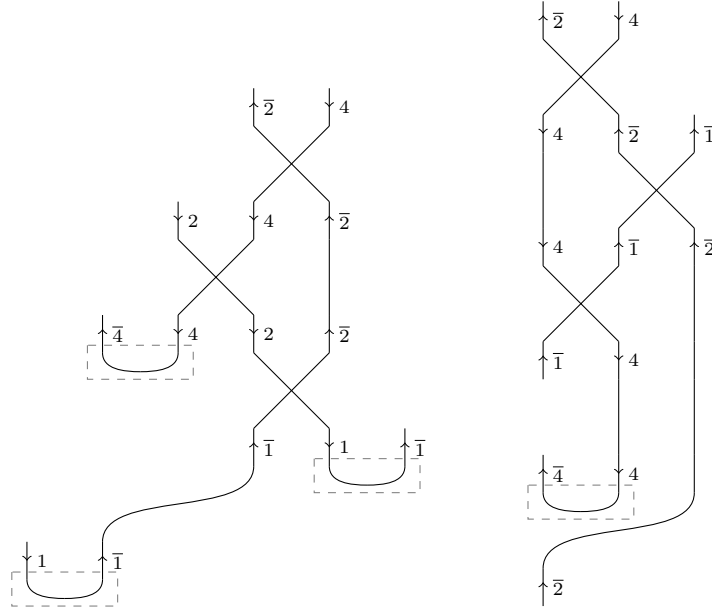


FIGURE 32. Appending end caps to oriented triangles in linearized diagrams.

5.7. Growth rules and descents. Here, we define descents of fluctuating tableaux and show how they appear in the growth algorithm.

Definition 5.30. Let w be a lattice word on \mathcal{A}_r . Say $\text{osc}(w) = w_1 \cdots w_n$. The *descent set* of w is

$$\text{Des}(w) = \{i \in [n-1] : 0 < w_i < w_{i+1} \text{ or } w_i < w_{i+1} < 0\}.$$

Lemma 5.31. Let G be an hourglass plabic graph obtained by repeatedly applying growth rules starting from a balanced lattice word $w = w_1 \cdots w_n$ of oscillating type. If $i \in \text{Des}(w)$, then the boundary nodes associated to w_i and w_{i+1} are connected by an edge in G .

Proof. Consider a descent $w_i w_{i+1} = 14$. Growth rules with $14 \rightarrow 41$ have the required property. None of the growth rules can change only the 4 or only the 1, so $14 \rightarrow 41$ must eventually be applied.

Now consider a descent 13 . Growth rules with $13 \rightarrow 31$ or $13 \rightarrow \bar{2}4$ have the required property. Other growth rules may only change the 3, namely $3\bar{1} \rightarrow \bar{1}3$, $34 \rightarrow \bar{1}2$, $34 \rightarrow 43$. The first two will result in $13 \cdots \rightarrow \bar{1}\bar{1} \cdots$, and $\bar{1}\bar{1}$ must eventually result in an end cap. The third would require $134 \rightarrow 143$, but that rule requires witnesses 3 or $\bar{4}$ rather than 1, so it does not apply.

The remaining descents may be handled similarly. The details are omitted. \square

5.8. Growth rules and fully reduced graphs. We now show that the output $\mathcal{G}(T)$ of the growth algorithm is fully reduced. By Corollary 3.33, we may equivalently show that $\mathcal{G}(T)$ is monotonic (see Definition 3.30). Our argument is inductive and verifies, by further analyzing promotion appliances, that growth rules preserve monotonicity. We begin with the significantly simpler trip_2 conditions.

Definition 5.32. Let $\{a, c\}, \{b, d\}$ be four distinct numbers in $[n]$. By relabeling if necessary, we may suppose $a < c, b < d$, and $a < b$. We say they form a *crossing* if $a < b < c < d$.

Lemma 5.33. *Let T' be a tableau of oscillating type with $w' = L(T')$. Suppose that G' is an hourglass plabic graph of the same boundary type as w' and with $\text{trip}_\bullet(G') = \text{prom}_\bullet(w')$. Suppose further that G is obtained from G' by applying one of growth rules in Figure 22. If the trip_2 -strands in G' have no self-intersections or double crossings, then the same is true of G .*

Proof. First, consider self-intersections of trip_2 -strands in G . Since G' has no trip_2 self-intersections, the only way to introduce a self-intersection by attaching an X is for a trip_2 -strand to leave and re-enter the X through the bottom two edges. That is, $\text{trip}_2(G')(i) = i + 1$ where $i, i + 1$ are the positions corresponding to the X in w' . Since $\text{trip}_\bullet(G') = \text{prom}_\bullet(w')$, we have $\text{prom}_2(w')(i) = i + 1$. By Lemma 5.10, $\rho_2(\vec{e}, v', \vec{f})(i') = i' + 1$ where $i', i' + 1$ are the positions corresponding to the X in w' . Graphically, the second promotion appliance of v' would need a “cup” below where the X is placed. We see in Example 5.12 that this does not occur, and one may check directly that the same is true for all short rules, so G does not contain trip_2 -strand self-intersections in these cases.

Now, consider double intersections of trip_2 -strands in G . Since G' has no trip_2 -strand double intersections, they arise in G only from the two trip_2 -strands leaving the bottom two edges of the X and crossing in G' . This configuration occurs if and only if $\{i, \text{trip}_2(G')(i)\}, \{i + 1, \text{trip}_2(G')(i + 1)\}$ form a crossing. As before, such a crossing would be apparent as a crossing in the promotion appliance of v' ; we see this does not occur in Example 5.12, and we may check it does not occur for any short rule. Hence, G does not contain trip_2 -strand double crossings in these cases. The trip_2 conditions may be summarized as requiring that $\rho_2(\vec{e}, v', \vec{f})(i') \neq i' + 1$ and that $\{i', \rho_2(\vec{e}, v', \vec{f})(i')\}, \{i' + 1, \rho_2(\vec{e}, v', \vec{f})(i' + 1)\}$ do not form a crossing.

Finally, consider the long rules. The preceding trip_2 conditions may be directly checked for the promotion appliances of the targets of Lemma 5.16(i)-(ii), e.g. by inspecting the second row of Figure 29. For the full long rules, we may repeat the inductive argument in Theorem 5.17 with the additional hypothesis that the promotion appliances of the targets of the long rules satisfy the trip_2 conditions. The base cases are short rules and Lemma 5.16(i)-(ii). We describe how to modify a representative inductive step. Recall that we used the substitutions $14 \cdots \bar{2}2 \rightarrow 14 \cdots 3\bar{3} \rightarrow 41 \cdots 3\bar{3} \rightarrow 41 \cdots \bar{2}2$, where the first and third steps use the plumbings in Lemma 5.14(i) and the second step uses a shorter long rule. By induction, $\rho_2(\vec{e}, 41 \cdots 3\bar{3}, \vec{f})$ satisfies the trip_2 conditions. Now $\rho_2(\vec{e}, 41 \cdots 3\bar{3}, \vec{f}) = \rho_2(\vec{e}, 41 \cdots \bar{2}2, \vec{f}) \circ (\text{id}^{k+1} \times H_2)$ and H_2 is the identity, so $\rho_2(\vec{e}, 41 \cdots \bar{2}2, \vec{f})$ satisfies the trip_2 conditions. The other cases use the $s = 2$ plumbings in Figure 26 in place of H_2 , which likewise do not interfere with the trip_2 conditions. \square

We give a similar but more technical argument for the $\text{trip}_1, \text{trip}_2$ monotonicity conditions. First, we show that promotion appliances can detect the touching of trip_1 - and trip_2 -strands.

Lemma 5.34. *Let T be a tableau of oscillating type with $w = L(T)$, where w has a fixed consecutive subword v . Let G be an hourglass plabic graph of the same boundary type as w , with $\text{trip}_\bullet(G) = \text{prom}_\bullet(w)$. Suppose $i \neq j$ are indices in w corresponding to v , while $\text{trip}_1(G)(i) = \text{trip}_2(G)(j)$ is an index in w not corresponding to v . Then $\{i, \rho_3(\vec{e}, v, \vec{f})(i)\}, \{j, \rho_2(\vec{e}, v, \vec{f})(j)\}$ form a crossing, where \vec{e}, \vec{f} are as in Lemma 5.10 applied to v in w .*

Proof. Let $k = \text{trip}_1(G)(i) = \text{trip}_2(G)(j)$. By construction of promotion appliances, $\rho_3(\vec{e}, v, \vec{f})(i) \neq \rho_2(\vec{e}, v, \vec{f})(j)$, and they are distinct from i, j . However, the function h from Lemma 5.10 is non-injective here and gives no information about the necessary inequalities.

Instead, let y be obtained from w by replacing the letter at index k with its standardized complement, e.g. $y \rightarrow w$ could be obtained by $123 \rightarrow \bar{4}$. Correspondingly, let H be obtained from G by attaching a “claw” at the boundary vertex k . By Lemma 3.34(c), $\text{trip}_1(H)(i) \neq \text{trip}_2(H)(j)$ and the two strands cross. Attaching a claw preserves monotonicity by inspection, so $\{i, \text{trip}_1(H)(i)\}, \{j, \text{trip}_2(H)(j)\}$ form a crossing. Since $\text{trip}_\bullet(G) = \text{prom}_\bullet(w)$, we see $\text{trip}_\bullet(H) = \text{prom}_\bullet(v)$. By Lemma 5.10 applied to v in y , we see that $\{i, \rho_3(\vec{e}_0, v, \vec{f}_0)(i)\}, \{j, \rho_2(\vec{e}_0, v, \vec{f}_0)(j)\}$ form a crossing.

We claim that $\vec{e}_0 = \vec{e}$ and $\vec{f}_0 = \vec{f}$. Indeed, they are each obtained by tracking the subword v in w or y through the promotion algorithm. The crystal operators applied to the positions of v are the same in either case since y and w differ by, e.g., $123 \rightarrow \bar{4}$, which is applied at indices disjoint from the positions of v and which comes from a crystal isomorphism. \square

Definition 5.35. Let v be a subword of a word w of oscillating type, suppose $\rho_\bullet = \rho_\bullet(\vec{e}, v, \vec{f})$ from Lemma 5.10 applied to v in w , and let $a \neq b$ be indices in w corresponding to v . We say that $\rho_i(a)$ intersects $\rho_j(b)$ if

- (i) $\rho_i(a) = b$; or
- (ii) $\rho_j(b) = a$; or
- (iii) $\rho_i(a) = \rho_j(b)$; or
- (iv) $a, b, \rho_i(a), \rho_j(b)$ are all distinct and $\{a, \rho_i(a)\}, \{b, \rho_j(b)\}$ form a crossing.

Lemma 5.36. *Under the hypotheses of Lemma 5.33, if G' is monotonic, then G is monotonic.*

Proof. By Lemma 5.33, we need only show that G satisfies the $\text{trip}_1, \text{trip}_2$ condition from Definition 3.30. As before, a violation of this condition in G must involve one of the trip_1 -strands in the additional plumbing through the attached X . Let $\rho_\bullet = \rho_\bullet(\vec{e}, v', \vec{f})$ from Lemma 5.10 applied to v' in w' and pick $a \neq b$ corresponding to positions of v' in w' . Combining $\text{trip}_\bullet(G') = \text{prom}_\bullet(w')$, monotonicity in G' , and Lemma 5.34, we see that if the $\text{trip}_i(G')(a)$ - and $\text{trip}_j(G')(b)$ -strands cross or touch, then $\rho_{r-i}(a)$ and $\rho_{r-j}(b)$ intersect.

One may check that requiring the following conditions on promotion appliances of v' (in addition to the trip_2 conditions verified above) ensures that G is monotonic. We may examine only a single τ, ϖ, ϵ representative plumbing π_\bullet by Lemma 5.7. Let a, b be the consecutive indices of the X of v' in w' .

- (i) $\pi_\bullet = X_{-+}^+ \times \text{id}^k$: $\{\rho_3(a), \rho_2(b)\}; \{\rho_1(a), \rho_2(b)\}; \{\rho_1(b), \rho_2(a)\};$ and $\{\rho_3(b), \rho_2(a)\}$ do not intersect.
- (ii) $\pi_\bullet = X_{+-}^- \times \text{id}^{k+1}$ or $\pi_\bullet = X_{++}^+ \times \text{id}^{k+1}$: $\{\rho_3(a), \rho_2(b)\}$ as well as $\{\rho_1(b), \rho_2(a)\}$ do not intersect. Further, $\rho_1(c) = b$ for some $c > b$ in v' , and for all $k \in [b, c]$, $\{\rho_2(k), \rho_1(a)\}$ do not intersect.

These conditions may be checked directly for the promotion appliances of the short rules in Figure 22. They may also be checked for the promotion appliances of the targets of Lemma 5.16(i)-(ii), e.g. by inspecting the second row of Figure 29.

It again remains to consider the long rules. It suffices to consider those which apply X_{++}^+ or X_{+-}^- with target of the form $41wx$ where w is a word consisting of $\bar{2}, \bar{3}$'s and $x \in \{4, 3, 2, \bar{1}\}$. Hence we must check condition (ii) for these targets. We may slightly strengthen the inductive proof of Theorem 5.17 to see that $\rho_3(b) = c$ where c corresponds to the position of the $\bar{1}, 2, 3, 4$ in the long rule. We also note that $\rho_s(a) < a$ for $s = 1, 2, 3$, since $v' = 41 \cdots$ begins with 4, which must be turned into a 1 by the first phase of the crystal raising algorithm. In particular, $\rho_s(a) \neq b, c, c + 1$. Similarly, $\rho_s(b) \geq a$. Hence $\{\rho_3(a), \rho_2(b)\}$ and $\{\rho_1(b), \rho_2(a)\}$ do not intersect.

We also now see that all conditions hold for $\{\rho_2(k), \rho_1(a)\}$ to not intersect for $k \in [b, c]$, except perhaps the crossing condition. This is significantly more difficult to rule out. Equivalently, we must show that when applying raising operators to $41wx$, after applying e_1 to the first letter we never apply e_2 to any other letter. This condition may be read off directly from Figure 33 where $x \in \{4, 3, 2\}$. The $x = \bar{1}$ case is similar and is omitted. \square

All that remains is to prove the correctness of Figure 33. Here we use notation like $\langle \bar{2}^\alpha, \bar{3}^\beta \rangle$ to denote any of the $\binom{\alpha+\beta}{\alpha}$ words with α copies of $\bar{2}$ and β copies of $\bar{3}$.

Lemma 5.37. *The portion of the crystal above any $41\langle \bar{2}^\alpha, \bar{3}^\beta \rangle 4$ is a subset of the diagram in Figure 33.*

Proof. Beginning at the bottom of the diagram in Figure 33, one may verify its correctness through routine applications of the bracketing rule, except for $41\langle \bar{2}^\alpha, \bar{3}^\beta, \bar{4}^\gamma \rangle^{(5)} 2$, which is more complex. The additional constraint is as follows.

- ⁽⁵⁾ For clarity, we write $\bar{2} = ()$ and $\bar{3} = (.$ Begin with an unmatched initial sequence $(\cdots) (\cdots ($. Add (possibly empty) complete matchings of $($ and $)$'s on either side of each of the letters of the initial sequence. Finally, add $\bar{4}$'s arbitrarily after the rightmost matched $($.

Note that ⁽⁵⁾ implies that the suffix of the word starting after the rightmost matched $($ is of the form (\cdots) (all matched) followed by $(\cdots) (\cdots ($ (all unmatched), with $\bar{4}$'s placed arbitrarily. All $\bar{4}$'s are in the suffix.

As an example, suppose ⁽⁵⁾ and ⁽⁶⁾ each hold, so all $($'s are paired with $\bar{4}$'s to their left. Then all $($'s are in the suffix and are hence unmatched. Thus the complete matchings from ⁽⁵⁾ are all empty, and every $($ is left of every $)$, which is ⁽⁷⁾.

We verify the correctness of ⁽⁵⁾. The initial conditions from ⁽¹⁾ and ⁽²⁾ give all $($'s left of all $\bar{4}$'s, and all $($'s are matched with an $)$, so ⁽⁵⁾ holds. We may restate the action of ⁽³⁾ as replacing the rightmost unmatched $($ with $(.$ This does not affect the matching and so preserves ⁽⁵⁾.

Finally, we may restate the action of ⁽⁴⁾ as pairing $\bar{4}$'s and $($'s and replacing the rightmost $($ (not paired with a $\bar{4}$ to its left with a $\bar{4}$. First suppose the replaced $($ is in the suffix, so it is unmatched, and replacing it with $\bar{4}$ preserves ⁽⁵⁾. Now suppose the replaced $($ is in the prefix. The prefix contains no $\bar{4}$'s, so the replaced $($ must be the final letter of the prefix. This operation does, however, affect the matching. In the original suffix, in the (\cdots) (all matched), the rightmost matched $)$ will now be searching for a partner. There are two cases.

- (a) The rightmost unmatched parenthesis in the prefix was $($. This will now match with the aforementioned rightmost matched $)$.
- (b) The rightmost unmatched parenthesis in the prefix was $)$ or did not exist. The aforementioned rightmost matched $)$ becomes unmatched.

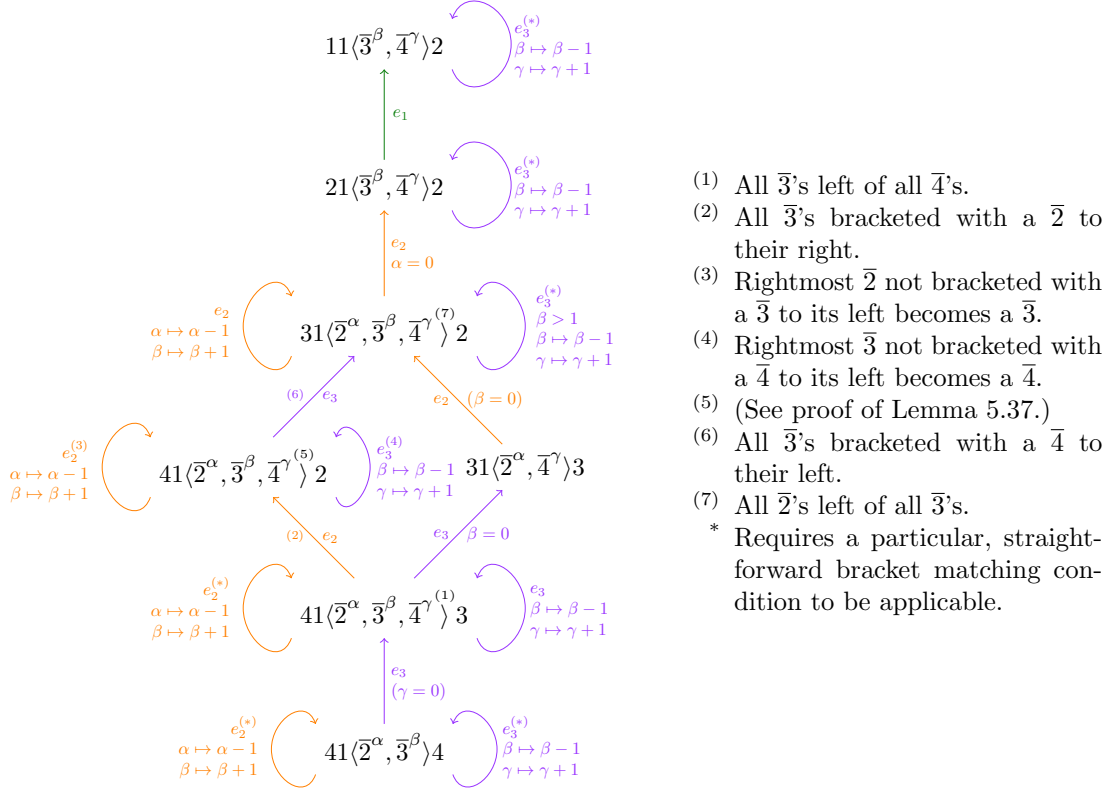
In each case, ⁽⁵⁾ continues to hold. □

5.9. Proving the growth algorithm. We now piece together the preceding results to establish the growth algorithm theorem.

Proof of Theorem 5.3. We begin with the oscillating case. The growth algorithm terminates in an hourglass plabic graph by Lemma 5.20 and Corollary 5.24, using induction on lattice words of oscillating type under length and then $\tilde{\text{l\`e}x}$ -order. The same induction using Theorem 5.11 gives condition (ii), $\text{trip}_\bullet(G) = \text{prom}_\bullet(T)$ for $G = \mathcal{G}(T)$ with $w = L(T)$ of oscillating type. Condition (i) now follows from Lemma 5.36 and Corollary 3.33. Conditions (iii) and (iv) are Theorem 5.25. The forward implication of (v) is Lemma 5.31. Conversely, suppose b_i and b_{i+1} of G are connected to the same vertex, where $i \in [n-1]$. Their boundary labels must have the same sign, and they must increase by the $\tilde{\text{l\`e}x}$ -minimality condition (iv), which completes the argument for (v). Each property extends immediately to the general fluctuating case. □

6. THE HOURGLASS WEB BASIS

6.1. The main bijection. Theorem 4.13 shows that the separation labeling determines a map \mathcal{T} from contracted fully reduced hourglass plabic graphs to rectangular fluctuating tableaux of the same type. Since move-equivalent graphs have the same trip permutations (Proposition 3.7), and

FIGURE 33. Finite state machine for upper crystal of $41\langle \bar{2}^\alpha, \bar{3}^\beta \rangle 4$.

thus the same separation labels on the boundary edges (Proposition 4.11), we can in fact consider this function as a map

$$\mathcal{T} : \text{CRG}(\underline{c})/\sim \rightarrow \text{RFT}(\underline{c}).$$

Theorem 5.3 shows that growth rules define a map $\mathcal{G} : \text{RFT}(\underline{c}) \rightarrow \text{CRG}(\underline{c})$, which induces a map

$$\mathcal{G} : \text{RFT}(\underline{c}) \rightarrow \text{CRG}(\underline{c})/\sim.$$

Theorem 6.1 below shows that \mathcal{T} and \mathcal{G} are mutually inverse bijections; this is our main combinatorial result, enabling the construction of our web basis.

Theorem 6.1. *The maps $\mathcal{T} : \text{CRG}(\underline{c})/\sim \rightarrow \text{RFT}(\underline{c})$ and $\mathcal{G} : \text{RFT}(\underline{c}) \rightarrow \text{CRG}(\underline{c})/\sim$ are mutually inverse bijections. Furthermore, this bijection satisfies $\text{trip}_\bullet(G) = \text{prom}_\bullet(\mathcal{T}(G))$. Consequently, it intertwines promotion and evacuation of tableaux with rotation and reflection of hourglass plabic graphs.*

Proof. Let $T \in \text{RFT}(\underline{c})$ and $G = \mathcal{G}(T)$. By Theorem 5.3, we have $G \in \text{CRG}(\underline{c})$ and $\text{trip}_\bullet(G) = \text{prom}_\bullet(T)$. By Theorem 4.13, $\mathcal{T}(G) \in \text{RFT}(\underline{c})$. Thus by Proposition 4.11 and [GPPSS24a, Thm. 6.12], we have $\mathcal{T}(G) = T$, so $\mathcal{T} \circ \mathcal{G}$ is the identity on $\text{RFT}(\underline{c})$.

Now let $G \in \text{CRG}(\underline{c})$ and let $T = \mathcal{T}(G)$. By Theorem 4.13, $T \in \text{RFT}(\underline{c})$. By Theorem 4.16, we therefore have that $\mathcal{T}(\text{rot}^i(G)) = \mathcal{P}^i(T)$ for all i . Let $\sigma = (12 \dots n) \in \mathfrak{S}_n$. It is easy to see that if $\text{Aexc}(\sigma^i \pi \sigma^{-i}) = \text{Aexc}(\sigma^i \pi' \sigma^{-i})$ for all i , then $\pi = \pi'$. Thus by [GPPSS24a, Thms. 6.7 & 6.12] and Proposition 4.11 we have $\text{prom}_\bullet(T) = \text{trip}_\bullet(G)$. Let $G' = \mathcal{G}(T)$; by Theorem 5.3, we have $\text{prom}_\bullet(T) = \text{trip}_\bullet(G')$. Thus by Theorem 3.13, we have $G' \sim G$, so that $\mathcal{G} \circ \mathcal{T}$ is the identity on $\text{CRG}(\underline{c})/\sim$.

We have now shown that \mathcal{T} and \mathcal{G} are mutually inverse bijections satisfying $\text{trip}_\bullet = \text{prom}_\bullet$. The rest of the theorem then follows from Theorem 4.16. \square

6.2. Unitriangularity from separation words. We now make precise the conversion from fully reduced hourglass plabic graphs to webs. Note that the following tagging convention only affects $[W]_q$ by a sign.

Definition 6.2. Let $W \in \text{CRG}(\underline{c})$. We view W as a web of type \underline{c} (see Definition 2.3) by considering each m -hourglass as an edge of multiplicity m , and by tagging the vertices v of W as follows:

- If v is incident to a 2-hourglass and two simple edges, place the tag between the simple edges.
- If v is incident to four simple edges, then the two trip_2 -strands passing through v divide the disk into four sectors (they do not double-cross since W is fully reduced). Place the tag in the sector containing the base face of W .
- If v is incident to a boundary 3-hourglass and a simple edge, place the tag on the side of the trip_2 strand through the simple edge which contains the base face.
- If v is incident to two boundary 2-hourglasses, place the tag on the side of the base face.

Note that there is no choice when v is incident to a boundary 4-hourglass.

The following unitriangularity result is analogous to [KK99, Thm. 2] (see also [BDG⁺22, Thm. 3.2]).

Theorem 6.3. *Let $G \in \text{CRG}(\underline{c})$. Then the separation word $w = \mathbf{w}(G)$ is the unique $\tilde{\text{lex}}$ -minimal boundary word among all proper labelings of G . Thus*

$$(6.1) \quad [G]_q = \pm q^a x_w + \sum_{v >_{\tilde{\text{lex}}} w} d_w^v(q) x_v$$

for some $a \in \mathbb{Z}$ and $d_w^v(q) \in \mathbb{Z}[q, q^{-1}]$, where v ranges over words of type \underline{c} .

Proof. If $G = \mathcal{G}(T)$ arises from the growth algorithm, the result follows from (2.1) and Theorem 5.3(iii)–(iv). (The tagging only results in a global sign change.) If G' is benzene-equivalent to such G , the result holds for G' by Theorem 5.25 and Lemma 5.29. Finally, if G'' is square-move-equivalent to such G' , then $[G']_q = [G'']_q$. By Corollary 3.37, we may apply benzene moves before square moves; hence, by Theorem 6.1, this covers all $G \in \text{CRG}(\underline{c})$. \square

6.3. Distinguished representatives and the web basis. The bijection from Theorem 6.1 implies that $|\text{CRG}(\underline{c})/\sim| = |\text{RFT}(\underline{c})|$. By Proposition 4.2, this quantity is also equal to $\dim_{\mathbb{C}} \text{InV}(\bigwedge^{\underline{c}} V) = \dim_{\mathbb{C}(q)} \text{InV}_{U_q(\mathfrak{sl}_4)}(\bigwedge_q^{\underline{c}} V_q)$. In this section, we obtain our $U_q(\mathfrak{sl}_4)$ -web basis $\mathcal{B}_q^{\underline{c}}$ by producing a distinguished web invariant from each move-equivalence class of $\text{CRG}(\underline{c})$.

Definition 6.4. A *benzene face* in an hourglass plabic graph is a face that admits a benzene move. We say a benzene face is *clockwise* (resp. *counterclockwise*) if in each hourglass edge the white vertex precedes the black vertex in clockwise (resp. counterclockwise) order; equivalently, if the corresponding triangle in the symmetrized six-vertex configuration is oriented clockwise (resp. counterclockwise). Let \mathcal{B} be a benzene-move-equivalence class of contracted fully reduced hourglass plabic graphs. For $x, y \in \mathcal{B}$, write $x \prec y$ and say y *covers* x when y is obtained by applying a benzene move to a clockwise benzene face in x , resulting in a counterclockwise benzene face in y . Let \preceq be the reflexive, transitive closure of this relation on \mathcal{B} .

Proposition 6.5. *The relation (\mathcal{B}, \preceq) is a partially ordered set with a unique maximum, which may be reached by starting at an arbitrary element and applying covering relations arbitrarily until no more apply.*

Proof. Consider a sequence of covers in (\mathcal{B}, \preceq) , corresponding to benzene moves on faces F_1, F_2, \dots . Between any two benzene moves at the same face F , a benzene move must be applied to all faces F' sharing an edge with F . Since no moves can be applied to boundary faces, this implies that F

appears finitely many times in the sequence. This guarantees antisymmetry, so that \preceq is a partial order.

Now, \mathcal{B} possesses the *diamond property*: if $x \prec y_0$ and $x \prec y_1$, then there is some $z \in \mathcal{B}$ with $y_0 \prec z$ and $y_1 \prec z$. Indeed, y_0 and y_1 are obtained from x by benzene moves on two distinct faces which, by the orientation condition, must be non-adjacent, so the two benzene moves commute. The diamond property implies that \mathcal{B} contains upper bounds, and thus has a unique maximal element, by Newman's Lemma [New42, Thm. 1]. \square

Remark 6.6. Standard techniques (see e.g. [Ken04, § 3.1]) can be used to prove that \mathcal{B} is in fact a distributive lattice, but we will not use this fact.

Definition 6.7. A contracted fully reduced hourglass plabic graph G that is maximal in its benzene-move-equivalence class (in the sense of Proposition 6.5) is called *top fully reduced*. Equivalently, $G \in \text{CRG}(\underline{c})$ is top fully reduced if and only if it has no clockwise benzene faces.

Theorem 6.8. *The collection*

$$\mathcal{B}_q^{\underline{c}} := \{[W]_q : W \text{ a top fully reduced hourglass plabic graph of type } \underline{c}\}$$

is a rotation-invariant web basis for $\text{Inv}_{U_q(\mathfrak{sl}_4)}(\bigwedge_q^{\underline{c}} V_q)$.

Proof. Let \mathcal{C} be a move-equivalence class of graphs from $\text{CRG}(\underline{c})$. By Corollary 3.37, square moves and benzene moves on fully reduced graphs commute: any $G, G' \in \mathcal{C}$ may be connected by first applying a sequence of benzene moves and then a sequence of square moves. By [CKM14, Eq. 2.10], square moves do not affect the web invariant; thus any top fully reduced hourglass plabic graphs $W, W' \in \mathcal{C}$ satisfy $[W]_q = [W']_q$. We write $[\mathcal{C}]_q$ for this common value.

By Theorem 2.9 and Theorem 6.3, the invariants $[\mathcal{C}]_q$ for $\mathcal{C} \in \text{CRG}(\underline{c})/\sim$ are linearly independent, since they have distinct leading terms. Since

$$|\text{CRG}(\underline{c})/\sim| = |\text{RFT}(\underline{c})| = \dim_{\mathbb{C}(q)} \text{Inv}_{U_q(\mathfrak{sl}_4)}(\bigwedge_q^{\underline{c}} V_q)$$

by Theorem 6.1 and Proposition 4.2, the invariants $[\mathcal{C}]_q$ form a web basis.

Rotation invariance follows by observing that the rotation of a top fully reduced graph is again top fully reduced. \square

Corollary 6.9. *For any complete collection of representatives \mathcal{R} for $\text{CRG}(\underline{c})/\sim$, the corresponding invariants $[G]_q$ for $G \in \mathcal{R}$ form a $\mathbb{C}(q)$ -basis for $\text{Inv}_{U_q(\mathfrak{sl}_4)}(\bigwedge_q^{\underline{c}} V_q)$.*

Proof. They are linearly independent by Theorem 6.3, and there are the right number by (4.1) and Theorem 6.1. \square

We thank Greg Kuperberg for suggesting Corollary 6.10 towards making connections with the dual canonical basis.

Corollary 6.10. *Let $E = ([x_v][G_w]_q)$ be a matrix whose rows are indexed by words v of type \underline{c} listed in decreasing $\tilde{\text{lex}}$ order and whose columns are indexed by $w \in \text{RFT}(\underline{c})$ listed in decreasing $\tilde{\text{lex}}$ order, where $G_w \in \text{CRG}(\underline{w})$ with $\mathbf{w}(G) = w$. Then E is in row echelon form, and each column has a pivot of the form $\pm q^a$ for $a \in \mathbb{Z}$.*

Proof. This follows by inspecting the matrix E and using Theorem 6.3. \square

7. UNCROSSING AND REDUCTION RELATIONS

Using the braiding of the representation category for $U_q(\mathfrak{sl}_r)$ (see [CKM14, §6]), one may assign invariants $[T]_q$ to *tensor diagrams* T , variants of webs in which edges may cross over one another. When T is the projection of a (colored) knot, link, or tangle, $[T]_q$ yields quantum knot invariants (e.g., [Jon85, Kau87, Tur94, Kho00, Kho04, MN08]) of great interest. The reader may take the

relations in Figure 34 (adapted to our conventions from [CKM14, Cor. 6.2.3]) as defining $[T]_q$ in the case $r = 4$.

In Algorithm 7.1 below, we describe how the invariant $[T]_q$ of an arbitrary $U_q(\mathfrak{sl}_4)$ -tensor diagram may be expanded in the web basis $\mathcal{B}_q^{\underline{c}}$ of Theorem 6.8. The relations appearing in this section are drawn from [CKM14] and adapted to our conventions. As noted by Kuperberg [Kup96b, §8.3], such reduction algorithms to a web basis allow for the efficient computation of quantum link and tangle invariants. In the case $\underline{c} = (1, \dots, 1)$, where the representation of \mathfrak{S}_n on $\text{Inv}(\bigwedge^{\underline{c}} V)$ via permutation of tensor factors is a rectangular Specht module, the uncrossing relations also allow for the computation of the actions of the simple reflections in the basis $\mathcal{B}^{\underline{c}}$.

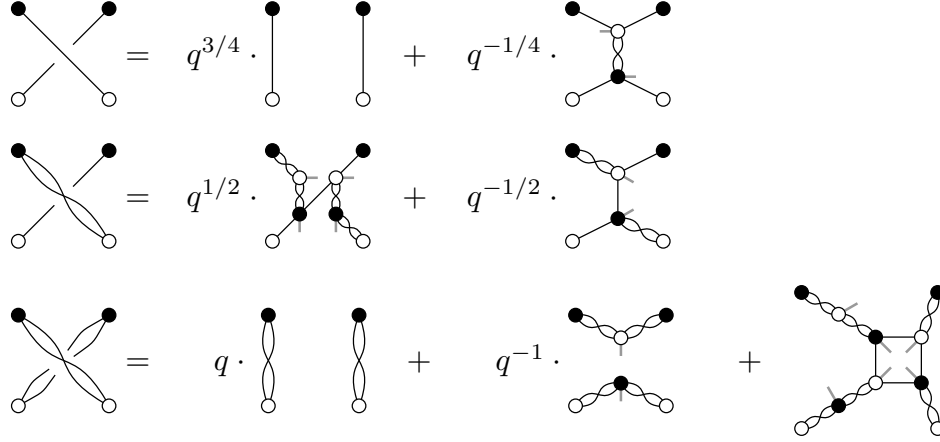


FIGURE 34. The uncrossing relations for invariants of $U_q(\mathfrak{sl}_4)$ -tensor diagrams.

Let $[k]_q := (q^k - q^{-k})/(q - q^{-1})$.

Algorithm 7.1 (REDUCTION ALGORITHM). Let T be any $U_q(\mathfrak{sl}_4)$ -tensor diagram.

- (1) Apply uncrossing relations (Figure 34) to T to remove any crossings.
- (2) For each web appearing in this expansion, apply relations from Figure 35 to decompose all forbidden 4-cycles.
- (3) For each web appearing in this expansion, remove any loops using the relations from Figure 36.
- (4) For each web W appearing in this expansion, if W is not fully reduced, apply the benzene relation of Figure 37 to create a forbidden 4-cycle and return to Step (2). Otherwise continue.
- (5) Apply benzene relations to express a fully reduced web invariant as

$$[W]_q = [W']_q + \left(\sum_{\alpha} \pm [W_{\alpha}]_q \right),$$

where W' is top fully reduced and the W_{α} have fewer faces. Return to Step (2) to decompose each W_{α} .

Theorem 7.2. For T a tensor diagram of type \underline{c} , Algorithm 7.1 expresses $[T]_q$ in the basis $\mathcal{B}_q^{\underline{c}}$.

Proof. If T is a tensor diagram, then the uncrossing relations unambiguously express $[T]_q$ as a combination of web invariants. By Definition 3.9, each web that is not fully reduced is modified by one of the Steps (2–4). If a web is modified only by a benzene move in Step (4), then it will also be modified by Step (2) on the subsequent iteration. Since the loop deletion and 4-cycle relations (Figures 35 and 36) all decrease the number of faces, the algorithm terminates in a fully reduced web. Finally, by Proposition 6.5, there is a sequence of benzene moves converting any fully reduced web into a basis web (and in fact this sequence may be chosen arbitrarily). \square

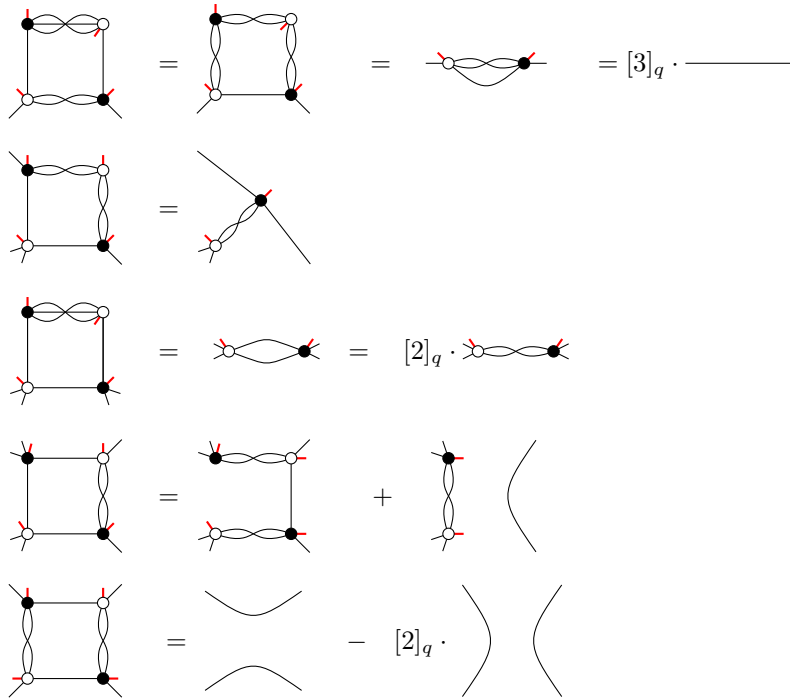


FIGURE 35. Relations decomposing the forbidden 4-cycles of $U_q(\mathfrak{sl}_4)$ -webs. Here, $[k]_q := (q^k - q^{-k})/(q - q^{-1})$. Tags are drawn in red (■) for clarity.

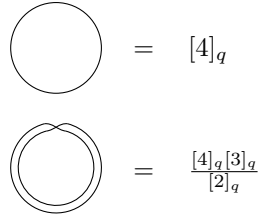


FIGURE 36. The loop deletion relations for $U_q(\mathfrak{sl}_4)$ -webs.

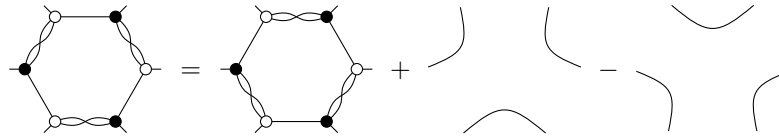


FIGURE 37. The benzene relation on invariants of $U_q(\mathfrak{sl}_4)$ -webs.

8. COMBINATORIAL APPLICATIONS OF THE WEB BASIS

In this section, we collect results related to our web basis \mathcal{B}_q^c that are of particular interest in combinatorics. We first re-prove a cyclic sieving result. We then summarize two particular extreme move-equivalence classes relating to alternating sign matrices and plane partitions, respectively.

8.1. Cyclic sieving and basis webs. Theorem 6.8 can be used to easily recover the 4-row case of a celebrated cyclic sieving result of Rhoades [Rho10], originally proved using Kazhdan–Lusztig theory. The 3-row case was re-proven in [PPR09], using Kuperberg’s $U_q(\mathfrak{sl}_3)$ -web basis. For the definition of the q -hook length polynomial below, see [Sta99, Cor. 7.21.6] or [Rho10].

Corollary 8.1. *Let $n = 4k$, $\lambda = (k, k, k, k)$, and $\zeta = e^{2\pi i/n}$. The number of standard tableaux of shape λ fixed by \mathcal{P}^d is $f^\lambda(\zeta^d)$, where $f^\lambda(q)$ is the q -hook length polynomial.*

Proof. Let $\sigma = (1\ 2\ \cdots\ n) \in \mathfrak{S}_n$. By Springer’s theory of regular elements [Spr74, Prop. 4.5], we have $\chi^\lambda(\sigma^d) = (-1)^d f^\lambda(\zeta^d)$, where χ^λ is the character of the Specht module $\mathcal{S}^\lambda \cong \text{Inv}(V^{\otimes n})$. On the other hand, since the basis $\mathcal{B}^{(1^n)}$ is permuted up to sign by the action of σ and is in \mathcal{P} -equivariant bijection with standard tableaux of shape λ , this character value is a signed count of the number of \mathcal{P}^d -fixed tableaux.

Moreover, each fixed point contributes a sign of precisely $(-1)^d$ as follows. Suppose $W \in \text{CRG}((1^n))$. Using our tagging conventions, $[\text{rot}(W)]_q = (-1)^k \cdot \sqcup([W]_q)$ where k is the number of vertices of simple degree 4 on the $\text{trip}_2(1)$ -strand of W , and \sqcup is the cyclic shift isomorphism from Section 1.2. For a symmetrized six-vertex configuration $\varphi(W)$, this strand has two incoming boundary edges. There must be an odd number of direction changes of the arrows along the strand, which occur precisely at sources or sinks, so k is odd. The result follows. \square

8.2. Alternating sign matrices and square moves. The set \mathcal{ASM}_n of alternating sign matrices consists of $n \times n$ matrices with entries from $\{-1, 0, 1\}$ where the nonzero entries of each row and column begin and end with 1 and alternate between 1 and -1 . Alternating sign matrices have long been of interest in enumerative combinatorics (see, e.g., [MRR83, Zei96, Kup96a, Pro01, Kup02]). Recently, they have obtained further significance through connections [Wei21] to back stable Schubert calculus [LLS21].

Permutation matrices are instances of alternating sign matrices. Indeed, \mathcal{ASM}_n is the MacNeille completion of the strong Bruhat order on \mathfrak{S}_n [LS96], i.e. \mathcal{ASM}_n is the smallest lattice containing Bruhat order. More strongly, \mathcal{ASM}_n is a distributive lattice with covering relations given by adding $\begin{pmatrix} -1 & 1 \\ 1 & -1 \end{pmatrix}$ where possible. The sub-poset of join-irreducible elements can be realized as a certain tetrahedral poset embedded in three-dimensional space (see [Str15, Fig. 5] and [EKLP92, Str11]). Hence \mathcal{ASM}_n can be viewed as the order ideals of this tetrahedral poset.

Proposition 8.2. *Let T be the “superstandard” 4-row standard tableau with lattice word $1^n 2^n 3^n 4^n$. The move-equivalence class of $\mathcal{G}(T)$ is in bijection with \mathcal{ASM}_n , with square moves corresponding to covering relations. No benzene moves apply to elements of this class.*

Proof. Consider the symmetrized six-vertex configurations obtained by placing $4n$ incoming strands around a square grid and assigning orientations to the middle in all possible ways. Such configurations are in bijection with configurations of the classical six-vertex model (with domain wall boundary conditions) by reversing all horizontal arrows, and these in turn are in bijection with \mathcal{ASM}_n by [Kup96a]. The composite bijection from the symmetrized six-vertex configurations to \mathcal{ASM}_n may be realized by replacing sinks with 1, sources with -1 , and transmitting vertices with 0. See Figure 38 for examples.

These symmetrized six-vertex configurations are clearly well-oriented by Proposition 3.21 and admit no Yang–Baxter moves, since they contain no big triangles. It is easy to check that the corresponding fully reduced hourglass plabic graphs (see Theorem 3.25) have separation word $1^n 2^n 3^n 4^n$. \square

See Remark 3.17 for further connections between square moves and alternating sign matrix dynamics.

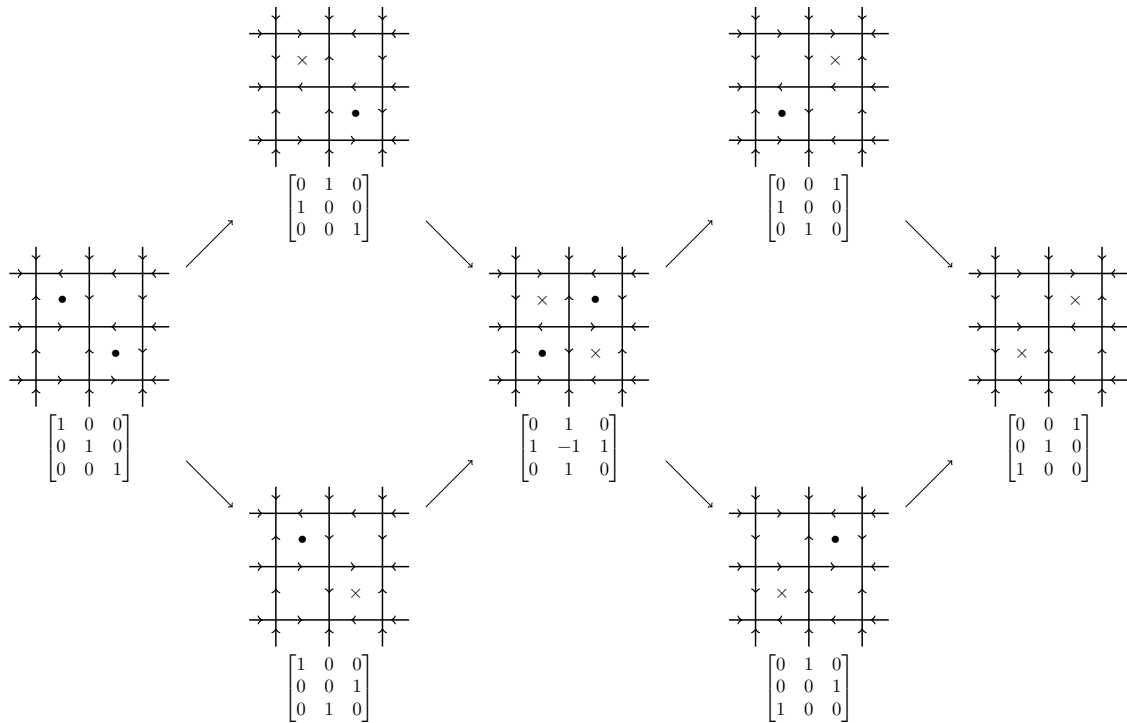


FIGURE 38. The 7 elements of \mathcal{ASM}_3 together with the corresponding symmetrized six-vertex configurations in the move-equivalence class of $\varphi(\mathcal{G}(T))$. Here T is the standard tableau with lattice word $L = 111222333444$. ASM moves going up (resp. down) in the poset are marked with \bullet (resp. \times).

8.3. Plane partitions and benzene moves. The set $\mathcal{PP}(a \times b \times c)$ of *plane partitions* in the $a \times b \times c$ box consists of the $a \times b$ matrices of nonnegative integers that weakly decrease along rows and columns and have maximum entry at most c . Like alternating sign matrices, plane partitions have long been prominent in enumerative combinatorics (see, e.g., [And77, And79, Ste90]) and representation theory (see, e.g., [Pro84, GPT23]). They are now one of the central objects of study in the burgeoning area of dynamical algebraic combinatorics (e.g., [SW12, Str17, Hop20, PP20]).

The plane partitions $\mathcal{PP}(a \times b \times c)$ may be equivalently viewed as the configurations of stacked unit cubes in the prism $[0, a] \times [0, b] \times [0, c]$ where gravity acts parallel to $(-1, -1, -1)$. Such plane partitions form a distributive lattice and may be seen as order ideals of the product of chains poset $[a] \times [b] \times [c]$. They have further alternative interpretations as rhombus tilings or perfect matchings on particular subsets of the hexagonal lattice.

Proposition 8.3. *Let $a, b, c \in \mathbb{Z}_{\geq 1}$. If $a \geq c$, let $L = 1^a \bar{4}^b 2^c \bar{1}^{a-c} \bar{2}^c 4^b \bar{1}^c$, and if $a \leq c$, let $L = 1^a \bar{4}^b 2^a 1^{c-a} \bar{2}^a 4^b \bar{1}^c$. Let T be the tableau with lattice word L . The move-equivalence class of $\mathcal{G}(T)$ is in bijection with $\mathcal{PP}(a \times b \times c)$, with benzene moves corresponding to covering relations. No square moves apply to elements of this class.*

Proof. In the hexagonal lattice, begin with a “large hexagon” with a, b, c, a, b, c hexagons, respectively, on each side in cyclic order; see Figure 39. The perfect matchings on this large hexagon can be converted to rhombus tilings by considering the dual graph and omitting edges of the dual graph that cross matched edges of the large hexagon. Alternatively, perfect matchings on the large hexagon may be converted to hourglass plabic graphs by replacing matched edges with hourglass edges. It is not difficult to see that the resulting hourglass plabic graphs are fully reduced, and one

may check that the separation labeling gives L . There are no square faces, so no square moves apply. See Figure 40 for an example. \square

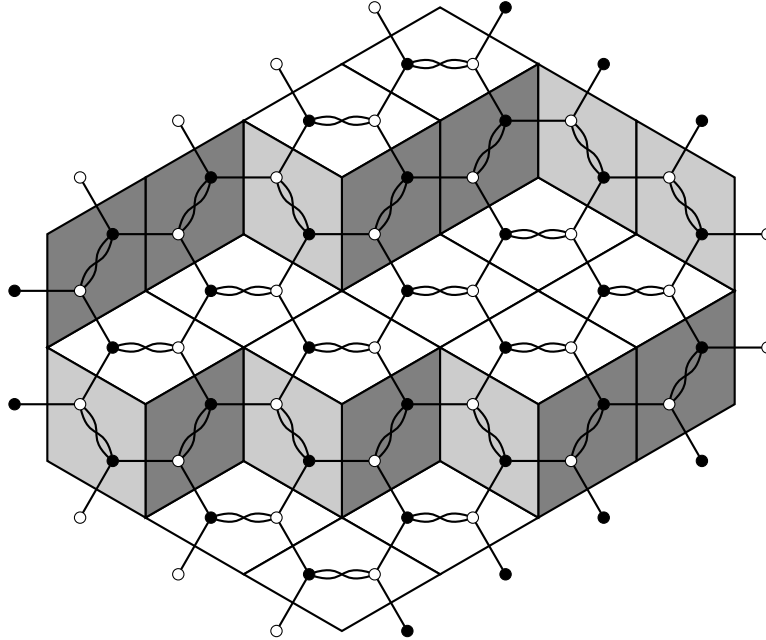


FIGURE 39. The large hexagon associated to $\mathcal{PP}(3 \times 2 \times 4)$ as in Proposition 8.3. A sample hourglass plabic graph in the move-equivalence class of $\mathcal{G}(T)$ has been drawn, together with the dual rhombus tiling. Here T is the oscillating tableau with lattice word $L = 111442221222441111$.

9. HOURGLASS PLABIC GRAPHS RECOVER KNOWN WEB BASES

In this section, we discuss how all known rotation-invariant web bases fit within our framework of hourglass plabic graphs, forbidden 4-cycles, and the $\text{trip}_\bullet = \text{prom}_\bullet$ property, and give an extension of these bases to the “semistandard” setting.

9.1. A uniform characterization for small r . We may extend Definition 3.1 by defining an $U_q(\mathfrak{sl}_r)$ -hourglass plabic graph exactly as before, but with all internal vertices of degree r . We define the trip permutations $\text{trip}_\bullet(G) = (\text{trip}_1(G), \dots, \text{trip}_{r-1}(G))$ of such a graph G in the natural way, extending Definition 3.4.

In general, $U_q(\mathfrak{sl}_r)$ -hourglass plabic graphs admit contraction moves as in Figure 9, which preserve trip_\bullet . As before, we say a $U_q(\mathfrak{sl}_r)$ -hourglass plabic graph G is *contracted* if all possible contraction moves have been applied. For $r = 2$ or 3 , the contraction moves are the only moves on hourglass plabic graphs.

Definition 9.1. A 4-cycle of an $U_q(\mathfrak{sl}_r)$ -hourglass plabic graph G is called *forbidden* if the sum of its edge multiplicities exceeds r . For $r = 2, 3$, or 4 , we write $G \sim G'$ for the move-equivalence relation. We say such a graph G with no isolated components is *fully reduced* if no $G' \sim G$ contains a forbidden 4-cycle. *Top* fully reduced graphs are distinguished contracted representatives in each move-equivalence class of fully reduced graphs (as in Definition 6.7); when $r = 2$ or 3 , every contracted fully reduced graph is top.

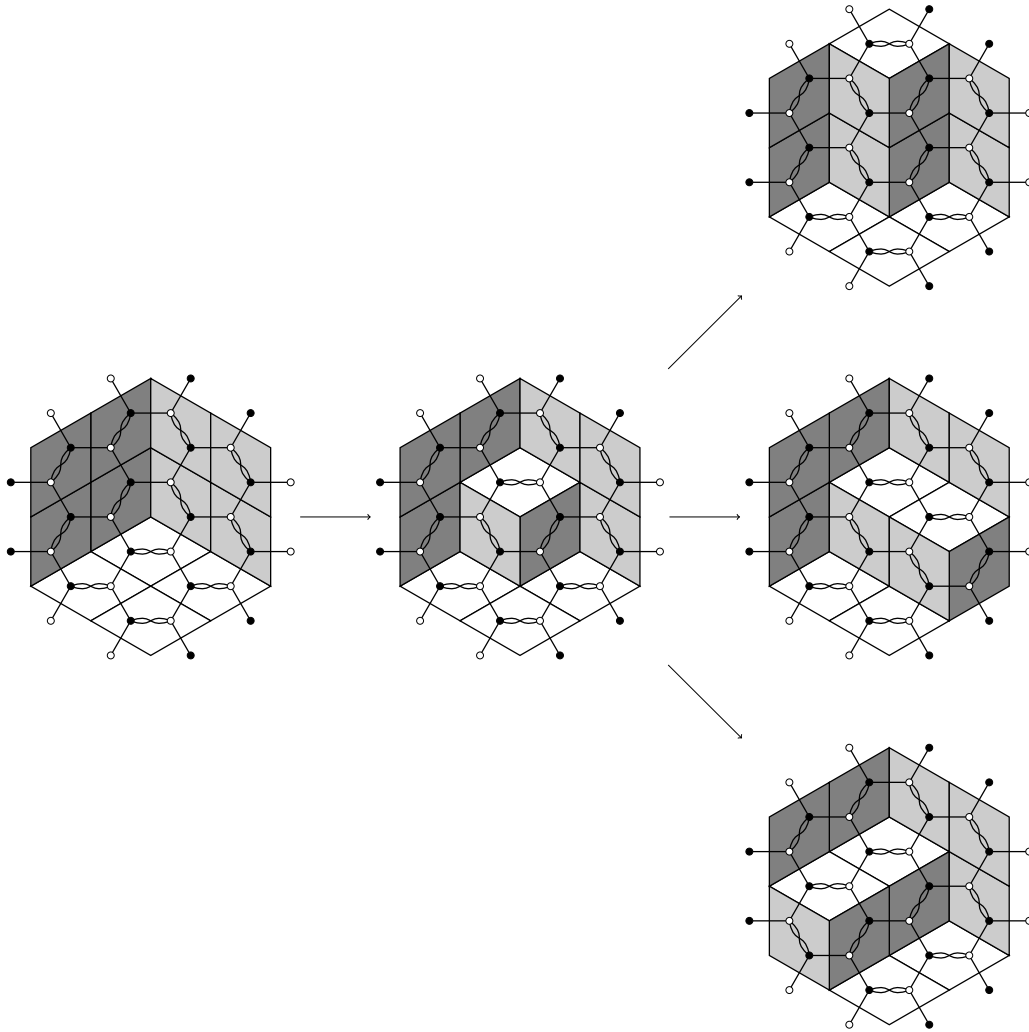


FIGURE 40. The 5 elements in the first three ranks of $\mathcal{PP}(2 \times 2 \times 2)$ drawn as rhombus tilings, together with the corresponding hourglass plabic graphs in the move-equivalence class of $\mathcal{G}(T)$. Here T is the oscillating tableau with lattice word $L = 114422224411$.

Theorem 9.2 below shows how our hourglass plabic graph perspective with forbidden 4-cycles and $\text{trip}_\bullet = \text{prom}_\bullet$, unifies the Temperley–Lieb $U_q(\mathfrak{sl}_2)$ -basis, the Kuperberg’s $U_q(\mathfrak{sl}_3)$ -basis, and our $U_q(\mathfrak{sl}_4)$ -basis from Theorem 6.8.

Theorem 9.2. *Let $r = 2, 3$, or 4 . Then $\text{CRG}(\underline{c}; r)/\sim$ is in bijection with $\text{RFT}(\underline{c}; r)$ via $\text{trip}_\bullet = \text{prom}_\bullet$, and this bijection intertwines rotation and promotion. Furthermore,*

$$\mathcal{B}_q^{\underline{c}; r} := \{[W]_q : W \text{ a top fully reduced } U_q(\mathfrak{sl}_r)\text{-hourglass plabic graph of type } \underline{c}\},$$

is a rotation-invariant web basis of $\text{Inv}_{U_q(\mathfrak{sl}_r)}(\bigwedge_q^{\underline{c}} V_q)$.

Proof. When $r = 2$, all hourglass plabic graphs consist of a non-crossing matching of the boundary vertices, with some internal vertices along each arc. Such a graph is contracted if there are 0 or 1 internal vertices on each arc; all such graphs are in the basis and this is exactly the Temperley–Lieb

basis. The $\text{trip}_\bullet = \text{prom}_\bullet$ condition is an easy verification, and this property implies that rotation corresponds to promotion.

When $r = 3$, the fully reduced graphs are those whose contraction contains no 2-cycles or 4-cycles, since a 2-cycle may be uncontracted into a 4-cycle with edge multiplicities 1, 1, 1, 2. Thus the fully reduced graphs are exactly Kuperberg’s *non-elliptic* web basis. Hopkins–Rubey [HR22] showed that the standard bijection between these webs and 3-row standard Young tableaux (for example, via the growth rules of [KK99, PPR09]) is characterized by $\text{trip}_\bullet = \text{prom}_\bullet$. Finally, the $r = 4$ case is Theorem 6.8. \square

9.2. The 2-column case. In [Fra23], Fraser found a rotation-invariant SL_r -web basis for $\text{Inv}(V^{(1^{2r})})$ with r arbitrary, the “2-column” case. He describes a bijection φ_r from rectangular standard tableaux of shape $r \times 2$ to a basis \mathcal{W}_r of SL_r -webs, which are only characterized as the outputs of the map φ_r (see Figure 41 for an example). For $G = \varphi_r(T) \in \mathcal{W}_r$, all internal faces are 4-cycles. The map φ_r in fact requires certain choices to be made, but all possible outputs are connected by the square relation of [FLL19, Eq. 6.9], so that the invariant $[G]$ is well-defined.

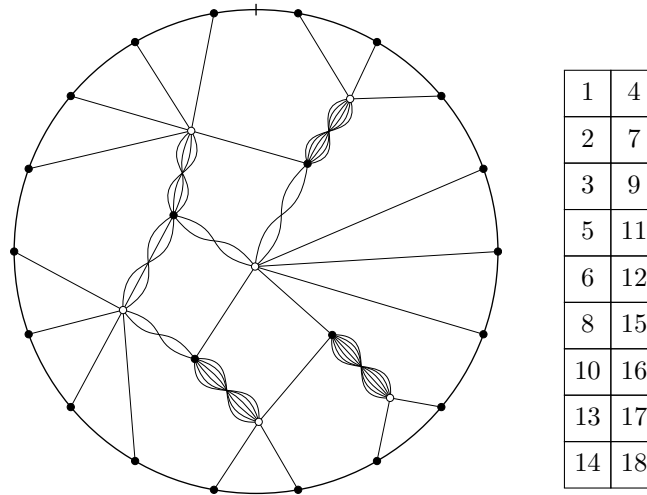


FIGURE 41. The SL_9 -web from [Fra23, Fig. 1] converted to an SL_9 -hourglass plabic graph and the corresponding tableau.

In follow-up work [GPPSS24b], we have extended the perspective of this paper to show that the bijection φ_r satisfies $\text{trip}_\bullet(\varphi_r(T)) = \text{prom}_\bullet(T)$ and that after lifting to hourglass plabic graphs, the general square relation preserves trip permutations. Furthermore, the web basis elements $[W]_q$ for $W \in \mathcal{W}_r$ are characterized as the web invariants of suitably defined fully reduced $U_q(\mathfrak{sl}_r)$ -hourglass plabic graphs; full reducedness again includes the prohibition of the forbidden 4-cycles of Definition 9.1 in move-equivalent graphs.

9.3. The semistandard web basis. We now show how the growth rules and the reduction algorithm allow for the extension of the top fully reduced bases to bases for general graded pieces of the coordinate ring $\mathbb{C}[\widetilde{\text{Gr}}_r(\mathbb{C}^n)]$ of the (affine cone over) the Plücker embedding of the Grassmannian, for $r \leq 4$. See [Fra23, §6] for similar results in the 2-column setting.

For the remainder of this section, we consider tensor diagrams at $q = 1$ all of whose boundary edges have multiplicity one, but such that a boundary vertex b_i may be incident to any number $\mu_i \geq 0$ of such edges. Any such tensor diagram T determines an element $[T] \in \text{Inv}_{\text{SL}_r}(\text{Sym}^\mu(V))$, where $\text{Sym}^\mu(V) := \text{Sym}^{\mu_1}(V) \otimes \cdots \otimes \text{Sym}^{\mu_n}(V)$. This element is the restriction of the invariant $[\check{T}] \in \text{Inv}_{\text{SL}_r}(\bigotimes_i V^{\otimes \mu_i})$ of the diagram \check{T} obtained from T by splitting b_i into μ_i separate boundary vertices, each incident to a single edge. In terms of the polynomial expressions from Section 2.2, $[T]$

can be computed from $[\check{T}]$ by setting equal, for each i , the corresponding μ_i vectors of boundary variables. Call such a tensor diagram T a *web of semistandard type* if it is planar; as before, we move freely between the language of webs and of hourglass plabic graphs. We now extend the definition of top full reducedness to such graphs.

Definition 9.3. We say an hourglass plabic graph G of semistandard type is *top fully reduced* if the hourglass plabic graph \check{G} is top fully reduced and if no boundary vertex of G is adjacent to a single interior vertex by more than one edge.

Theorem 9.4. *Let $r = 2, 3$, or 4 . Then the collection $\mathcal{B}^r(\underline{\mu})$ of invariants of top fully reduced r -hourglass plabic graphs of semistandard type with boundary multiplicities $\underline{\mu}$ is a rotation-invariant web basis of $\mathbb{C}[\widetilde{\text{Gr}}_r(\mathbb{C}^n)]_{\underline{\mu}}$.*

Remark 9.5. Fomin and Pylyavskyy [FP16] conjecture close connections between the SL_3 -web basis and the cluster algebra structure on $\mathbb{C}[\widetilde{\text{Gr}}_3(\mathbb{C}^n)]$, having assumed that the SL_3 -web basis extends to the semistandard setting as we describe above. In light of Theorem 9.4, it would be very interesting to study whether these conjectures might also hold for the SL_4 -web basis and the cluster algebra structure on $\mathbb{C}[\widetilde{\text{Gr}}_4(\mathbb{C}^n)]$. The rotation-invariance of our basis is particularly important in this context, as rotation induces an automorphism of the cluster structure.

Proof of Theorem 9.4. Suppose that $\underline{\mu}$ is a composition of rN into n parts. The First Fundamental Theorem of invariant theory (see [Wey97]) implies that the graded piece $\mathbb{C}[\widetilde{\text{Gr}}_r(\mathbb{C}^n)]_{\underline{\mu}} \cong \text{Inv}_{\text{SL}_r} \text{Sym}^{\underline{\mu}}(V)$ is spanned by products $\Delta_{I_1} \cdots \Delta_{I_N}$ of Plücker coordinates such that i lies in exactly μ_i of the sets I_j for $i = 1, \dots, n$. Such a product equals $[T]$ where T is the tensor diagram with boundary multiplicities $\underline{\mu}$ obtained by overlaying N r -valent star graphs using boundary vertices I_1, \dots, I_N . Using the relations from Algorithm 7.1 when $r = 4$ or using the relations from [Kup96b] when $r = 2$ or 3 , which apply equally well in the semistandard setting, we can write $[T]$ as a linear combination of invariants $[W]$ of webs W of semistandard type $\underline{\mu}$ such that \check{W} is top fully reduced. If such a W has a boundary vertex incident to a single interior vertex by more than one edge, then $[W] = 0$ since $[\check{W}]$ is alternating in the corresponding two arguments, so we may in fact write $[T]$ as a linear combination of elements of $\mathcal{B}^r(\underline{\mu})$. This shows that $\mathcal{B}^r(\underline{\mu})$ spans $\mathbb{C}[\widetilde{\text{Gr}}_r(\mathbb{C}^n)]_{\underline{\mu}}$.

It is well-known (see e.g. [Ses14, Ch. 1]) that $\dim \mathbb{C}[\widetilde{\text{Gr}}_r(\mathbb{C}^n)]_{\underline{\mu}}$ is equal to the cardinality of the set $\text{SSYT}(r \times N, \underline{\mu})$ of semistandard tableaux of shape $r \times N$ and content $\underline{\mu}$. Thus, to prove that $\mathcal{B}^r(\underline{\mu})$ is a basis, it suffices to give an injection from the top fully reduced graphs of semistandard type, modulo moves, to $\text{SSYT}(r \times N, \underline{\mu})$. We define such a map ψ as follows: given a top fully reduced graph G of semistandard type, form the standard tableau $\mathcal{T}(\check{G})$ and make it of content $\underline{\mu}$ by relabeling the boxes labeled $1 + \sum_{j=1}^{i-1} \mu_j, \dots, \mu_i + \sum_{j=1}^{i-1} \mu_j$ by i ; call this tableau $\psi(G)$.

We first argue that $\psi(G)$ is indeed semistandard. If boxes labeled a and $a+1$ are both relabeled by i , then the boundary vertices \check{b}_a and \check{b}_{a+1} of \check{G} both come from splitting the same boundary vertex b_i of G . Since G is top fully reduced of semistandard type, this means that \check{b}_a and \check{b}_{a+1} do not share a neighbor in \check{G} . By Theorem 5.3(v), this is equivalent to $a \notin \text{Des}(\mathcal{T}(\check{G}))$, so $a+1$ is not in a lower row than a in $\mathcal{T}(\check{G})$. Applying this for each a in $1 + \sum_{j=1}^{i-1} \mu_j, \dots, \mu_i + \sum_{j=1}^{i-1} \mu_j$, we see that the boxes with these labels in $\psi(G)$ occur left to right in a skew strip having no two boxes in the same column. Thus $\psi(G)$ is semistandard. We now check that ψ is injective. Clearly $G_1 \sim G_2$ if and only if $\check{G}_1 \sim \check{G}_2$, so, since \mathcal{T} is injective on CRG/\sim by Theorem 9.2, it only remains to check that the relabeling step is injective. But this also follows from the observation about the skew strip.

Finally, it is clear that rotation of graphs sends the basis $\mathcal{B}^r(\underline{\mu})$ to the basis $\mathcal{B}^r((\mu_2, \dots, \mu_n, \mu_1))$ for the rotated weight. \square

ACKNOWLEDGEMENTS

This project began during the 2021 BIRS Dynamical Algebraic Combinatorics program hosted at UBC Okanagan, and we are very grateful for the excellent research environment provided there. At that conference, Sam Hopkins and Martin Rubey introduced us to their perspective from [HR22] of webs-as-plabic graphs which was foundational in this work. We completed the main result at NDSU (partially supported by NSF DMS-2000592), for whose hospitality we are very thankful. Finally, we are grateful for the resources provided at ICERM, where much of this paper was written.

We also thank the following people for their helpful comments: Ben Elias, Sergey Fomin, Chris Fraser, Pavel Galashin, Joel Kamnitzer, Rick Kenyon, Mikhail Khovanov, Allen Knutson, Greg Kuperberg, Thomas Lam, Ian Le, Gregg Musiker, Rebecca Patrias, Alex Postnikov, Kevin Purbhoo, Pavlo Pylyavskyy, Brendon Rhoades, Anne Schilling, Travis Scrimshaw, David Speyer, Hugh Thomas, Julianna Tymoczko, Bruce Westbury, Lauren Williams, Haihan Wu, and Paul Zinn-Justin.

REFERENCES

- [ABC⁺16] Nima Arkani-Hamed, Jacob Bourjaily, Freddy Cachazo, Alexander Goncharov, Alexander Postnikov, and Jaroslav Trnka, *Grassmannian geometry of scattering amplitudes*, Cambridge University Press, Cambridge, 2016.
- [And77] George E. Andrews, *MacMahon's conjecture on symmetric plane partitions*, Proc. Nat. Acad. Sci. U.S.A. **74** (1977), no. 2, 426–429.
- [And79] George E. Andrews, *Plane partitions. III. The weak Macdonald conjecture*, Invent. Math. **53** (1979), no. 3, 193–225.
- [Bax89] Rodney J. Baxter, *Exactly solved models in statistical mechanics*, Academic Press, Inc. [Harcourt Brace Jovanovich, Publishers], London, 1989, Reprint of the 1982 original.
- [BB05] Anders Björner and Francesco Brenti, *Combinatorics of Coxeter groups*, Graduate Texts in Mathematics, vol. 231, Springer, New York, 2005.
- [BDG⁺22] Véronique Bazier-Matte, Guillaume Douville, Alexander Garver, Rebecca Patrias, Hugh Thomas, and Emine Yıldırım, *Leading terms of SL_3 web invariants*, Int. Math. Res. Not. IMRN (2022), no. 3, 1714–1733.
- [BS17] Daniel Bump and Anne Schilling, *Crystal bases: representations and combinatorics*, World Scientific Publishing Co. Pte. Ltd., Hackensack, NJ, 2017.
- [BZ08] Arkady Berenstein and Sebastian Zwicknagl, *Braided symmetric and exterior algebras*, Trans. Amer. Math. Soc. **360** (2008), no. 7, 3429–3472.
- [CKM14] Sabin Cautis, Joel Kamnitzer, and Scott Morrison, *Webs and quantum skew Howe duality*, Math. Ann. **360** (2014), no. 1-2, 351–390.
- [CS14] Luigi Cantini and Andrea Sportiello, *A one-parameter refinement of the Razumov-Stroganov correspondence*, J. Combin. Theory Ser. A **127** (2014), 400–440.
- [DKS22] Daniel C. Douglas, Richard Kenyon, and Haolin Shi, *Dimers, webs, and local systems*, preprint (2022), 33 pages, [arXiv:2205.05139](https://arxiv.org/abs/2205.05139).
- [EKLP92] Noam Elkies, Greg Kuperberg, Michael Larsen, and James Propp, *Alternating-sign matrices and domino tilings. I*, J. Algebraic Combin. **1** (1992), no. 2, 111–132.
- [Eli15] Ben Elias, *Light ladders and clasp conjectures*, preprint (2015), 69 pages, [arXiv:1510.06840](https://arxiv.org/abs/1510.06840).
- [FK97] Igor B. Frenkel and Mikhail G. Khovanov, *Canonical bases in tensor products and graphical calculus for $U_q(\mathfrak{sl}_2)$* , Duke Math. J. **87** (1997), no. 3, 409–480.
- [FK14] Bruce Fontaine and Joel Kamnitzer, *Cyclic sieving, rotation, and geometric representation theory*, Selecta Math. (N.S.) **20** (2014), no. 2, 609–625.
- [FKK13] Bruce Fontaine, Joel Kamnitzer, and Greg Kuperberg, *Buildings, spiders, and geometric Satake*, Compos. Math. **149** (2013), no. 11, 1871–1912.
- [FLL19] Chris Fraser, Thomas Lam, and Ian Le, *From dimers to webs*, Trans. Amer. Math. Soc. **371** (2019), no. 9, 6087–6124.
- [Fon12] Bruce Fontaine, *Generating basis webs for SL_n* , Adv. Math. **229** (2012), no. 5, 2792–2817.
- [FP16] Sergey Fomin and Pavlo Pylyavskyy, *Tensor diagrams and cluster algebras*, Adv. Math. **300** (2016), 717–787.
- [Fra20] Chris Fraser, *Braid group symmetries of Grassmannian cluster algebras*, Selecta Math. (N.S.) **26** (2020), no. 2, Paper No. 17, 51 pages.
- [Fra23] Chris Fraser, *Webs and canonical bases in degree two*, Combin. Theory **3** (2023), no. 3, Paper No. 11, 26 pages.

- [FZ03] Sergey Fomin and Andrei Zelevinsky, *Cluster algebras. II. Finite type classification*, Invent. Math. **154** (2003), no. 1, 63–121.
- [GHKK18] Mark Gross, Paul Hacking, Sean Keel, and Maxim Kontsevich, *Canonical bases for cluster algebras*, J. Amer. Math. Soc. **31** (2018), no. 2, 497–608.
- [GPPSS23] Christian Gaetz, Oliver Pechenik, Stephan Pfannerer, Jessica Striker, and Joshua P. Swanson, *An SL_4 -web basis from hourglass plabic graphs*, Sémin. Lothar. Combin. **89B** (2023), Art. 9, 12 pages.
- [GPPSS24a] Christian Gaetz, Oliver Pechenik, Stephan Pfannerer, Jessica Striker, and Joshua P. Swanson, *Promotion permutations for tableaux*, Combin. Theory (in press) (2024), 55 pages, [arXiv:2306.12506](https://arxiv.org/abs/2306.12506).
- [GPPSS24b] Christian Gaetz, Oliver Pechenik, Stephan Pfannerer, Jessica Striker, and Joshua P. Swanson, *Web bases in degree two from hourglass plabic graphs*, preprint (2024), [arXiv:2402.13978](https://arxiv.org/abs/2402.13978).
- [GPT23] Alexander Garver, Rebecca Patrias, and Hugh Thomas, *Minuscule reverse plane partitions via quiver representations*, Selecta Math. (N.S.) **29** (2023), no. 3, Paper No. 37, 48 pages.
- [Hag18] Colin Scott Hagemeyer, *Spiders and generalized confluence*, ProQuest LLC, Ann Arbor, MI, 2018, Thesis (Ph.D.)—University of California, Davis.
- [HJO22] Byung-Hak Hwang, Jihyeug Jang, and Jaeseong Oh, *A combinatorial model for the transition matrix between the Specht and web bases*, Sémin. Lothar. Combin. **86B** (2022), Art. 34, 12 pages.
- [HMN⁺17] Dylan Heuer, Chelsey Morrow, Ben Noteboom, Sara Solhjem, Jessica Striker, and Corey Vorland, *Chained permutations and alternating sign matrices—inspired by three-person chess*, Discrete Math. **340** (2017), no. 12, 2732–2752.
- [Hod43] W. V. D. Hodge, *Some enumerative results in the theory of forms*, Proc. Cambridge Philos. Soc. **39** (1943), 22–30.
- [Hop20] Sam Hopkins, *Cyclic sieving for plane partitions and symmetry*, SIGMA Symmetry Integrability Geom. Methods Appl. **16** (2020), Paper No. 130, 40 pages.
- [HR22] Sam Hopkins and Martin Rubey, *Promotion of Kreweras words*, Selecta Math. (N.S.) **28** (2022), no. 1, Paper No. 10, 38 pages.
- [IZ22] Mee Seong Im and Jieru Zhu, *Transitioning between tableaux and spider bases for Specht modules*, Algebr. Represent. Theory **25** (2022), no. 2, 387–399.
- [Jon85] Vaughan F. R. Jones, *A polynomial invariant for knots via von Neumann algebras*, Bull. Amer. Math. Soc. (N.S.) **12** (1985), no. 1, 103–111.
- [Kas90] Masaki Kashiwara, *Crystalizing the q -analogue of universal enveloping algebras*, Comm. Math. Phys. **133** (1990), no. 2, 249–260.
- [Kas91] M. Kashiwara, *On crystal bases of the q -analogue of universal enveloping algebras*, Duke Math. J. **63** (1991), no. 2, 465–516.
- [Kau87] Louis H. Kauffman, *State models and the Jones polynomial*, Topology **26** (1987), no. 3, 395–407.
- [Ken04] Richard Kenyon, *An introduction to the dimer model*, School and Conference on Probability Theory, ICTP Lect. Notes, XVII, Abdus Salam Int. Cent. Theoret. Phys., Trieste, 2004, pp. 267–304.
- [Kho00] Mikhail Khovanov, *A categorification of the Jones polynomial*, Duke Math. J. **101** (2000), no. 3, 359–426.
- [Kho04] Mikhail Khovanov, *$sl(3)$ link homology*, Algebr. Geom. Topol. **4** (2004), 1045–1081.
- [Kim03] Dongseok Kim, *Graphical calculus on representations of quantum Lie algebras*, ProQuest LLC, Ann Arbor, MI, 2003, Thesis (Ph.D.)—University of California, Davis.
- [KK99] Mikhail Khovanov and Greg Kuperberg, *Web bases for $sl(3)$ are not dual canonical*, Pacific J. Math. **188** (1999), no. 1, 129–153.
- [KL94] Louis H. Kauffman and Sóstenes L. Lins, *Temperley-Lieb recoupling theory and invariants of 3-manifolds*, Annals of Mathematics Studies, vol. 134, Princeton University Press, Princeton, NJ, 1994.
- [KO05] Richard Kenyon and Andrei Okounkov, *What is ... a dimer?*, Notices Amer. Math. Soc. **52** (2005), no. 3, 342–343.
- [KR84] Joseph P. S. Kung and Gian-Carlo Rota, *The invariant theory of binary forms*, Bull. Amer. Math. Soc. (N.S.) **10** (1984), no. 1, 27–85.
- [Kup96a] Greg Kuperberg, *Another proof of the alternating-sign matrix conjecture*, Internat. Math. Res. Notices (1996), no. 3, 139–150.
- [Kup96b] Greg Kuperberg, *Spiders for rank 2 Lie algebras*, Comm. Math. Phys. **180** (1996), no. 1, 109–151.
- [Kup02] Greg Kuperberg, *Symmetry classes of alternating-sign matrices under one roof*, Ann. of Math. (2) **156** (2002), no. 3, 835–866.
- [KW14] Yuji Kodama and Lauren Williams, *KP solitons and total positivity for the Grassmannian*, Invent. Math. **198** (2014), no. 3, 637–699.
- [LLS21] Thomas Lam, Seung Jin Lee, and Mark Shimozono, *Back stable Schubert calculus*, Compos. Math. **157** (2021), no. 5, 883–962.
- [LMS79a] V. Lakshmibai, C. Musili, and C. S. Seshadri, *Geometry of G/P . III. Standard monomial theory for a quasi-minuscule P* , Proc. Indian Acad. Sci. Sect. A Math. Sci. **88** (1979), no. 3, 93–177.
- [LMS79b] V. Lakshmibai, C. Musili, and C. S. Seshadri, *Geometry of G/P . IV. Standard monomial theory for classical types*, Proc. Indian Acad. Sci. Sect. A Math. Sci. **88** (1979), no. 4, 279–362.

- [LS78] V. Lakshmibai and C. S. Seshadri, *Geometry of G/P . II. The work of de Concini and Procesi and the basic conjectures*, Proc. Indian Acad. Sci. Sect. A **87** (1978), no. 2, 1–54.
- [LS96] Alain Lascoux and Marcel-Paul Schützenberger, *Treillis et bases des groupes de Coxeter*, Electron. J. Combin. **3** (1996), no. 2, Research paper 27, approx. 35 pages.
- [LS21] Thang T. Q. Lê and Adam S. Sikora, *Stated $SL(n)$ -skein modules and algebras*, preprint (2021), 79 pages, [arXiv:2201.00045](#).
- [Lus90] G. Lusztig, *Canonical bases arising from quantized enveloping algebras*, J. Amer. Math. Soc. **3** (1990), no. 2, 447–498.
- [Lus92] G. Lusztig, *Affine quivers and canonical bases*, Inst. Hautes Études Sci. Publ. Math. (1992), no. 76, 111–163.
- [Lus93] George Lusztig, *Introduction to quantum groups*, Progress in Mathematics, vol. 110, Birkhäuser Boston, Inc., Boston, MA, 1993.
- [Lus00] G. Lusztig, *Semicanonical bases arising from enveloping algebras*, Adv. Math. **151** (2000), no. 2, 129–139.
- [MN08] Scott Morrison and Ari Nieh, *On Khovanov’s cobordism theory for \mathfrak{su}_3 knot homology*, J. Knot Theory Ramifications **17** (2008), no. 9, 1121–1173.
- [Mor07] Scott Edward Morrison, *A diagrammatic category for the representation theory of $U_q(\mathfrak{sl}_n)$* , ProQuest LLC, Ann Arbor, MI, 2007, Thesis (Ph.D.)—University of California, Berkeley.
- [MOY98] Hitoshi Murakami, Tomotada Ohtsuki, and Shuji Yamada, *Homfly polynomial via an invariant of colored plane graphs*, Enseign. Math. (2) **44** (1998), no. 3–4, 325–360.
- [MRR83] W. H. Mills, David P. Robbins, and Howard Rumsey, Jr., *Alternating sign matrices and descending plane partitions*, J. Combin. Theory Ser. A **34** (1983), no. 3, 340–359.
- [New42] M. H. A. Newman, *On theories with a combinatorial definition of “equivalence”*, Ann. of Math. (2) **43** (1942), 223–243.
- [Pat19] Rebecca Patrias, *Promotion on generalized oscillating tableaux and web rotation*, J. Combin. Theory Ser. A **161** (2019), 1–28.
- [Pos06] Alexander Postnikov, *Total positivity, Grassmannians, and networks*, preprint (2006), 79 pages, [arXiv:math/0609764](#).
- [Pos18] Alexander Postnikov, *Positive Grassmannian and polyhedral subdivisions*, Proceedings of the International Congress of Mathematicians—Rio de Janeiro 2018. Vol. IV. Invited lectures, World Sci. Publ., Hackensack, NJ, 2018, pp. 3181–3211.
- [Pou22] Anup Poudel, *A comparison between SL_n spider categories*, preprint (2022), 25 pages, [arXiv:2210.09289](#).
- [PP20] Rebecca Patrias and Oliver Pechenik, *Dynamics of plane partitions: proof of the Cameron–Fon-Der-Flaass conjecture*, Forum Math. Sigma **8** (2020), Paper No. e62, 6 pages.
- [PP23] Rebecca Patrias and Oliver Pechenik, *Tableau evacuation and webs*, Proc. Amer. Math. Soc. Ser. B **10** (2023), 341–352.
- [PPR09] T. Kyle Petersen, Pavlo Pylyavskyy, and Brendon Rhoades, *Promotion and cyclic sieving via webs*, J. Algebraic Combin. **30** (2009), no. 1, 19–41.
- [PPS22] Rebecca Patrias, Oliver Pechenik, and Jessica Striker, *A web basis of invariant polynomials from non-crossing partitions*, Adv. Math. **408** (2022), Paper No. 108603, 33 pages.
- [Pro84] Robert A. Proctor, *Bruhat lattices, plane partition generating functions, and minuscule representations*, European J. Combin. **5** (1984), no. 4, 331–350.
- [Pro01] James Propp, *The many faces of alternating-sign matrices*, Discrete models: combinatorics, computation, and geometry (Paris, 2001), Discrete Math. Theor. Comput. Sci. Proc., AA, Maison Inform. Math. Discrèt. (MIMD), Paris, 2001, pp. 043–058.
- [Qin21] Fan Qin, *Cluster algebras and their bases*, Proceedings of ICRA2020, to appear (2021), 33 pages, [arXiv:2108.09279](#).
- [Rho10] Brendon Rhoades, *Cyclic sieving, promotion, and representation theory*, J. Combin. Theory Ser. A **117** (2010), no. 1, 38–76.
- [Rho19] Brendon Rhoades, *The polytabloid basis expands positively into the web basis*, Forum Math. Sigma **7** (2019), Paper No. e26, 8 pages.
- [RT19] Heather M. Russell and Julianna S. Tymoczko, *The transition matrix between the Specht and web bases is unipotent with additional vanishing entries*, Int. Math. Res. Not. IMRN (2019), no. 5, 1479–1502.
- [RT22] Heather M. Russell and Julianna Tymoczko, *The transition matrix between the Specht and \mathfrak{sl}_3 web bases is unitriangular with respect to shadow containment*, Int. Math. Res. Not. IMRN (2022), no. 5, 3371–3416.
- [Sco06] J. Scott, *Grassmannians and cluster algebras*, Proc. London Math. Soc. (3) **92** (2006), no. 2, 345–380.
- [Sel11] P. Selinger, *A survey of graphical languages for monoidal categories*, New structures for physics, Lecture Notes in Phys., vol. 813, Springer, Heidelberg, 2011, pp. 289–355.

- [Ses78] C. S. Seshadri, *Geometry of G/P . I. Theory of standard monomials for minuscule representations*, C. P. Ramanujam—a tribute, Tata Inst. Fund. Res. Studies in Math., vol. 8, Springer, Berlin-New York, 1978, pp. 207–239.
- [Ses14] C. S. Seshadri, *Introduction to the theory of standard monomials*, second ed., Texts and Readings in Mathematics, vol. 46, Hindustan Book Agency, New Delhi, 2014.
- [Sik05] Adam S. Sikora, *Skein theory for $SU(n)$ -quantum invariants*, Algebr. Geom. Topol. **5** (2005), 865–897.
- [Spr74] T. A. Springer, *Regular elements of finite reflection groups*, Invent. Math. **25** (1974), 159–198.
- [Sta99] Richard P. Stanley, *Enumerative combinatorics. Vol. 2*, Cambridge Studies in Advanced Mathematics, vol. 62, Cambridge University Press, Cambridge, 1999, with a foreword by Gian-Carlo Rota and appendix 1 by Sergey Fomin.
- [Ste90] John R. Stembridge, *Nonintersecting paths, Pfaffians, and plane partitions*, Adv. Math. **83** (1990), no. 1, 96–131.
- [Str09] Jessica Striker, *The alternating sign matrix polytope*, Electron. J. Combin. **16** (2009), no. 1, Research Paper 41, 15 pages.
- [Str11] Jessica Striker, *A unifying poset perspective on alternating sign matrices, plane partitions, Catalan objects, tournaments, and tableaux*, Adv. in Appl. Math. **46** (2011), no. 1-4, 583–609.
- [Str15] Jessica Striker, *The toggle group, homomesy, and the Razumov-Stroganov correspondence*, Electron. J. Combin. **22** (2015), no. 2, Paper 2.57, 17 pages.
- [Str17] Jessica Striker, *Dynamical algebraic combinatorics: promotion, rowmotion, and resonance*, Notices Amer. Math. Soc. **64** (2017), no. 6, 543–549.
- [SW12] Jessica Striker and Nathan Williams, *Promotion and rowmotion*, European J. Combin. **33** (2012), no. 8, 1919–1942.
- [SW20] Linhui Shen and Daping Weng, *Cyclic sieving and cluster duality of Grassmannian*, SIGMA Symmetry Integrability Geom. Methods Appl. **16** (2020), Paper No. 067, 41 pages.
- [TL71] H. N. V. Temperley and E. H. Lieb, *Relations between the “percolation” and “colouring” problem and other graph-theoretical problems associated with regular planar lattices: some exact results for the “percolation” problem*, Proc. Roy. Soc. London Ser. A **322** (1971), no. 1549, 251–280.
- [Tur94] V. G. Turaev, *Quantum invariants of knots and 3-manifolds*, De Gruyter Studies in Mathematics, vol. 18, Walter de Gruyter & Co., Berlin, 1994.
- [Wei21] Anna Weigandt, *Bumpless pipe dreams and alternating sign matrices*, J. Combin. Theory Ser. A **182** (2021), Paper No. 105470, 52 pages.
- [Wes12] Bruce W. Westbury, *Web bases for the general linear groups*, J. Algebraic Combin. **35** (2012), no. 1, 93–107.
- [Wey97] Hermann Weyl, *The classical groups*, Princeton Landmarks in Mathematics, Princeton University Press, Princeton, NJ, 1997, Their invariants and representations, Fifteenth printing, Princeton Paperbacks.
- [Wie00] Benjamin Wieland, *A large dihedral symmetry of the set of alternating sign matrices*, Electron. J. Combin. **7** (2000), Research Paper 37, 13 pages.
- [Zei96] Doron Zeilberger, *Proof of the alternating sign matrix conjecture*, Electron. J. Combin. **3** (1996), no. 2, Research Paper 13, approx. 84 pages, the Foata Festschrift.
- [Zhu17] Xinwen Zhu, *An introduction to affine Grassmannians and the geometric Satake equivalence*, Geometry of moduli spaces and representation theory, IAS/Park City Math. Ser., vol. 24, Amer. Math. Soc., Providence, RI, 2017, pp. 59–154.

(Gaetz) DEPARTMENT OF MATHEMATICS, UNIVERSITY OF CALIFORNIA, BERKELEY, CA, USA.
 Email address: gaetz@berkeley.edu

(Pechenik) DEPARTMENT OF COMBINATORICS & OPTIMIZATION, UNIVERSITY OF WATERLOO, ON, CANADA.
 Email address: oliver.pechenik@uwaterloo.ca

(Pfannerer) INSTITUTE OF DISCRETE MATHEMATICS AND GEOMETRY, TECHNISCHE UNIVERSITÄT WIEN, AUSTRIA.
 Email address: math@pfannerer-mittas.net

(Striker) DEPARTMENT OF MATHEMATICS, NORTH DAKOTA STATE UNIVERSITY, FARGO, ND, USA.
 Email address: jessica.striker@ndsu.edu

(Swanson) DEPARTMENT OF MATHEMATICS, UNIVERSITY OF SOUTHERN CALIFORNIA, LOS ANGELES, CA, USA.
 Email address: swansonj@usc.edu